INT 186/94 December 1994

TCV POSTERS

AT

APS MEETING 1994

MINNEAPOLIS, 7 - 11 NOVEMBER 1994

Content

INITIAL OHMIC CONFINEMENT RESULTS FROM TCV

F. Hofmann, J.B. Lister, R. Behn, M.J. Dutch, B.P. Duval, B. Joye, X. Llobet, Y. Martin, J.-M. Moret, Ch. Nieswand, Z.A. Pietrzyk, R.A. Pitts, A. Pochelon, G. Tonetti, H. Weisen and the TCV Team.

Centre de Recherches en Physique des Plasmas, Association EURATOM - Confédération Suisse, Ecole Polytechnique Fédérale de Lausanne, 21 Av. des Bains, CH-1007 Lausanne, Switzerland

Introduction

TCV (Tokamak à Configuration Variable) is a compact, highly-elongated tokamak capable of producing limited or diverted plasmas with currents up to 1MA. During the first year of operation, TCV has produced a large variety of plasma shapes and magnetic configurations, with $1.0 \leq Btor \leq 1.46T$, $Ip \leq 810kA$, $k \leq 2.05$, $-0.7 \leq d \leq 0.9$. A new shape control algorithm, based on a finite-element reconstruction of the plasma current in real time, has been implemented. Vertical growth rates up to 800 sec-1, corresponding to a stability margin f=1.15, have been stabilized. Ohmic H-modes, with energy confinement times reaching 80ms, normalized beta (btoraB/Ip) of 1.9 and tE/tE(ITER89-P) of 2.4 have been obtained in single-null X-point deuterium discharges with the ion —B drift towards the X-point. Limiter H-modes with maximum line-averaged electron densities of 1.7x1020 m-3 have been observed in D-shaped plasmas with $360kA \leq Ip \leq 600kA$. ELM control has been demonstrated in double-null Ohmic H-modes. This work was partly supported by the Swiss National Science Foundation.

TCV Objectives

The goals of TCV, as stated in the original 1985 Phase I Proposal, are to study:

"• scenarios for the creation of **strongly shaped** and **elongated** plasmas.

- the possibility of maintaining positional stability and optimization of the control system.
- the dependence of the maximum current on elongation.
- the scaling laws for the confinement time and density limit at high elongation.
- the dependence of the beta limit on current."

The **4.5 MW ECRH additional heating system** (3.0 MW X2, 82.6 GHz and 1.5 MW X3, 118 GHz) will allow these studies to be pursued at high input power levels and permit a host of related experiments, for example:

- dependence of the H-mode threshold and confinement properties on elongation and shape.
- clarification of scaling law discrepancies between ECRH and NBI / ICRH heated plasmas.
- control of MHD activity and current profile tailoring.

Research Program 1994-1995

- **Creation and control of highly elongated plasmas.** In TCV, plasma elongation and current are presently limited to values of approximately 2.1 and 800kA respectively, due to the limited bandwidth of the shaping coil power supplies. In November 1994, two additional coils, driven by a fast power supply, will be installed inside the TCV vacuum vessel. This will allow exploration of the limits in elongation and plasma current, as well as the creation of new divertor configurations with high triangularity.

- **H-mode.** The conditions for the L-H transition will be investigated as a function of the discharge parameters (plasma current, density, elongation and triangularity). Methods of actively controlling the transition from ELM-free to ELMy H-mode and vice versa will also be studied. This study will mainly be done in Ohmically heated plasmas, but will also include ECRH heated plasmas, as sources become available.

- **Influence of plasma shape on transport and confinement.** The effect of elongation and triangularity on operational limits and on plasma transport will be studied in the Ohmic regime and with ERCH, as sources become available.

- **Magnetic activity in highly elongated and shaped plasmas.** Magnetic activity due to a variety of phenomena (locked modes, ELMs, sawteeth, magnetic turbulence, disruptions) will be studied.

- **Use of non-magnetic measurements for position and shape control.**

- **Edge parameters.** Scaling of edge parameters (n_e, T_e, scrape-off length, power load) in diverted discharges with main discharge parameters (plasma current, density, magnetic configuration).

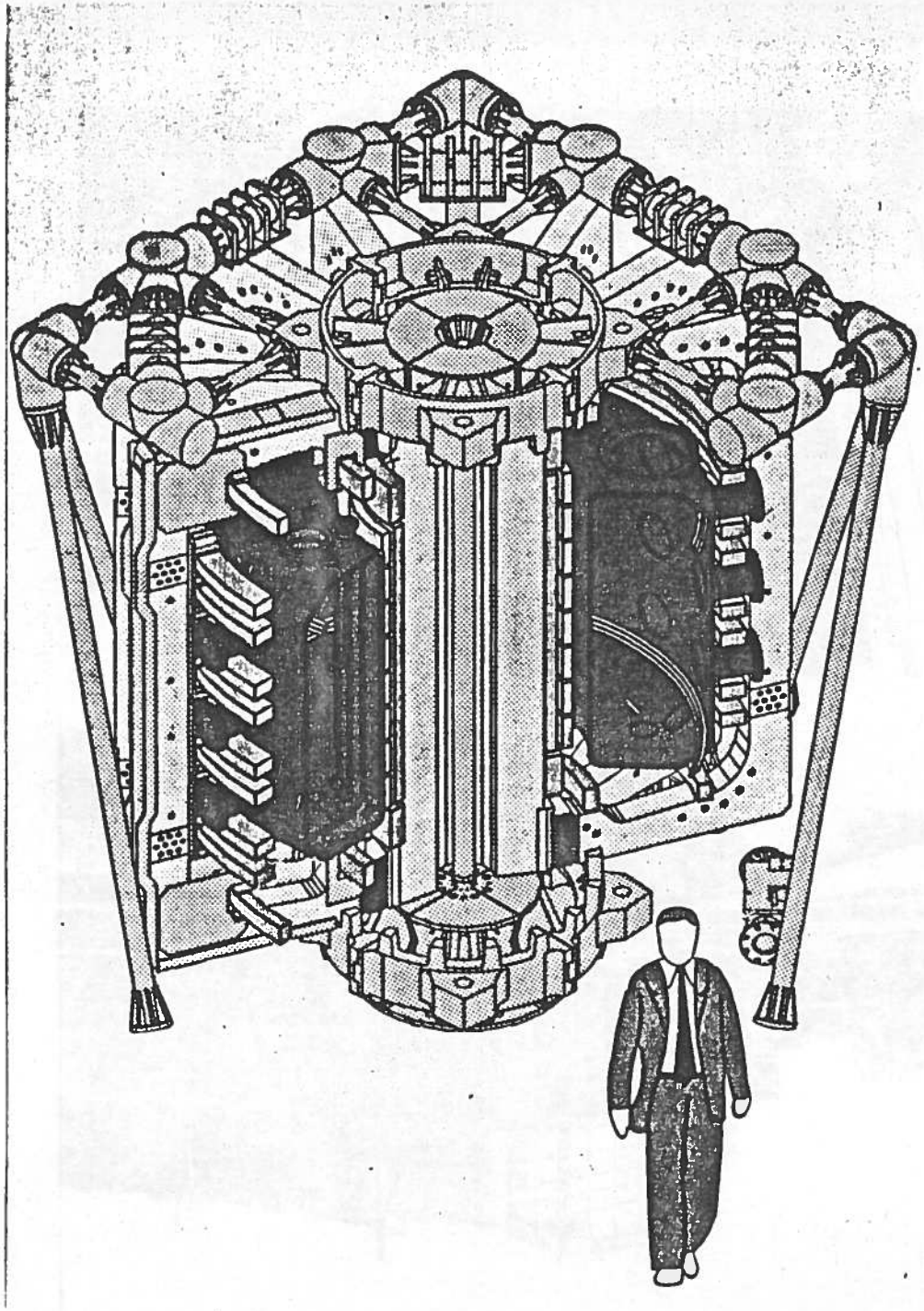

TCV DESIGN PARAMETERS

Major Radius	0.875 m
Vessel Internal Full Width	0.56 m
Vessel Internal Full Height	1.54 m
Nominal aspect ratio	3.66
Maximum Plasma Elongation	3.0
Toroidal Magnetic Field	1.43 T
Flux Swing from Air Core Transformer	3.4 Vsec (± 1.7)
Maximum Loop Voltage	10 V/turn
Maximum design Plasma Current	1.2 MA
Plasma Current, q=2 circular plasma	250 kA
Vacuum Vessel, Wall Thickness Resistance Time Constant (m=1)	1.8 cm s/steel 55 μΩ 8 msec
16 Independent Shaping Supplies	4 Quadrant 12 pulse 100 Hz
Auxiliary Heating (ECRH)	3.0 MW X2 1.5 MW X3

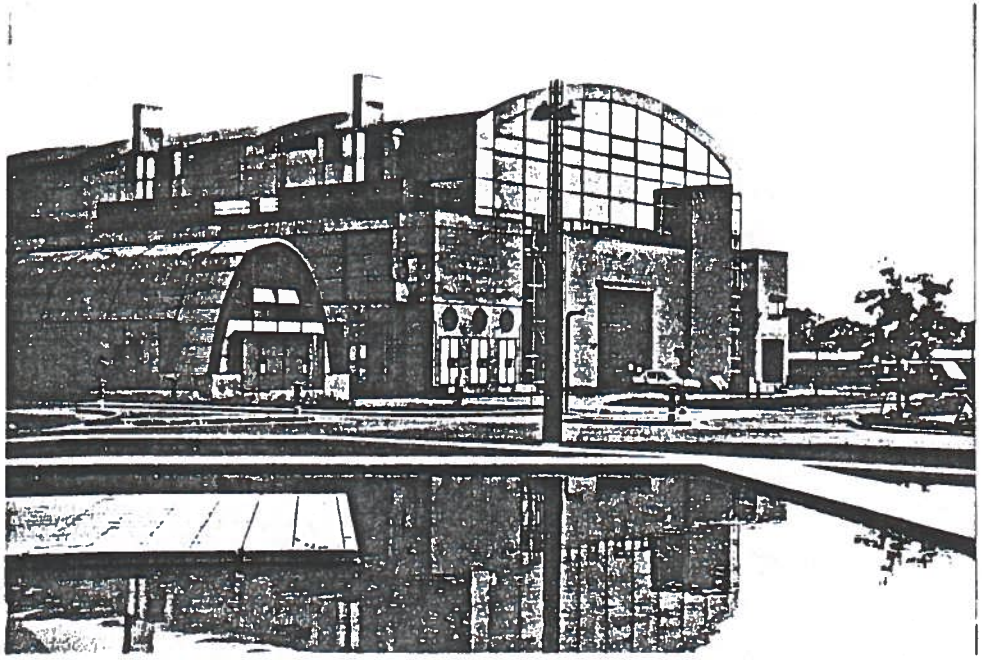

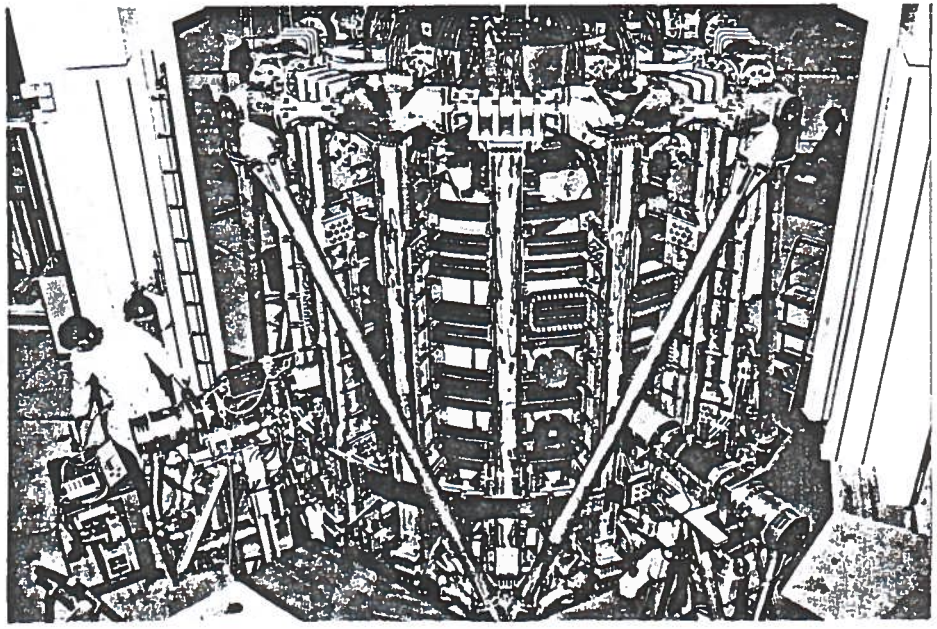

TCV PROGRAM

First Symbolic q=6 discharge	Nov 1992
First Campaign (Discharge Control + Shaping)	May - Oct 1993
Second Campaign (SNU, SNL, DND, Ohmic H-Mode)	Feb - Oct 1994
ECRH (1.....4.5 MW)	1995.....

ACHIEVED PERFORMANCE in TCV

Plasma current		--->	0.81 MA
Elongation	0.9	--->	2.05
Triangularity	-0.7	--->	0.9
Line-averaged density		--->	2.2e20 /m3
Normalized beta		--->	1.9
Energy confinement time		--->	80 msec
Regular Ohmic H-Modes		--->	1.5 seconds

Density control using ELMs in Ohmic H-Mode

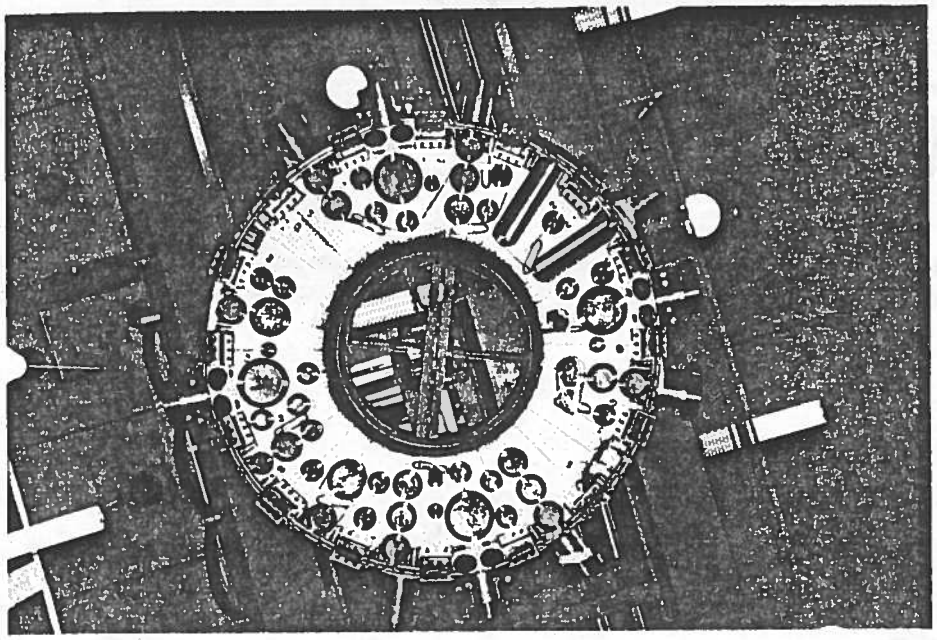

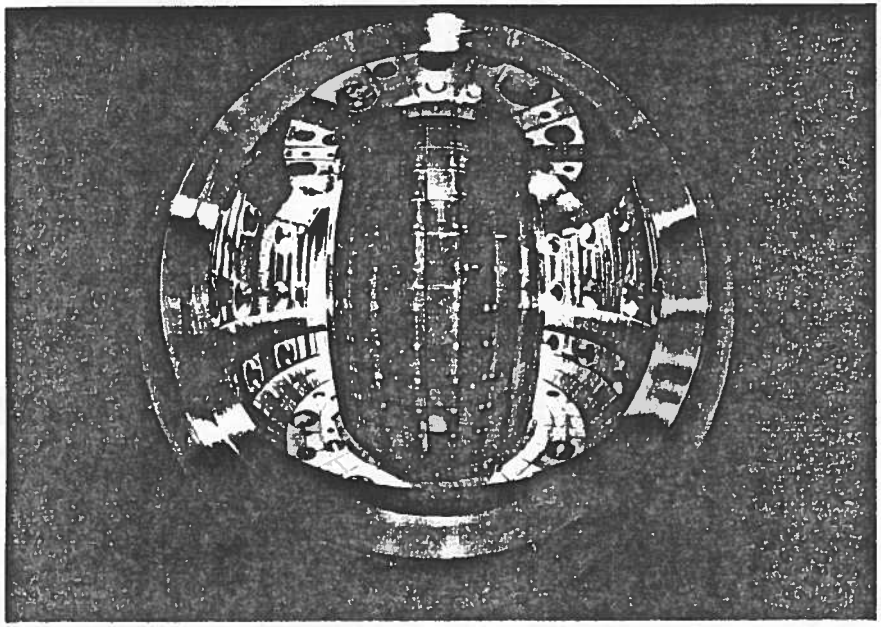

TCV diagnostics

Diagnostic	Measurements
Magnetics: 176 pick-up coils	Plasma equilibrium & shape
62 flux loops	MHD modes
Rogowski, DML	
Thomson scattering:	Electron temperature profile
30 (10) channels (vert.)	Electron density profile
30 channels (horiz.)	
4 Nd-Yag, 20 Hz	
FIR interferometer/polarimeter:	Electr. density profile (continuous)
215 μm, 15 (4) channels	Equilibrium reconstr. /CORK/
2mm microwave interferometer	Back-up for FIR
Infrared camera	Tile temperatures, power load
Langmuir Probes (44)	T_e and n_e at tiles
Multibolometer (64 chans, 5 cams)	P_{rad} profile
X-ray tomography	Plasma shape
200 (40) chans in 10 (2) cams	MHD phenomena
X-ray monitor diodes 12 (4)	$T_e(0)$ from foils, mode n-numbers,
Hard-X monitor	suprathermals
Visible tangential camera (2)	Plasma position and boundary shape
X-ray tangential camera	Core plasma shape
Neutral particle analyser	$T_i(0)$
Visible light monitors 20 (11)	Hα and impurity lines
Spectroscopy visible	Plasma purity Edge lines
VUV	Particle fluxes
USX	CV,CVI,BV ... /IPP Prague/
SX	metals, suprath. /CFN/
ECRH power transmission	Transmitted power (esp. X3)
Under discussion:	
SPRED spectrometer	Impurity surveillance ... /UKAEA?/
low power ECT	Changes in electron distr. function
laser scattering or imaging	n_e fluctuations, MHD act. /CFN?/
Reciprocating Langmuir probe	Edge T_e and n_e profiles. /UCSD?/

TCV TOKAMAK
VARIOUS CONFIGURATIONS ACHIEVED

TCV # 5559 @ 0.5 sec

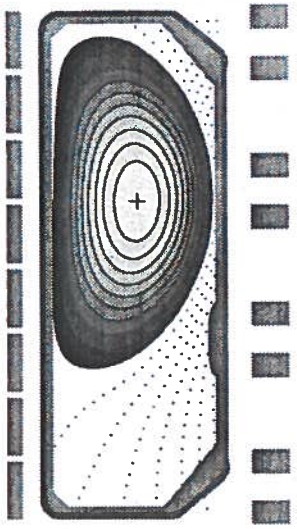

810kA q95=2.2 k=2.0 d=0.4

TCV # 5608 @ 0.266 sec

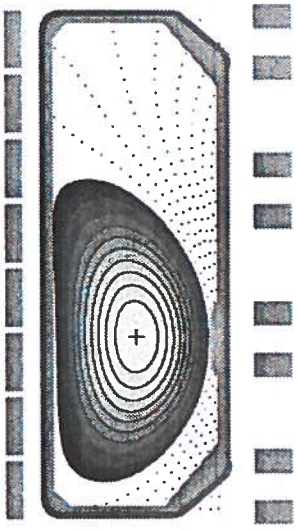

510kA q95=2.9 k=1.9 d=0.4

TCV # 5913 @ 0.552 sec

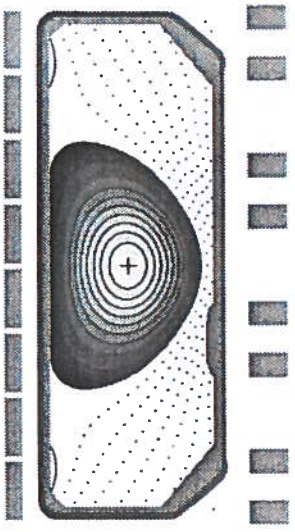

197kA q95=5.3 k=1.6 d=0.5

TCV # 6010 @ 0.6 sec

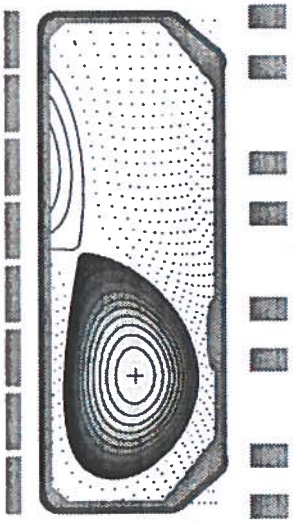

338kA q95=2.3 k=1.7 d=0.4

TCV # 5650 @ 0.466 sec

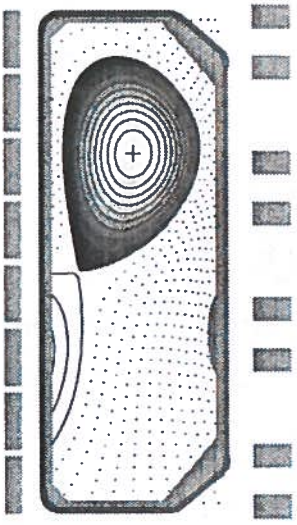

334kA q95=2.1 k=1.6 d=0.6

TCV # 4211 @ 0.432 sec

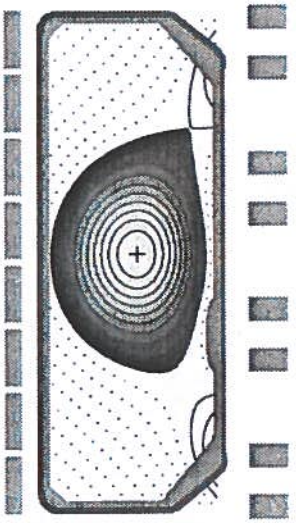

216kA q95=3.8 k=1.6 d=-0.6

TCV # 6398 @ 1.29 sec

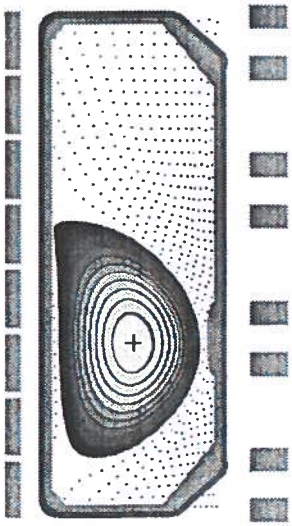

390kA q95=2.5 k=1.6 d=0.6

TCV # 6479 @ 0.4 sec

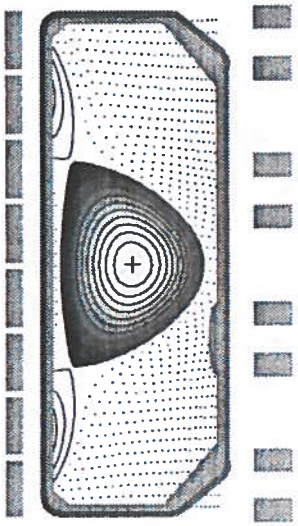

256kA q95=2.8 k=1.4 d=0.8

TCV # 6442 @ 0.259 sec

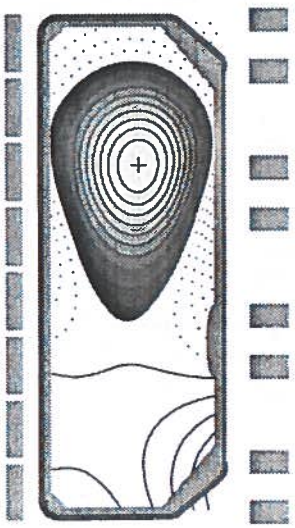

361kA q95=2.6 k=1.6 d=0.0

TCV MAGNETICS # 5559 @ 0.5 sec

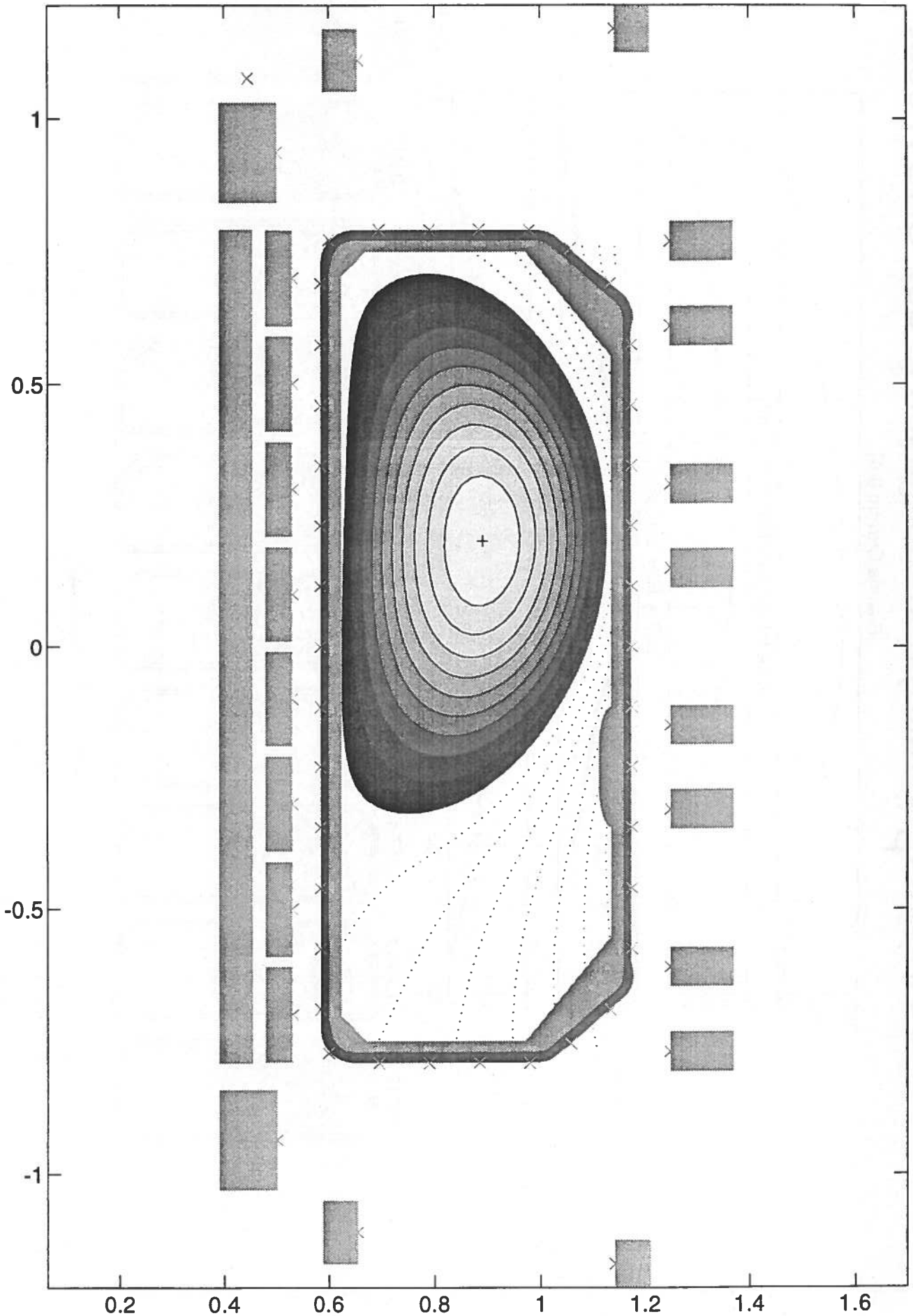

810kA q95=2.2 k=2.0 d=0.4

TCV Record I_P (810kA) and Elongation (2.05) SHOT: 5559

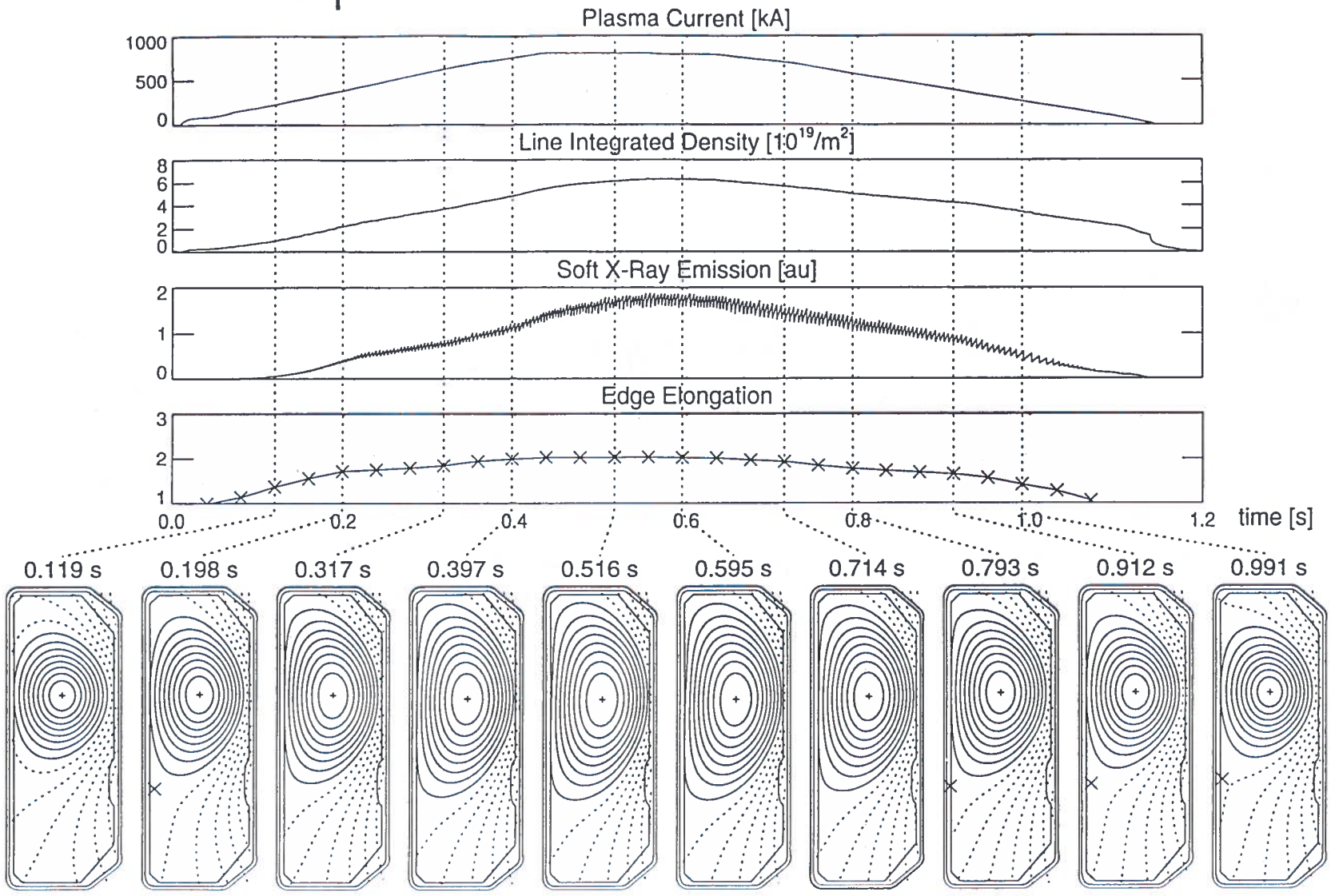

Record Density ($\overline{n}_e \geq 2.2e20\ m^{-3}$) and Confinement Time ($\tau_E \geq 80$ ms).

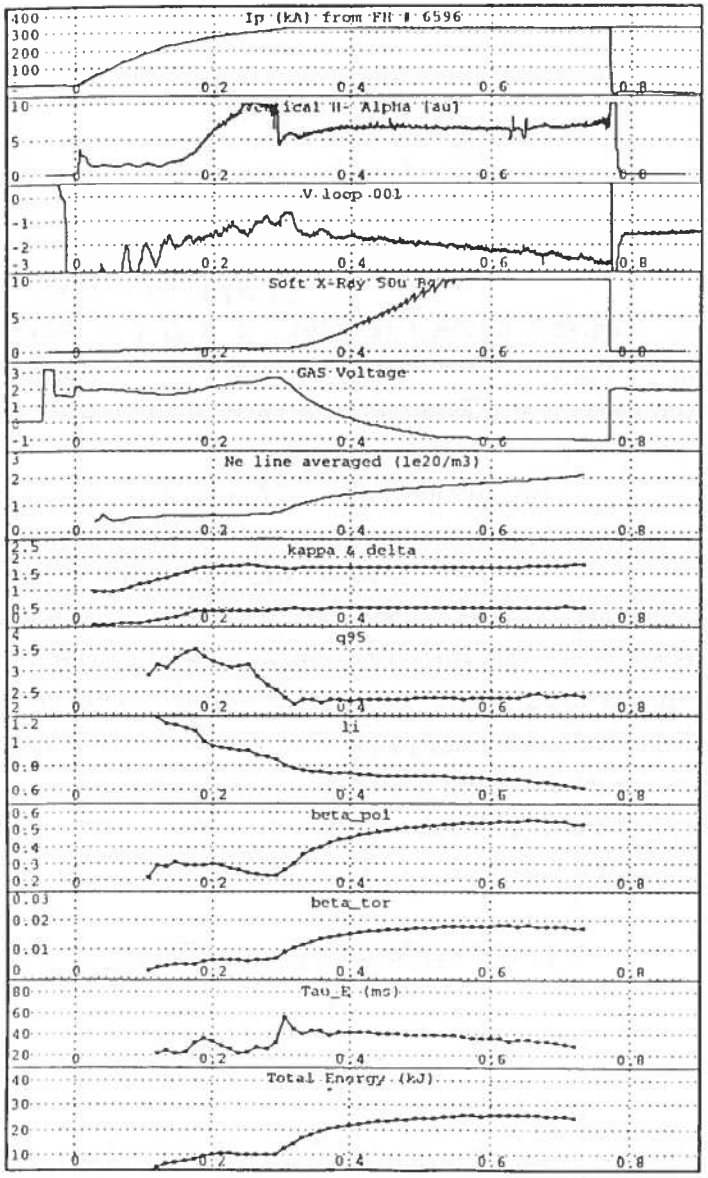

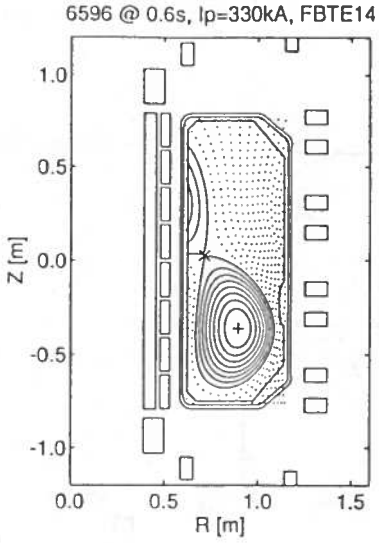

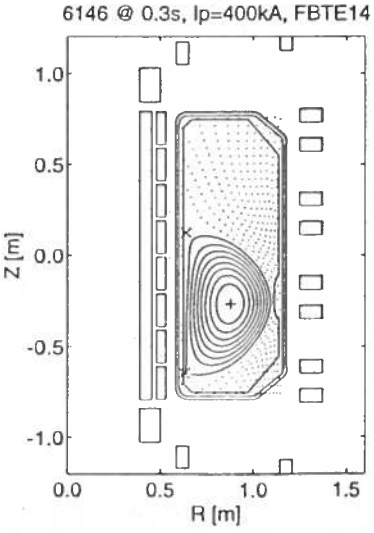

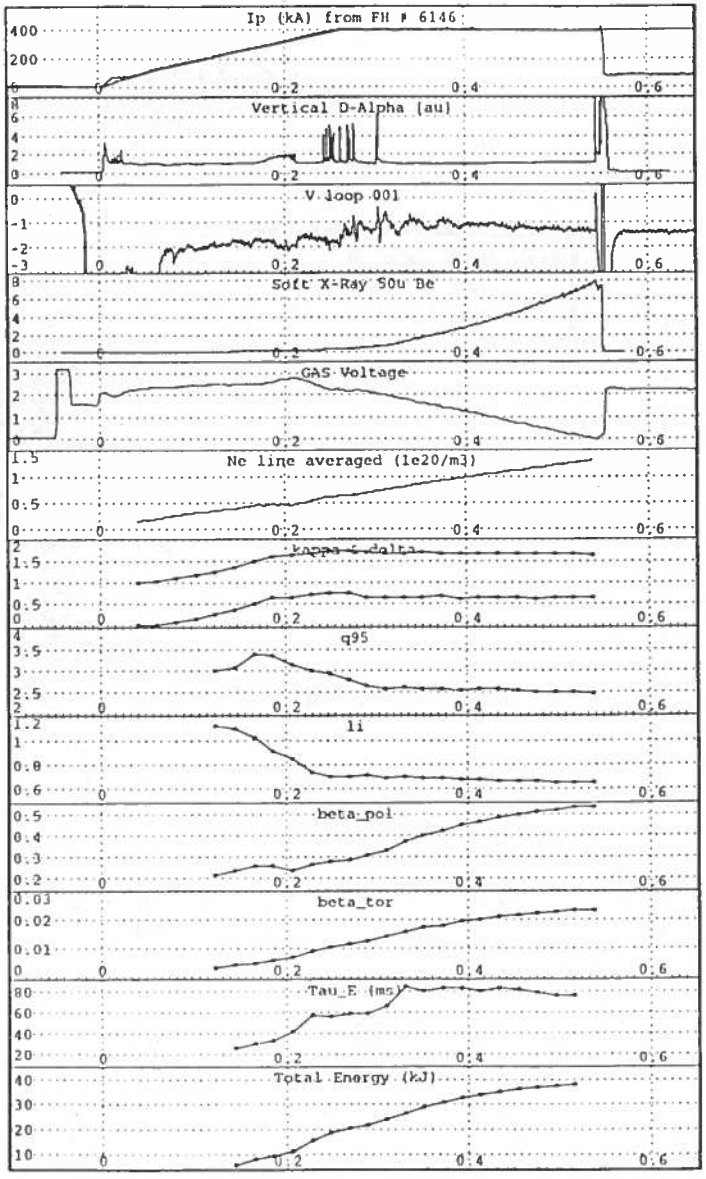

Energy Confinement Time in TCV

We present a preliminary analysis of the energy confinement time in L and H-mode discharges in TCV. Since electron density and temperature profiles are only available for a small fraction of the discharges and ion temperatures are not yet measured, τ_E is derived from equilibrium reconstructions (LIUQE) based on extensive magnetic pickup and flux measurements. The energy confinement time is calculated as:

$$\tau_E = W / (I_p V_l - dW/dt - dU/dt)$$

where W is the plasma thermal energy, $W = (3/2)\int p\, dV$, V_l is the loop voltage evaluated on the last closed flux surface and U is the internal poloidal magnetic field energy, $U = (\mu_o/4) l_i R_o I_p^2$

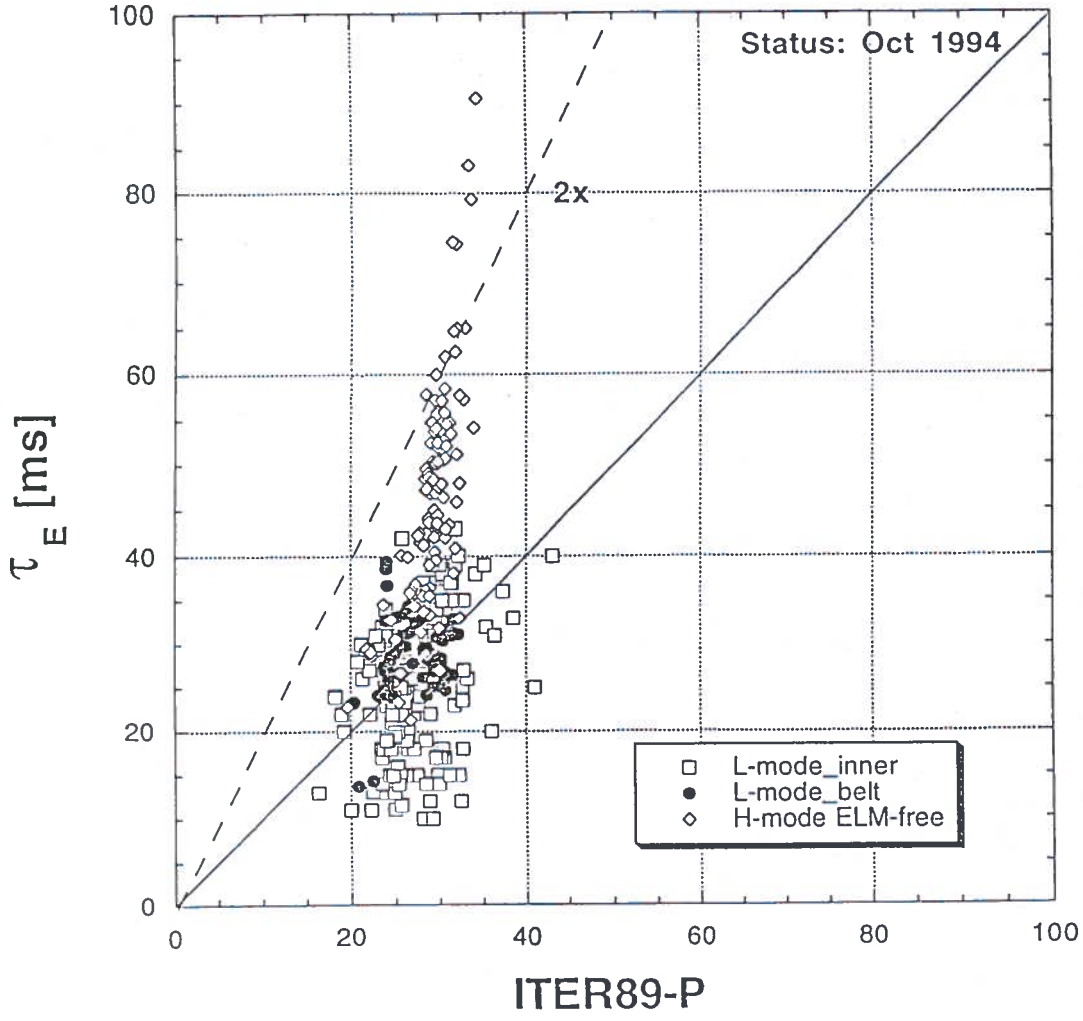

τ_E scalings

ITER89-P

$\tau_E^{ITER89\text{-}P} = 0.048\ I^{0.85}\ R^{1.2}\ a^{0.3}\ \kappa^{0.5}\ \bar{n}_{20}^{0.1}\ B^{0.2}\ A_i^{0.5}\ P^{-0.5}\ F$

$F = F[f_S^{\alpha s}\ f_q^{\alpha q}]$ = scale factor with $|\alpha_S| < 0.7$, $|\alpha_q| < 0.15$

$f_S = 0.3\ (R/a)^{0.75}\ R^{0.25}\ \kappa^{0.5}$ = shape-size index

$f_q = q95/3.2$ = q index

(here $f_S \sim 1$, $f_q \sim 1$, as in the ITER database)

Neo-Alcator OH scaling

$\tau_{NA} = 0.07\ n_{20}\ a\ R_o^2\ q_*$

q_* = cylindrical equivalent safety factor:

$q_* \sim (5a^2 B_o/R_o I)\ [1+\kappa^2(1+2\delta^2-1.2\delta^3)\ ] / 2$

JET-DIII-D scaling (ITER93H-P)

ELM-free:

$\tau_{th} = 0.036\ I^{1.06}\ B^{0.32}\ n_{19}^{0.17}\ P^{-0.67}\ R^{1.79}\ \kappa^{0.66}\ \varepsilon^{-0.11}\ A_i^{0.41}$

ELMy:

$\tau_{th} = 0.022\ I^{0.76}\ B^{0.15}\ n_{19}^{0.42}\ P^{-0.70}\ R^{2.60}\ \kappa^{1.05}\ \varepsilon^{-0.30}\ A_i^{0.30}$

Rebut-Lallia-Watkins

$\tau_{RLW} = f_R \times [\ 1.2\times10^{-2}\ I\ l^{1.5}/Z_{eff}^{0.5}$
$+ 0.146\ n_{20}^{0.75}\ I^{0.5}\ B^{0.5}\ l^{2.75}\ Z_{eff}^{0.25}\ /\ P\ ]\ (A_i/2)^{0.5}$

$l = (R\ a^2\ \kappa)^{1/3}$ characteristic scale length

f_R numerical factor to include ions: 1.8 and $Z_{eff} = 1.5$

[s, MA, T, m^{-3}, MW, m]
$\varepsilon = a/R$, A_i atomic nb.
$\bar{n}$ = line average density, n = volume-average electron density

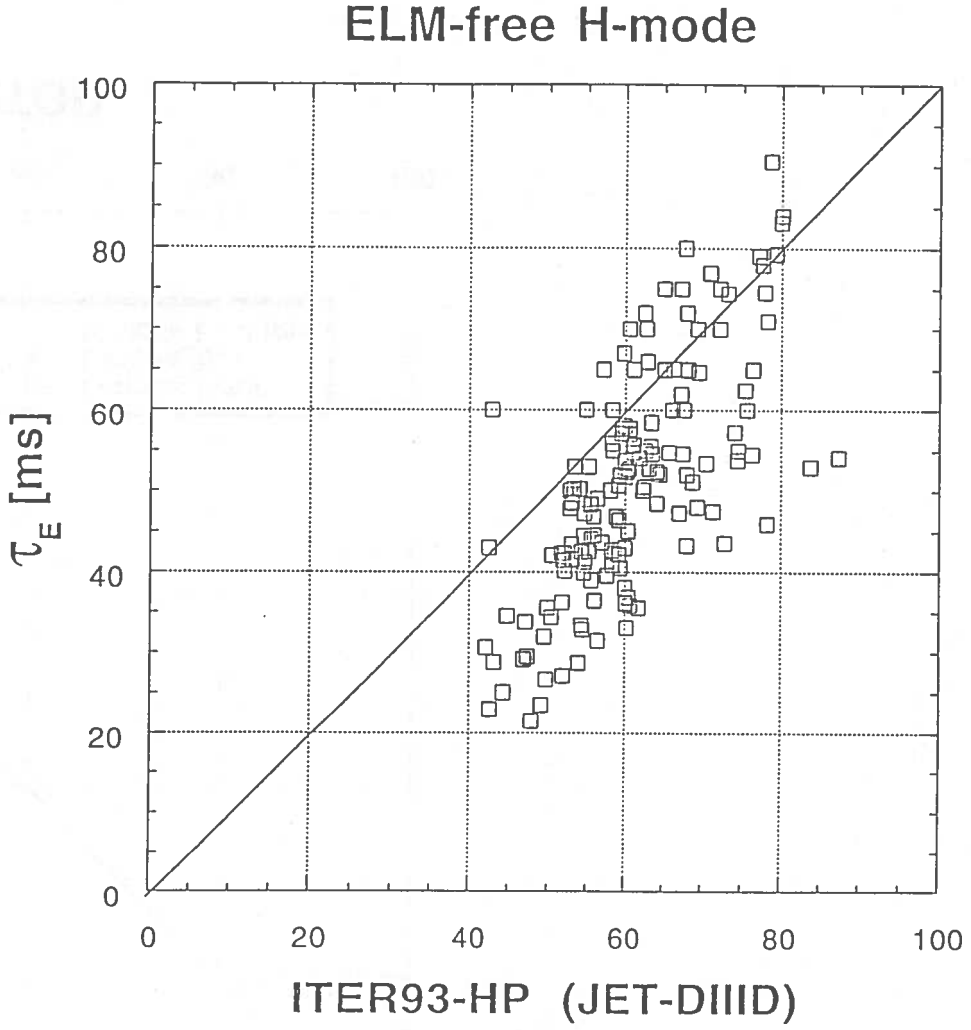

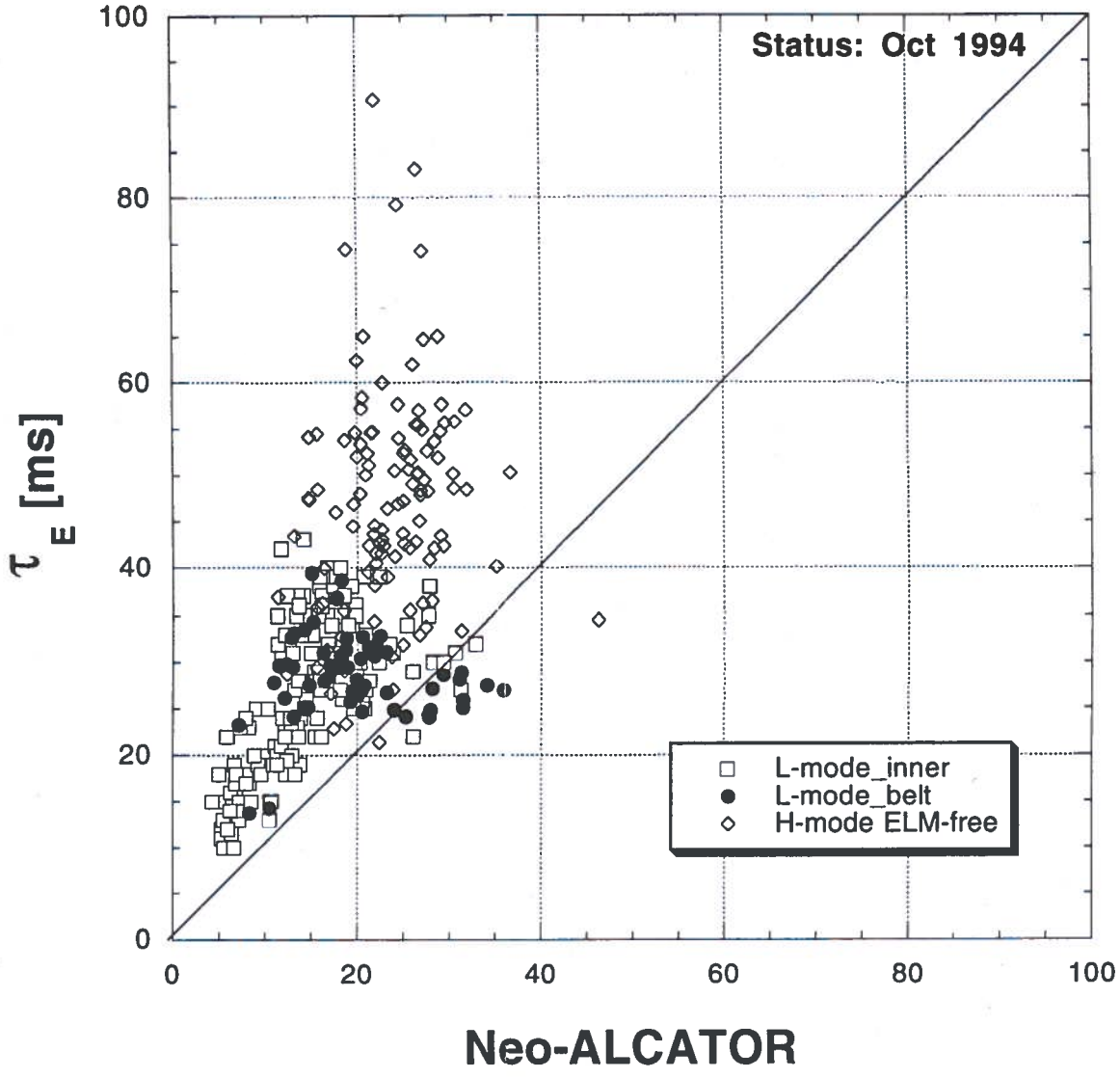
Status: Oct 1994
τ_E [ms]
Neo-ALCATOR
0
20
40
60
80
100
L-mode_inner
L-mode_belt
H-mode ELM-free

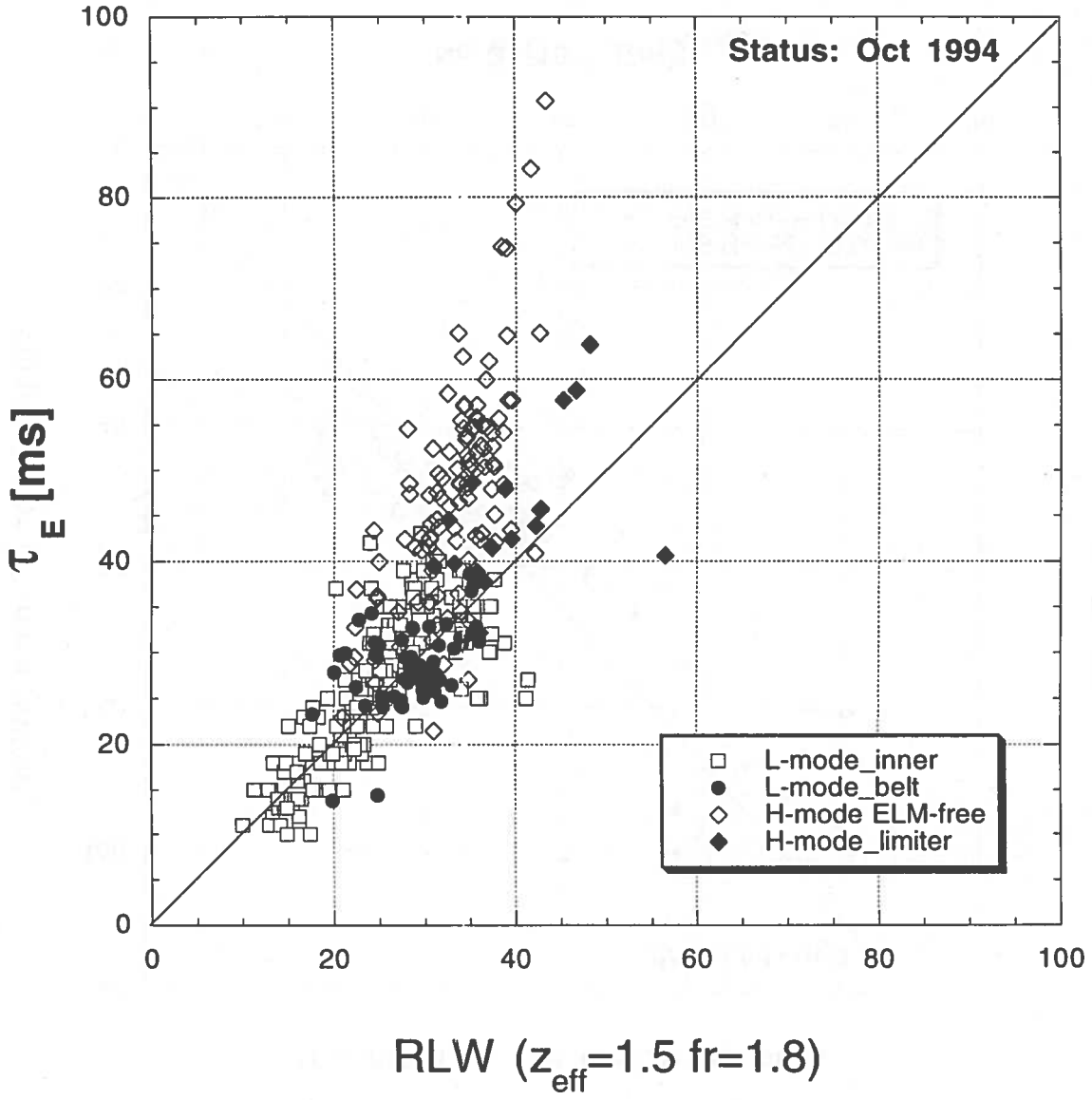
Status: Oct 1994
τ_E [ms]
RLW (z_{eff}=1.5 fr=1.8)
0
20
40
60
80
100
L-mode_inner
L-mode_belt
H-mode ELM-free
H-mode_limiter

Comparison with ASDEX H-mode threshold scaling

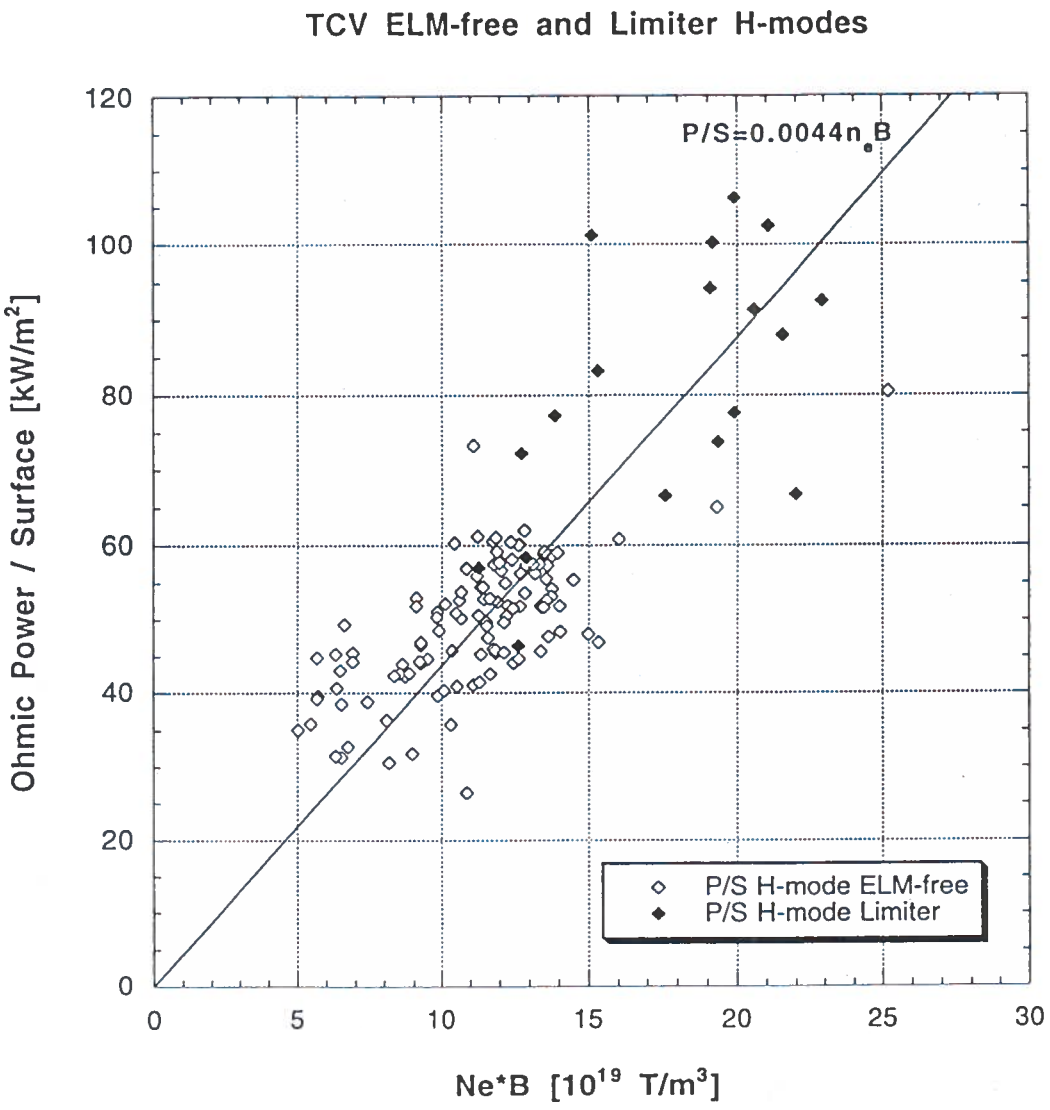

For detailed treatment of Ohmic H-modes in TCV, see Poster 2S25 at this session.

TCV TOKAMAK PLANT CONTROL

The plant control system provides:

- Man-Machine interface for physics, engineering and diagnostics.
- Automated control of some of the plant.
- Recording and display of the plant status.
- Control of the TCV Tokamak Pulse.

TCV plant to control includes:

- 340 MJ Motor Generator + Power Switchgear.
- Area access control.
- Coil Cooling + Vessel Heating subsystems.
- Pumps/Vacuum system + Diagnostics.
- Hybrid Plasma Control System. (See Poster 2S26)
- Plasma Waveform Generators.
- Fast distributed TCV pulse Timer.

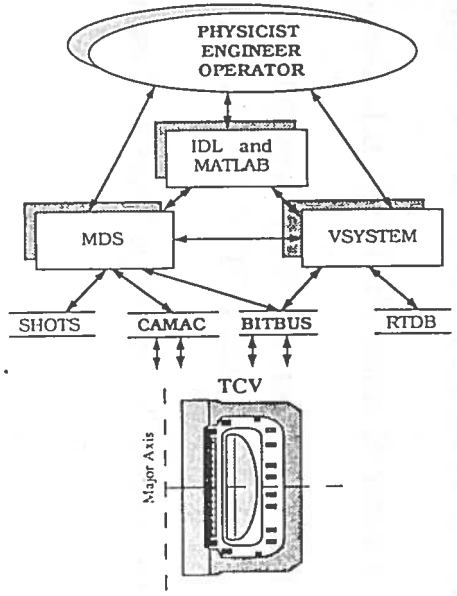

Integration of Data Flow using Existing Software

TCV Operator console display using the Vsystem package.

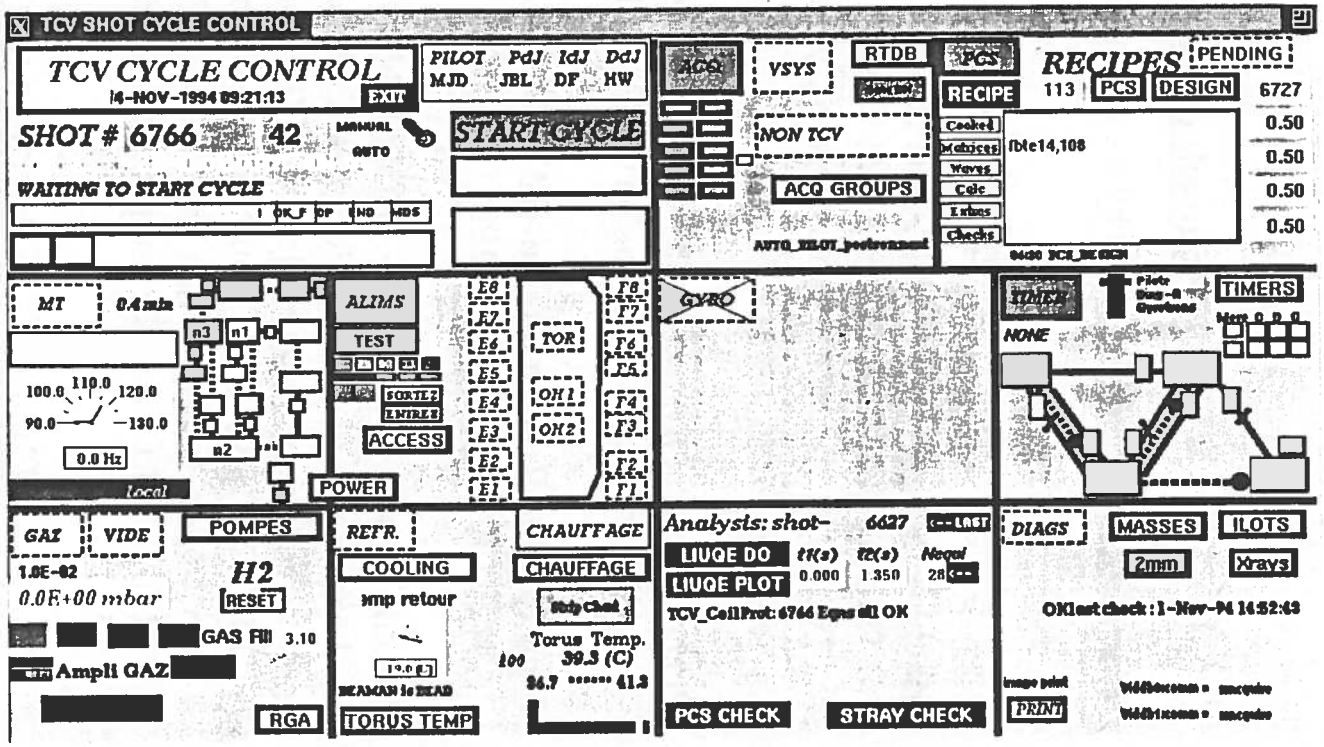

Acknowledgements

This work was partly supported by the Swiss National Science Foundation.

Bibliography

Machine Design - HOFMANN, F., et al., Proc. of 14th Symposium on Fusion Technology, Avignon (1986), Vol 1, p 587.
TONETTI, G., et al., Proc. of 16th Symposium on Fusion Technology, London (1990), Vol 1, p 687.

Plasma Control System (PCS) - ISOZ, P.F., et al., Proc. of 16th Symposium on Fusion Technology, London (1990), Vol 2, p 1264.

Equilibrium Reconstruction (LIUQE) - HOFMANN, F., TONETTI, G., NUCLEAR FUSION 28 (1988) 1871.

Initial Results from TCV - HOFMANN, F., et al., To be published in Proceedings of the 21st European Conference on Controlled Fusion and Plasma Physics, Montpellier. (EPS, Geneva, 1994).
LISTER, J.B., et al., 15th IAEA Conference on Plasma Physics and Controlled Nuclear Fusion Research, Seville (1994), Paper A-5-I-2.
DUTCH, M.J., et al., Submitted to NUCLEAR FUSION (Letters).

Other TCV Posters at this Session

2S24 "**MHD Activity** in Ohmic, Diverted and Limited L- and H-Mode Plasmas in the TCV Tokamak". H. Weisen , et al.

2S25 "**Ohmic H-modes** in TCV". B.P. Duval, et al.

2S26 **Plasma Control:** "Experimental and Modelling Study of the Plasma Dynamic Response in TCV". Y. Martin, J.B.Lister and J.-M. Moret.

2S27 (was 9R4) " First **Edge Physics** Results from TCV". R.A. Pitts, et al.

OHMIC H-MODES IN TCV

R. Behn, M.J. Dutch, B.P. Duval, F. Hofmann, B. Joye, J.B. Lister, X. Llobet, Y. Martin, J.-M. Moret, Ch. Nieswand, Z.A. Pietrzyk, R.A. Pitts, A. Pochelon, G. Tonetti, H. Weisen and the TCV Team.

Centre de Recherches en Physique des Plasmas, Association EURATOM - Confédération Suisse, Ecole Polytechnique Fédérale de Lausanne, 21 Av. des Bains, CH-1007 Lausanne, Switzerland

Introduction

TCV Machine

- Tokamak à Configuration Variable.
- For the experiments reported in this paper, additional heating was not yet available, so the plasma heating is purely OHMIC.
- Machine has been designed with a large number of independently controllable shaping coils permitting a wide variety of plasma shapes.
- Elongations up to k = 2 and triangularity +/- 0.7 with plasma currents up to 810kA have been achieved.
- For further information about the machine and the plasma control system, see posters presented by M.J. Dutch and Y. Martin at this conference.

Initial H-mode Results

- Signs of H-mode seen in SND configurations before first boronisation.
- Following Boronisation, a clear H-mode transition was observed for the SND configuration with the ion drift in the direction of the X-point (SND-U)
- Many types of Edge Localised Modes (ELMs) have been observed.
- A prolonged ELM-free phase inevitably resulted in a high density disruption. Transitions between the ELM phases appeared to be "spontaneous"

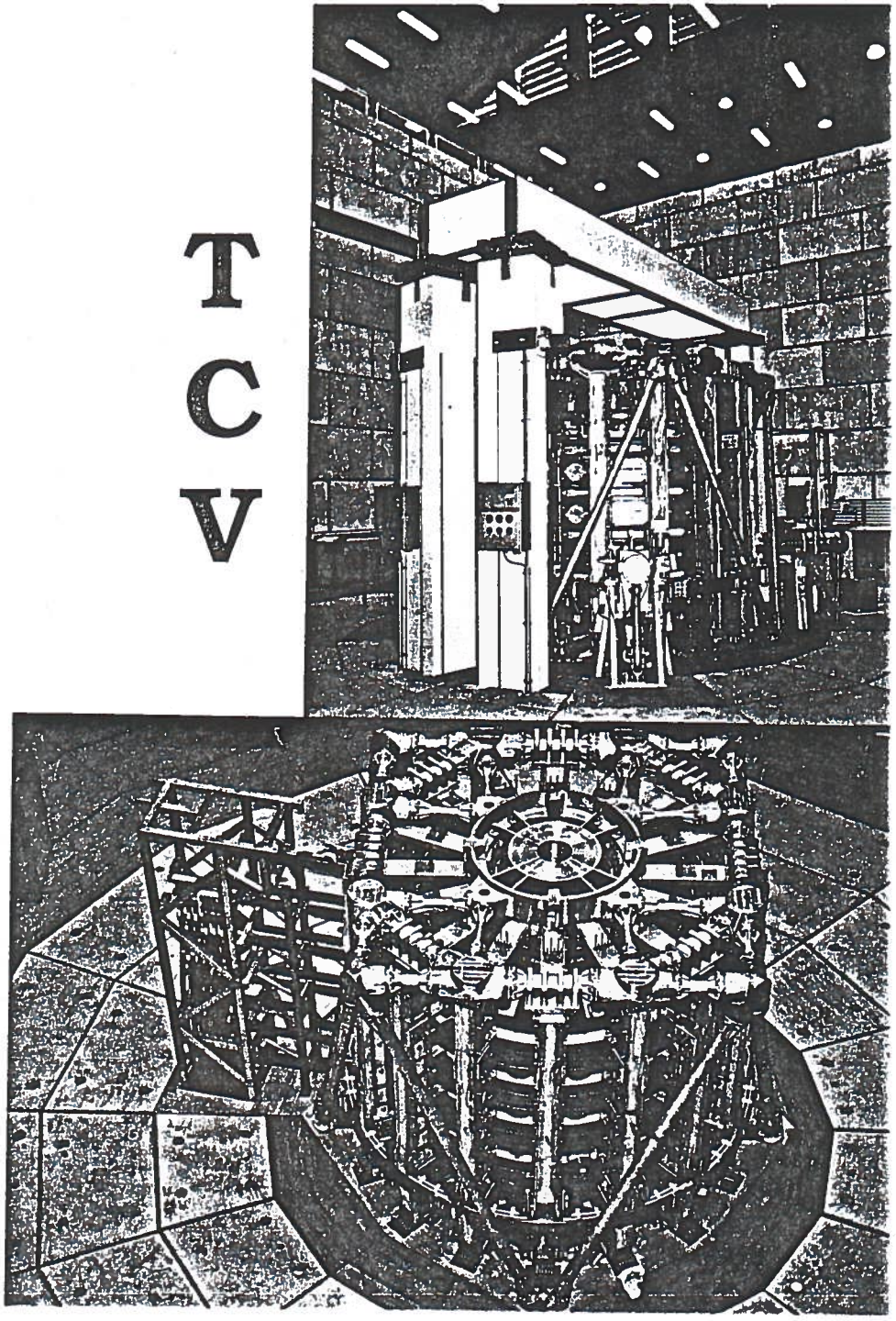

Single Null Configuration with Ion Drift Direction towards the X-point (favourable)

- There is a clear **DENSITY** threshold for transition to H-mode
- There is little effect on this threshold with plasma current
- Toroidal field of 1.4T and 1T showed same density threshold for same q

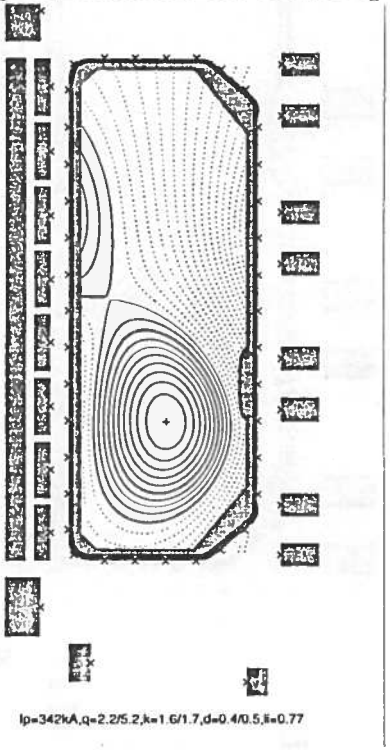

Reconstruction of the SND-U plasma configuration

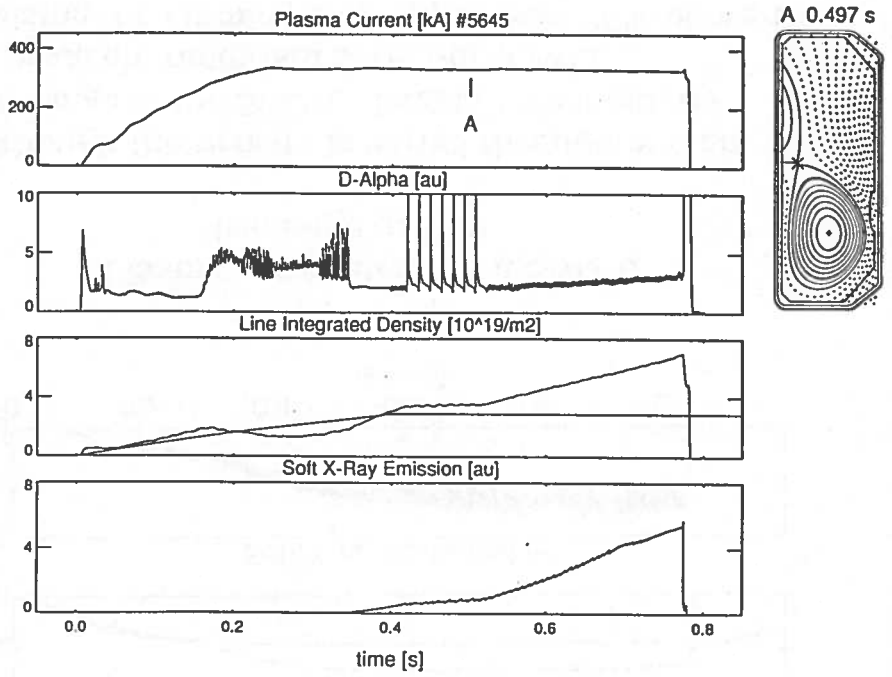

Plasma parameters for a "Typical" SND-U discharge in TCV

- An initial ELM-free period is followed by several large ELMs and "grassy" ELMs.
- The density rise is virtually halted during the large ELMs and appears less strong during the grassy ELMs
- The discharge terminates in a high density disruption.

Single Null Configuration with Ion Drift Direction away from the X-point (unfavourable)

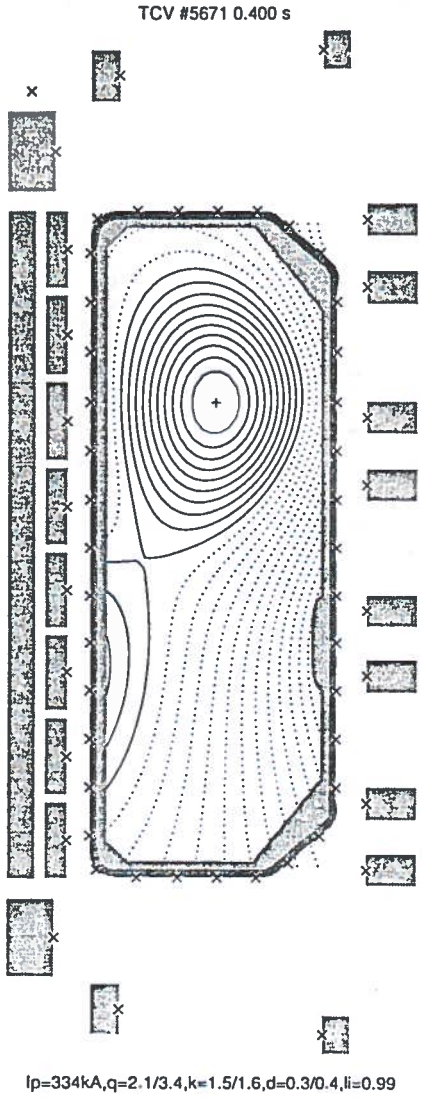

Reconstruction of the SND-L plasma configuration

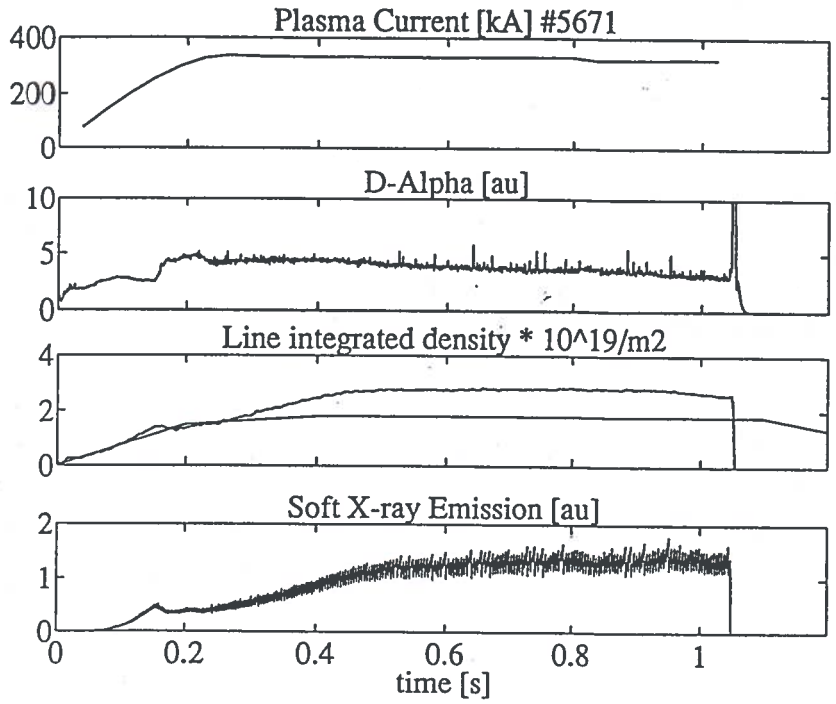

Plasma parameters for a SND-L discharge in TCV

- Although the density is varied through and above the range of the SND-U density threshold, no H-mode characteristics were observed.
- Raising the Ohmic power input over 30% above the threshold required for the SND-U configuration did not result in an H-mode transition

Power Threshold for H-mode Transition

- Following the ASDEX scaling proposition the plasma parameters at the first L-H mode transition are plotted with the surface normalised input power as a function of the product $n_e B$.
- The transition parameters are shown for most the configurations in this poster by selecting discharges in which the density threshold was the most representative and with the lowest threshold power.
- A Current scan was performed for the SND-U configuration to determine the power threshold. Although discharges at Ip = 240kA (b) passed easily into H-mode, a very similar discharges with Ip = 210kA showed no H-mode, despite an extensive density scan.
- Since all the discharges in this presentation were performed with the same magnetic field (1.4T) this scaling has not been investigated as a function of toroidal field.
- Although several TCV discharges had H-mode parameters slightly lower than the ASDEX scaling, the TCV data is consistent

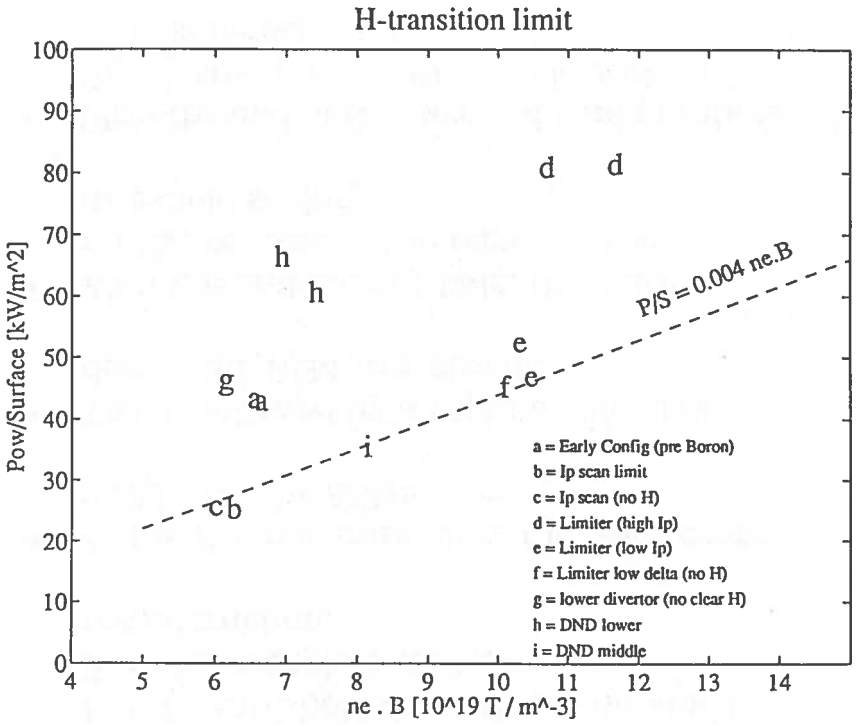

Locus of the Threshold Parameters Through a Discharge

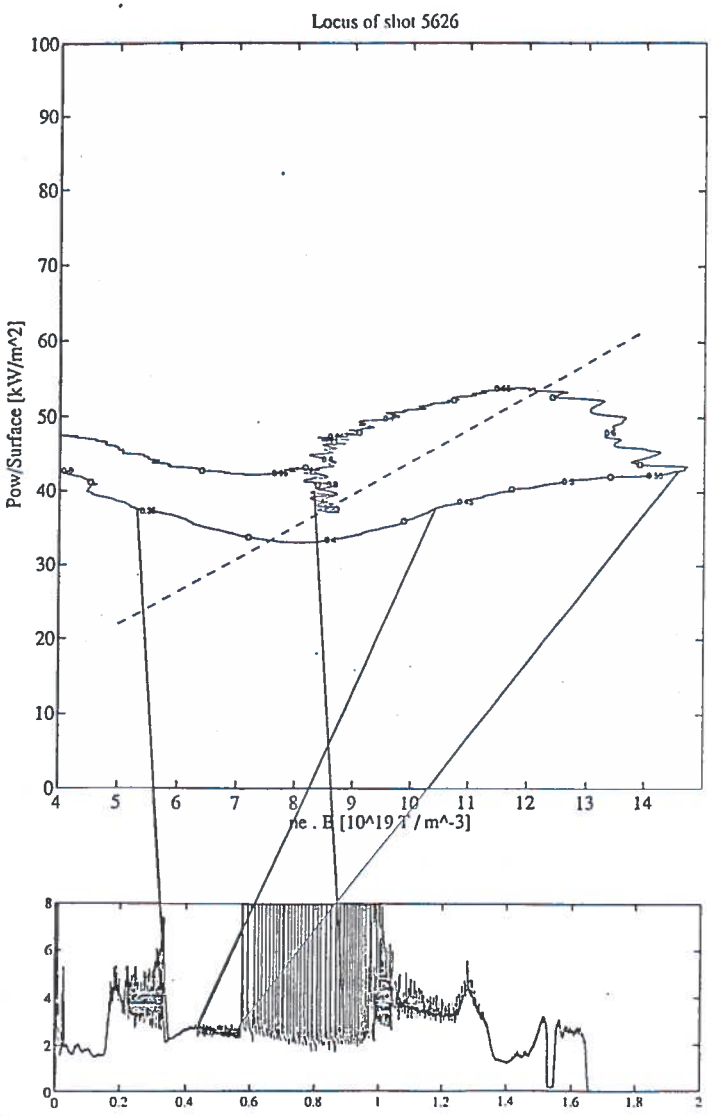

Locus of the threshold plasma parameters
through a SND-U discharge

- Since the plasma current is constant during the discharge, the Y-axis is proportional to the Surface Loop voltage. For the threshold data, this is obtained from the complete configuration reconstruction.
- At the H-mode transition, the trace drops well below the ASDEX scaling.
- This is followed by a rapid density rise during the ELM-free period.
- With the first Large ELMs, the trace rapidly returns to the region of the threshold scaling.
- With the end of the diverted configuration, the plasma returns to L-mode and the plasma density falls.

Density Limit in Long ELM-free Discharge

- The locus of a high density ELM-free discharge shows that the loop voltage rises as the plasma density increases
- It is interesting to note that this example, which is typical of most of the high density SND TCV discharges increasingly diverges from the ASDEX scaling.

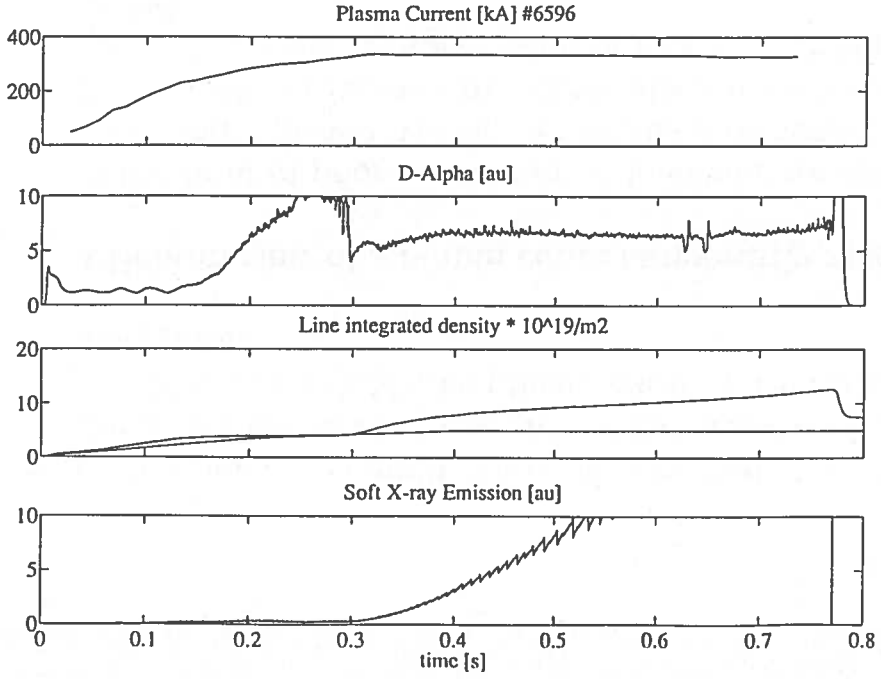

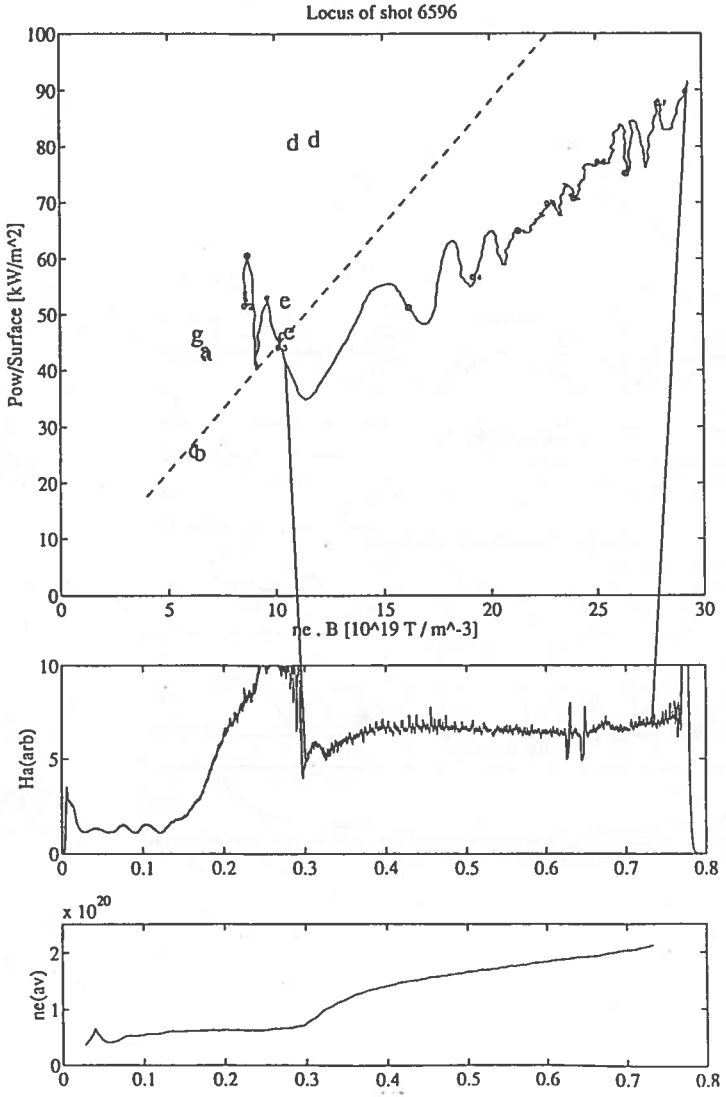

Locus of the threshold plasma parameters through a long ELM-free SND-U discharge

Effect of Vessel Conditioning

- As the machine conditioning deteriorated (100 x discharges), the ELMy phases became rarer. This increased the likelihood of a prolonged ELM-free phase resulting in a high density disruption.
- A Helium glow of > 30min could temporarily recover the ELMs
- In the limit of poor conditioning, following an extended operational period without a boronisation where a Helium glow could not recover the ELMs discharges were observed in which there were a succession of ELM-free and L-mode periods.
- Impurity analysis implies that the H-modes were curtailed by an increase in the radiated power from the accumulating impurities.
- The observation of ELM-free phases when the impurity content was known to be higher shows that large ELMs are favoured by "clean" plasma conditions

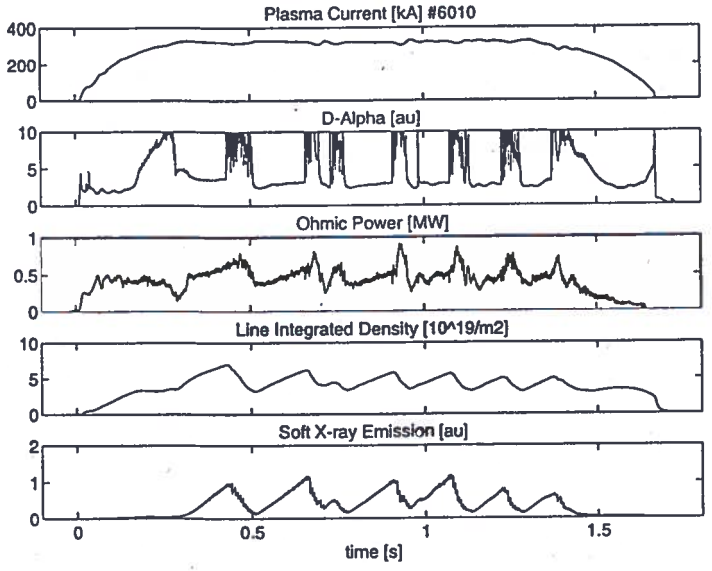

Long H-mode Discharge with Continuous Spontaneous ELMs

- Following a fresh boronisation and a Helium glow the probability of spontaneous ELMs is maximised.
- This resulted in a SND-U discharge with a 1.3 sec duration H-mode in a 2 sec discharge.
- The density and impurity accumulation remain bounded throughout the H-mode phase by the continuous presence of spontaneous ELMs.

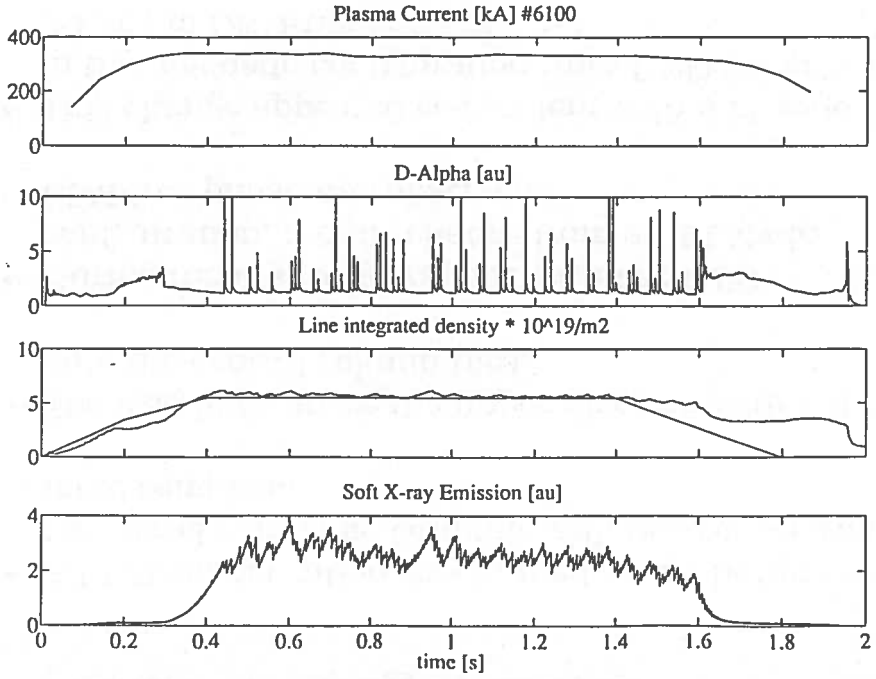

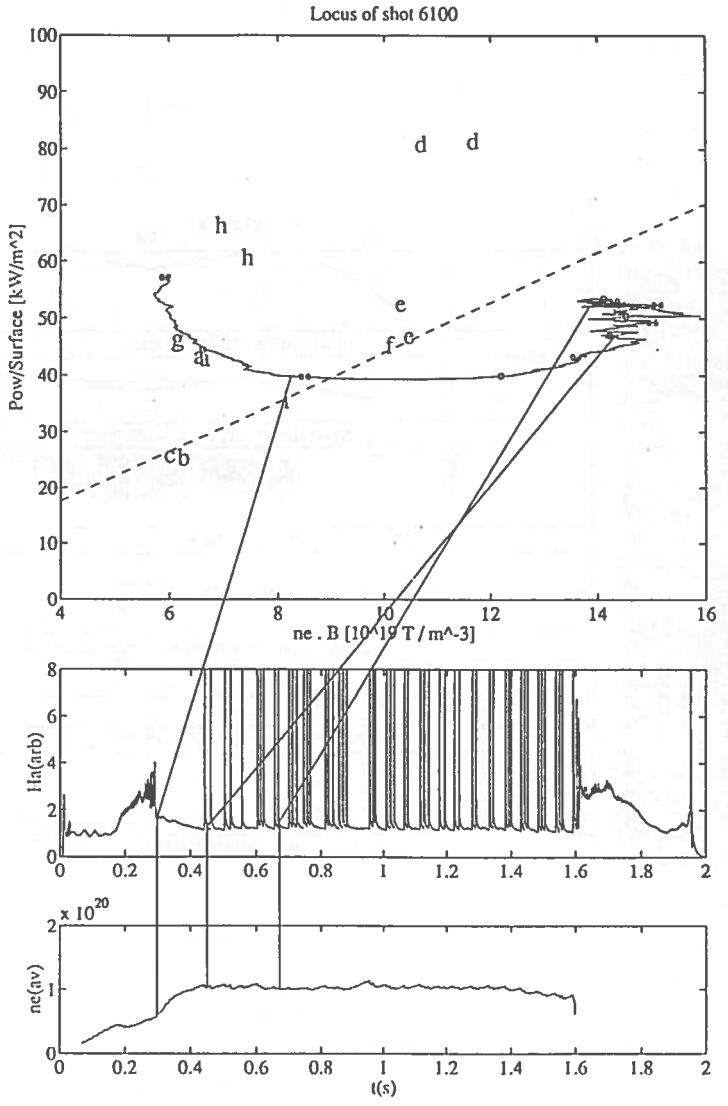

DND configuration

- A DND configuration was formed in the bottom of the vessel where the Graphite wall protection was more complete.
- The field lines above the upper divertor were put onto the central column tiles.
- During the first observations with the DND configuration, a clear change from an ELMy to ELM-free phase was observed.
- This change appeared co-incident with a change in the magnetic configuration from DND-lower (ELMy) to DND-upper (ELM-free).
- This change, was initially achieved with a modification of the magnetic field in the region of the lower X-point.

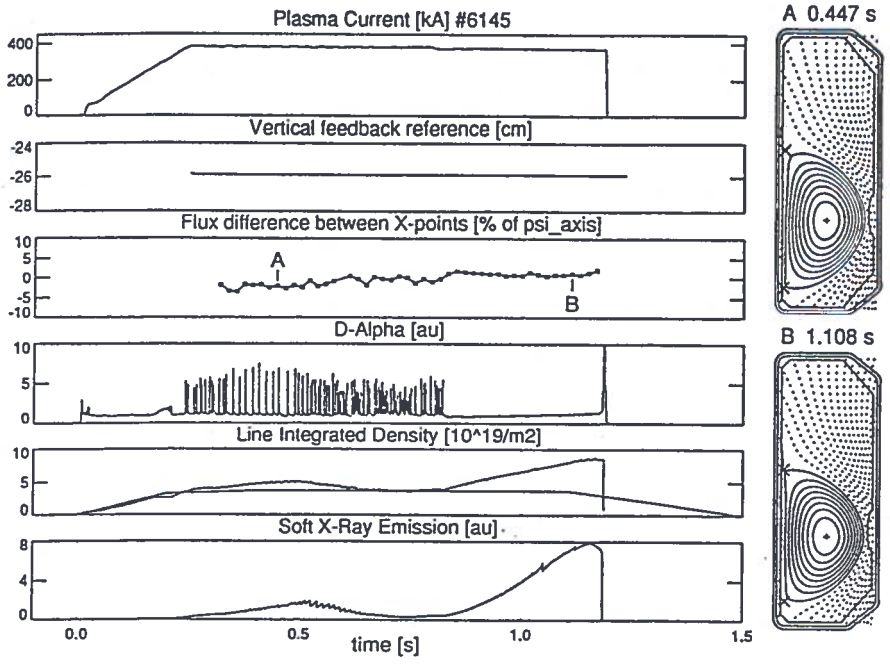

- In this configuration, there is often only one X-point defining the last closed flux surface.
- The power threshold for H-mode being somewhat higher than the ASDEX scaling, this configuration is more sensitive to the machine conditioning

DND X-point Toggling

- In the DND configuration, the X-point on the last closed flux surface can be toggled by changing the vertical position.
- In TCV this can be achieved by pre-programming a square wave perturbation into the vertical feedback reference.
- Since an ELMy period causes the plasma density fall, a reference plasma density was programmed which acts on the gas valve.
- The most striking feature in the resulting discharge is the synchronisation of the ELM-free and ELMy phases with the imposed modulation
- During the ELMy phases, the gas valve opened to limit the density drop
- The impurity accumulation during the ELM-free phase is removed during the ELMy phase.
- The plasma density and plasma impurity content remained bounded throughout the 1.5sec H-mode phase.

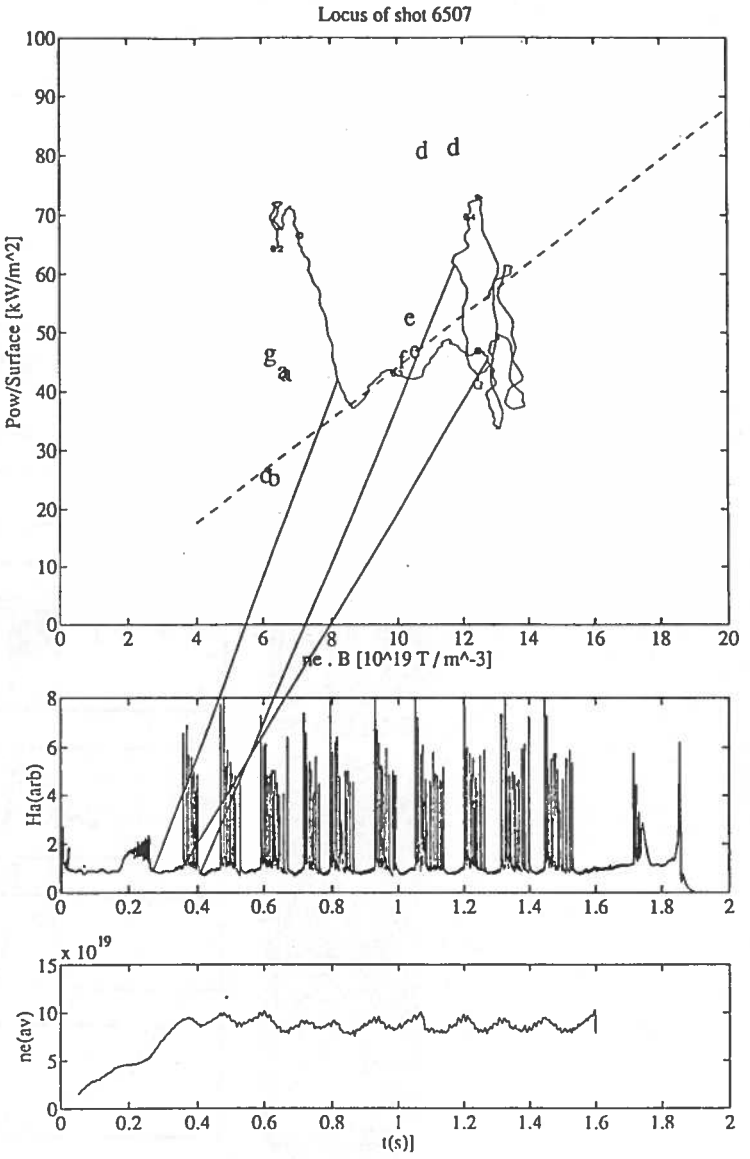

Evolution of the pre-programmed DND X-point toggling

Pre-Programmed X-point Toggling

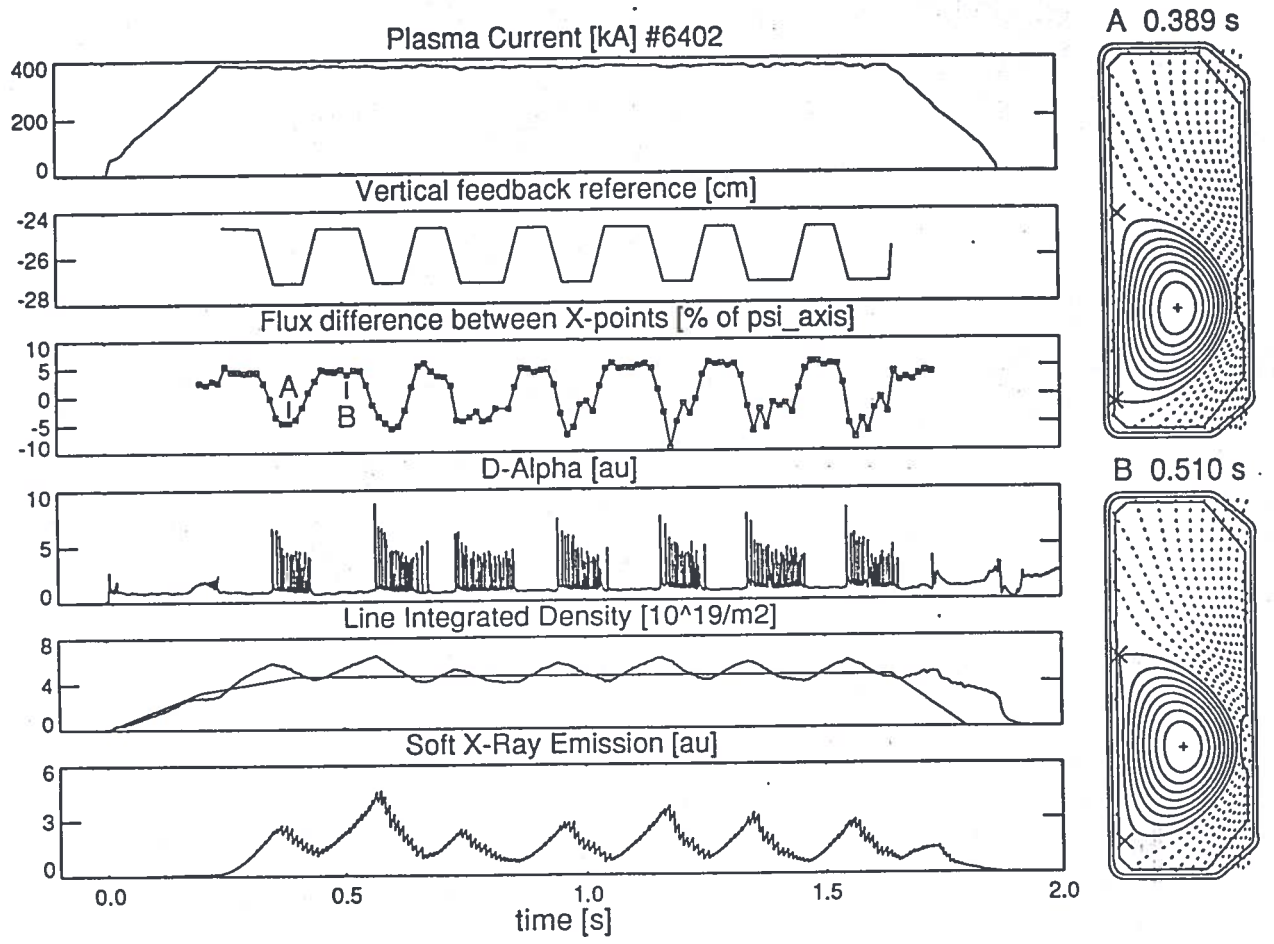

Second DND Configuration with X-point Toggling

- A centred symmetric DND configuration with:
  - ◊ lower plasma current (250kA)
  - ◊ lower elongation
  - ◊ greater distance from separatrix to vessel

- Despite all these differences, X-point toggling displays the same essential characteristics showing that this technique is not specific to a particular configuration

LIUQE Equilibrium Reconstruction SHOT: 6315 triang_6

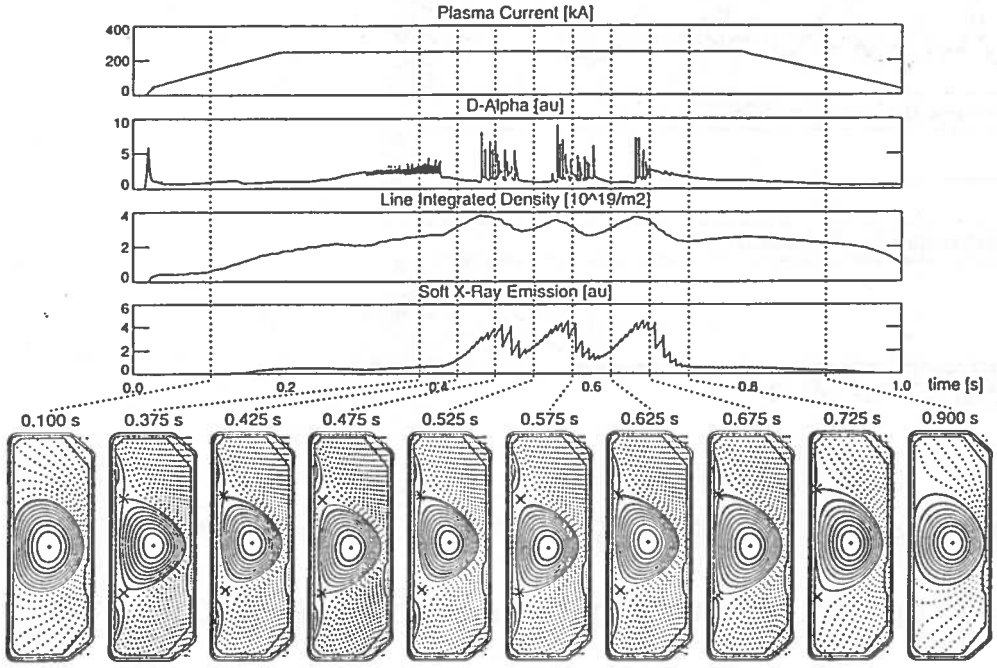

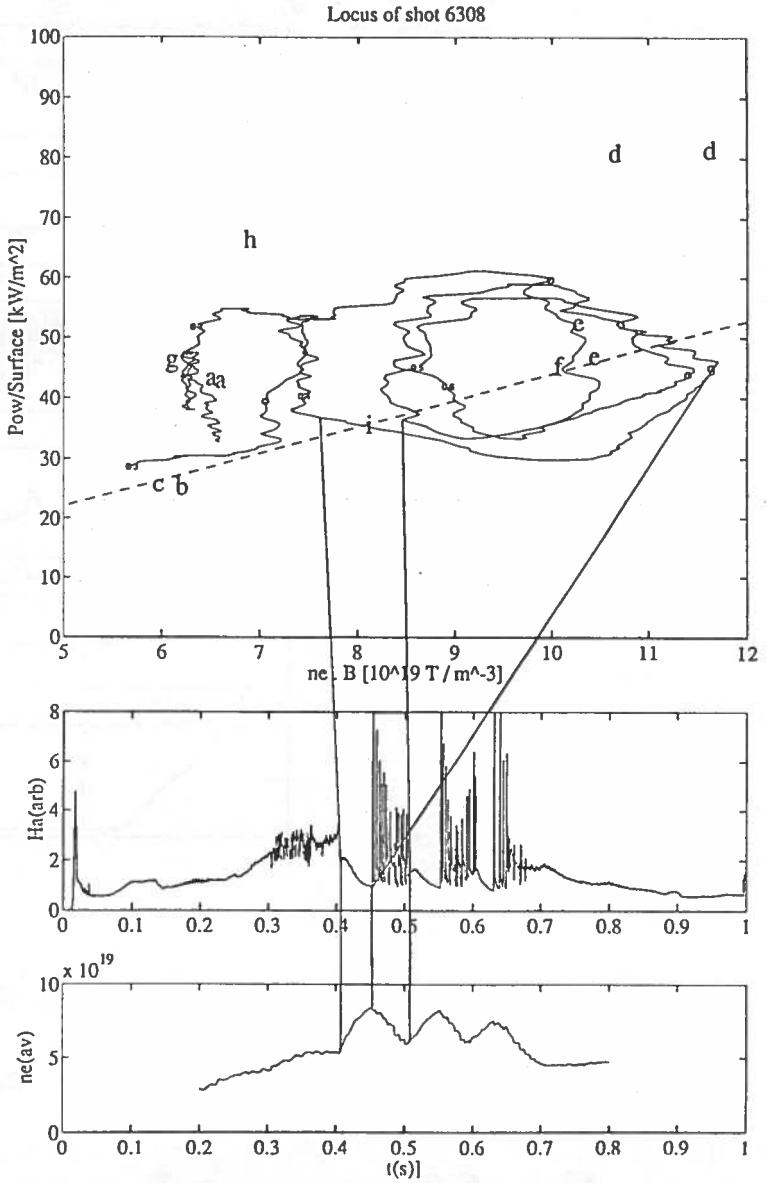

Plasma Density Control Feedback via X-point Toggling

- During the plasma current flat-top, the gas valve opening is fixed
- The error between the measured and reference plasma density is directly fed back to the vertical position

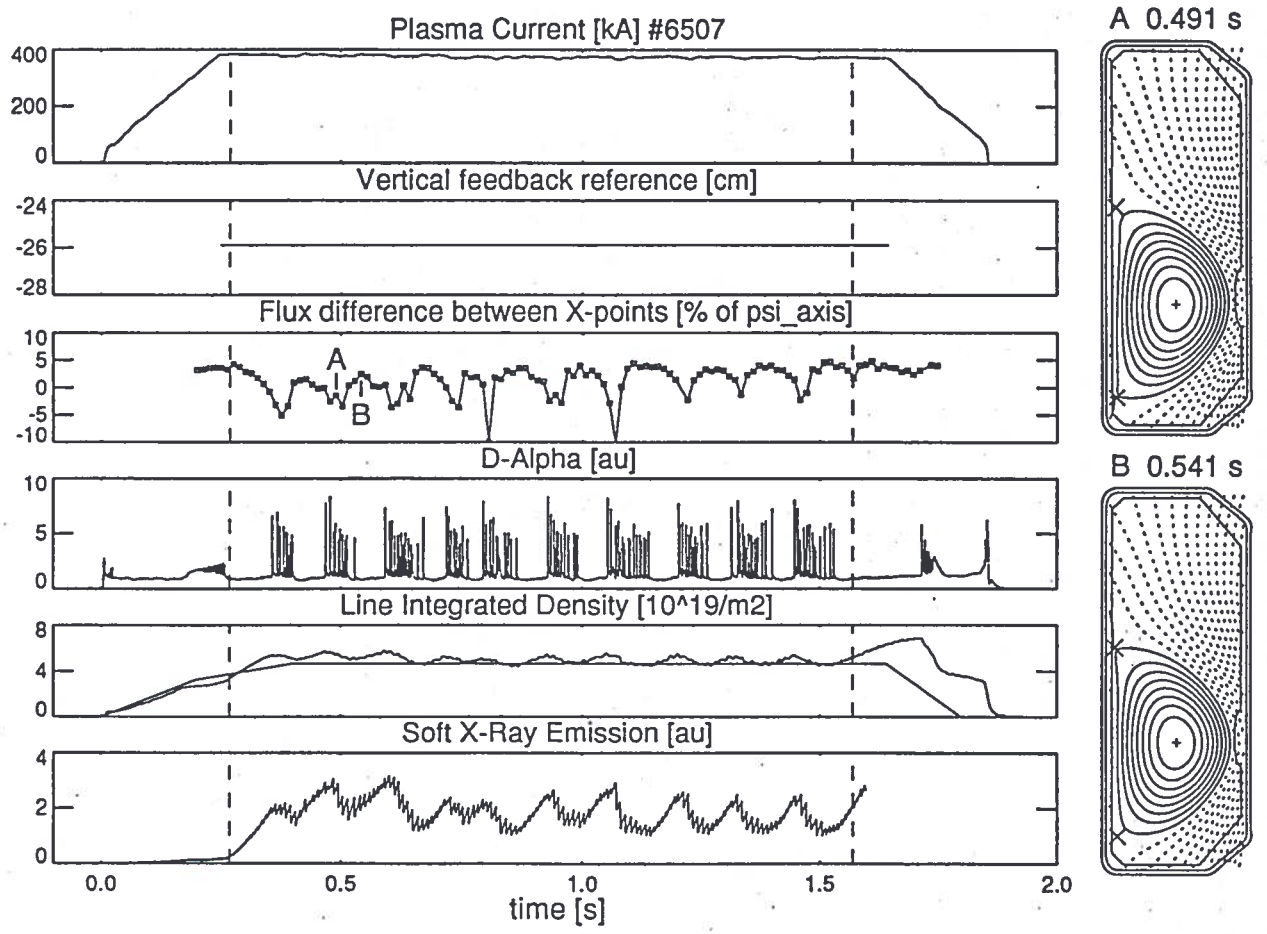

L -modes During DND-L

- During some of the ELMy periods, the discharge appeared to momentarily return to L-mode. During this period, a reasonably large Sawtooth crash was sufficient to cause a momentary return to H-mode, returning to L-mode with the Da and MHD signature of an ELM.

- Although several of these H-L-H transitions were observed during some of the ELMy phases, switching to the DND-U configuration resulted in a new ELM-free period.

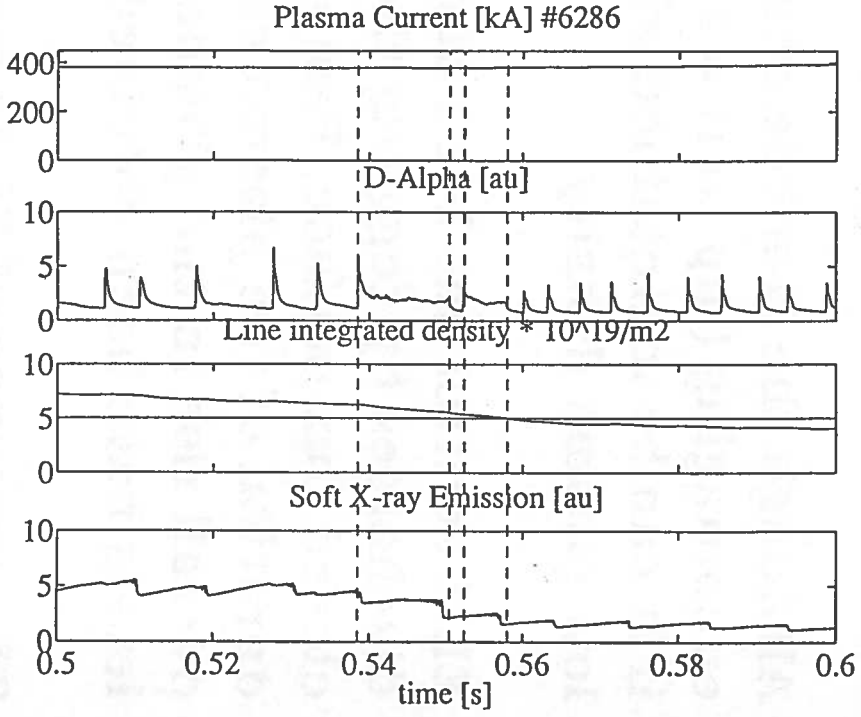

Thomson Scattering Te Profiles

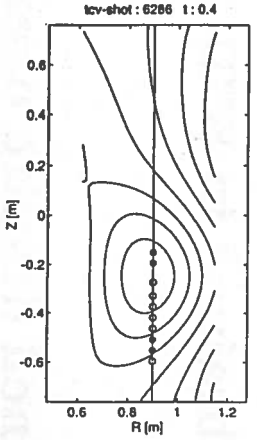

Viewing chords as a function of PSI

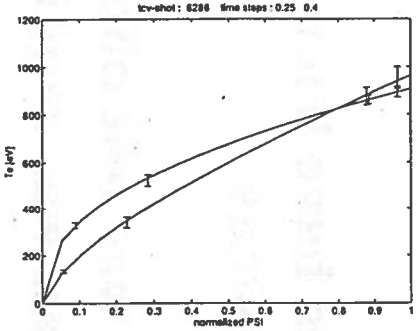

Profile change for initial L-H transition

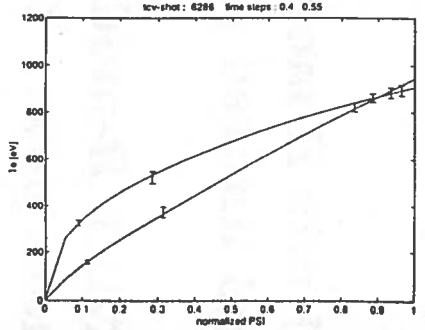

Profile change for short L-mode during DND-L

Conclusions

Ohmic H-modes have been obtained in SND, DND and limited plasmas.

SND-L H-mode was not obtained despite over 30% more power than was required for SND-U.

The thresholds for transition to H-mode do not disagree with the ASDEX scaling.

The effect of large ELMs is to return the locus of the plasma parameters in threshold space to the scaling value.

Although the H-mode confinement improvement is encouraging (up to H = 2.4), it remains to be seen if it can be maintained with ECRH and the implied low plasma density.

ELM control has been demonstrated in DND discharges by toggling the X-point on the last closed flux surface. H-modes lasting the full duration of the plasma current flat-top without an overall rise in the plasma density and impurity levels have been obtained.

The presence of ELMs has been used to control the plasma density in a feedback loop by coupling the X-point toggling with the difference between the measured plasma density and the reference signal.

MHD ACTIVITY IN OHMIC H-MODE PLASMAS IN TCV

H. Weisen, A. Hirt, A. Pochelon, M. Anton, Ch. Nieswand, R. Behn, M. Dutch, B.P. Duval, S. Franke, B. Joye, F. Hofmann, J.B. Lister, X. Llobet, Y. Martin, W. van Toledo and G. Tonetti

Centre de Recherches en Physique des Plasmas
Association Euratom-Confédération Suisse
Ecole Polytechnique Fédérale de Lausanne
CH-1015 LAUSANNE
Switzerland

Summary

- MHD activity in diverted Single-Null, Double-Null and limited H-modes studied.

- Dithering phase: Magnetic precursor activity to D_α pulses.

- H-L transition: Drop of broadband turbulence on all magnetic probes with exceptions at divertor legs.
  Reduction of amplitude of Mirnov oscillations.
  Flattening of density profile.

- ELM-free H-modes:
  Increase of density and impurity concentration.
  Step-wise increase of edge X-ray emission with heat pulses released by sawtooth collapses indicates existence of edge confinement barrier.
  Long ELM-free H-modes ($\geq$ 0.3 s) lead to central radiation collapse or high density H-L transition with subsequent disruption near Greenwald density limit.
  Unidentified mode with frequency above Mirnov frequency ($\geq$ 15 kHz) during ELM-free H-mode.

- Two types of ELMs, hereafter referred to as 'large' and 'grassy' Elms:

- Large Elms briefly puncture edge confinement barrier, releasing particles (~5%) and energy.
  Strong n=0, m=1 component and n=1, m=2,3
  Edge confinement in Elmy H-modes dominated by discrete MHD events: supply by sawtooth collapses and depletion by Elms.

- Grassy Elms (probably unrelated to DIII-D grassies) are localized to the divertor region (Dilms?) and cause no reduction in particle or energy confinement.

X-ray cameras

- Two 20 channel prototype X-ray cameras viewing lower third of TCV vessel.
- Based on 20 diode arrays (diode size 1×4 mm).
- 50 μm thick Be windows (flat).
- Present bandwidth 5 kHz.
- TCV and camera vacuum are independent.
- Tomography possible only on a few rare occasions, most plasmas not being entirely in field of view.
- Tomography system to be implemented 1995 will have 200 channels in 10 cameras equipped with curved Be windows.

Other diagnostics

- 4 channel FIR interferometer with λ=215 μm.
- Set of visible light diodes for D_α and impurity lines.
- 4 vertically viewing X-ray diodes with 50, 100, 250, 650 μm Be filters for T_e estimates.
- Estimate of impurity level using absolute signal from diode with 50 μm Be, X-ray temperature, line density from FIR interferometer, assuming carbon as the only impurity and fixed profile shapes.

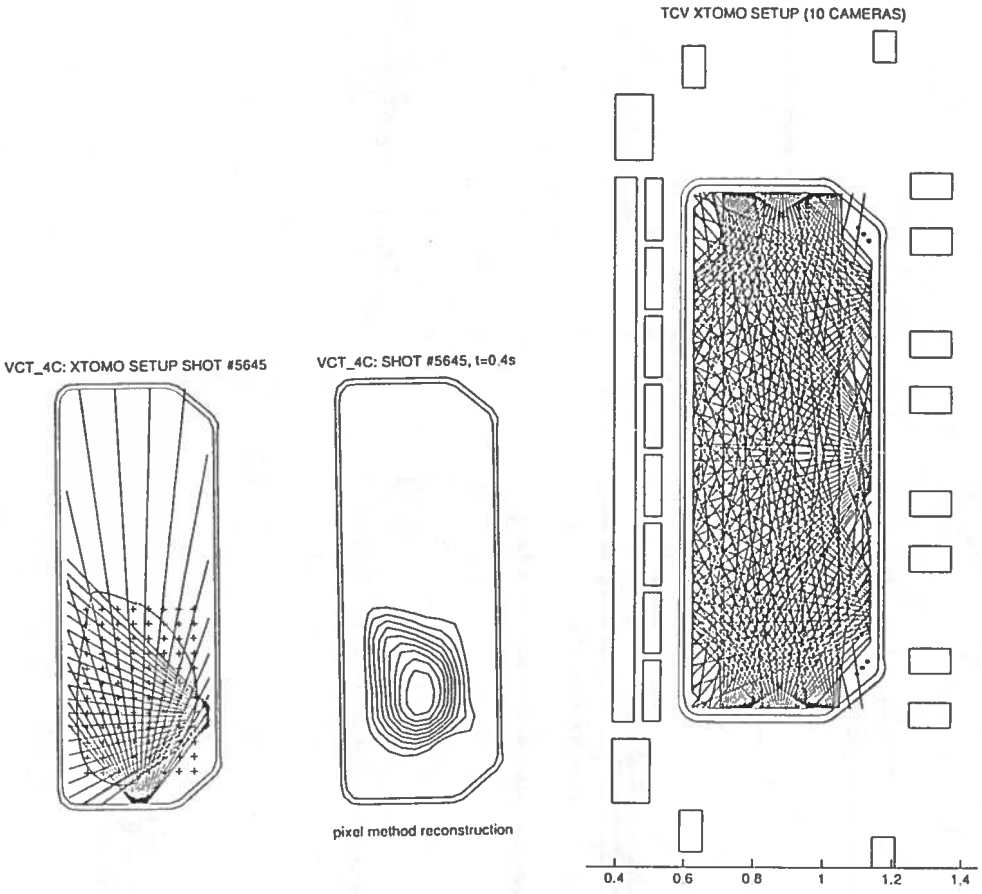

TCV X-ray cameras

Above: 1994 setup with Single-Null plasma. Right: 1995 setup.

Magnetic turbulence localisation

The spatial repartition of turbulence apparently depends on two main factors:

- the currents circulating in the SOL.
- the plasma configuration.

Plots A and B on the right side of this page show that, in some cases, **turbulence seems to be produced locally**, near the divertor legs. This turbulence is attributed to currents circulating in the SOL and does not always decrease at the L-H transition time.

Plot C shows the drop in magnetic turbulence through the L-H transition for a limited ohmic H-mode shot. The **turbulence level is higher on the HFS** for a given plasma-probe distance.

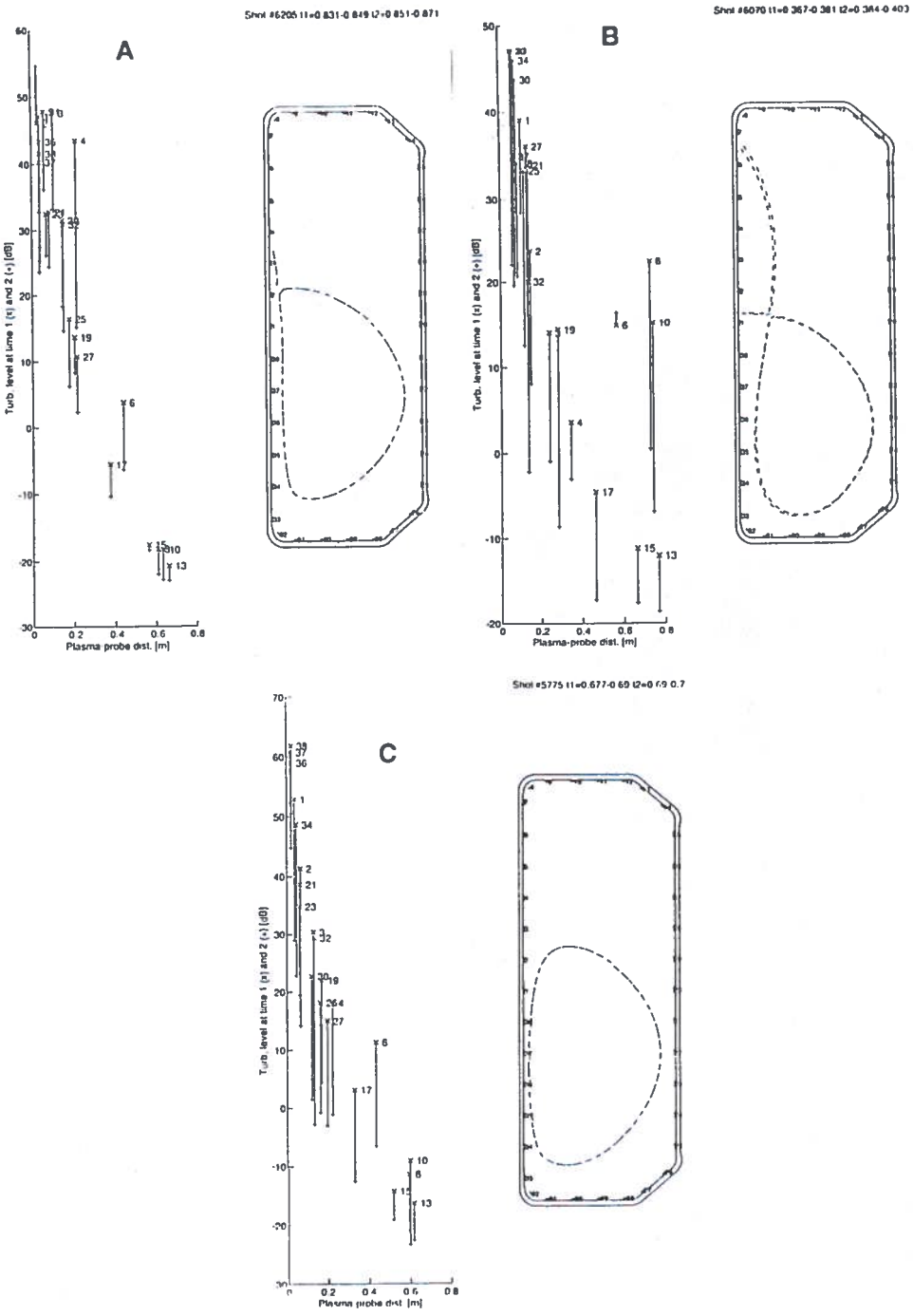

The three plots show the mean turbulence level [dB] before and after the L-H transition against the plasma-probe distance [m]. Plot A and B show probes in the divertor legs region showing a special behaviour: the turbulence level does not decrease at the transition time, it even increases (colored red on the plots).

Dithering phase

When the conditions required for the transition are only marginal, the plasma oscillates between L and H-mode. On TCV, this dithering phase is characterised by repeated (f= 1-3 kHz) peaks in the D_α intensity. A burst of turbulent magnetic activity is detected during the D_α intensity rise, preceded by a growing **coherent magnetic precursor (f=50-60 kHz) starting typically 0.3 ms before the burst.**

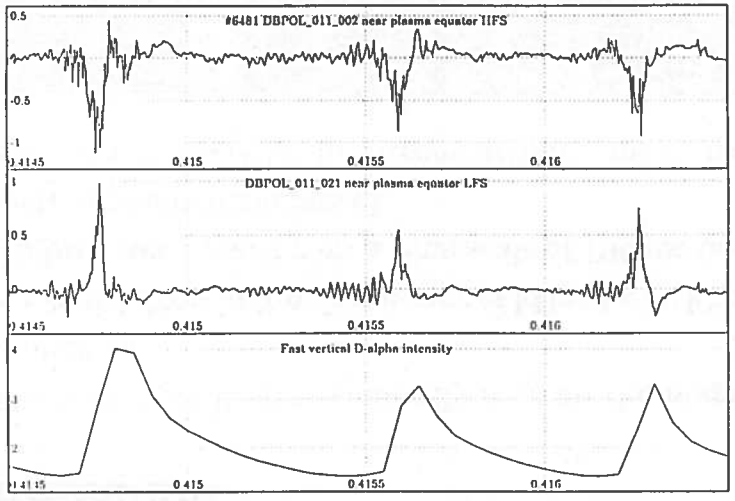

Magnetic precursors to D_α pulses during the dithering phase. Note that they are visible on the LFS as well as on the HFS.

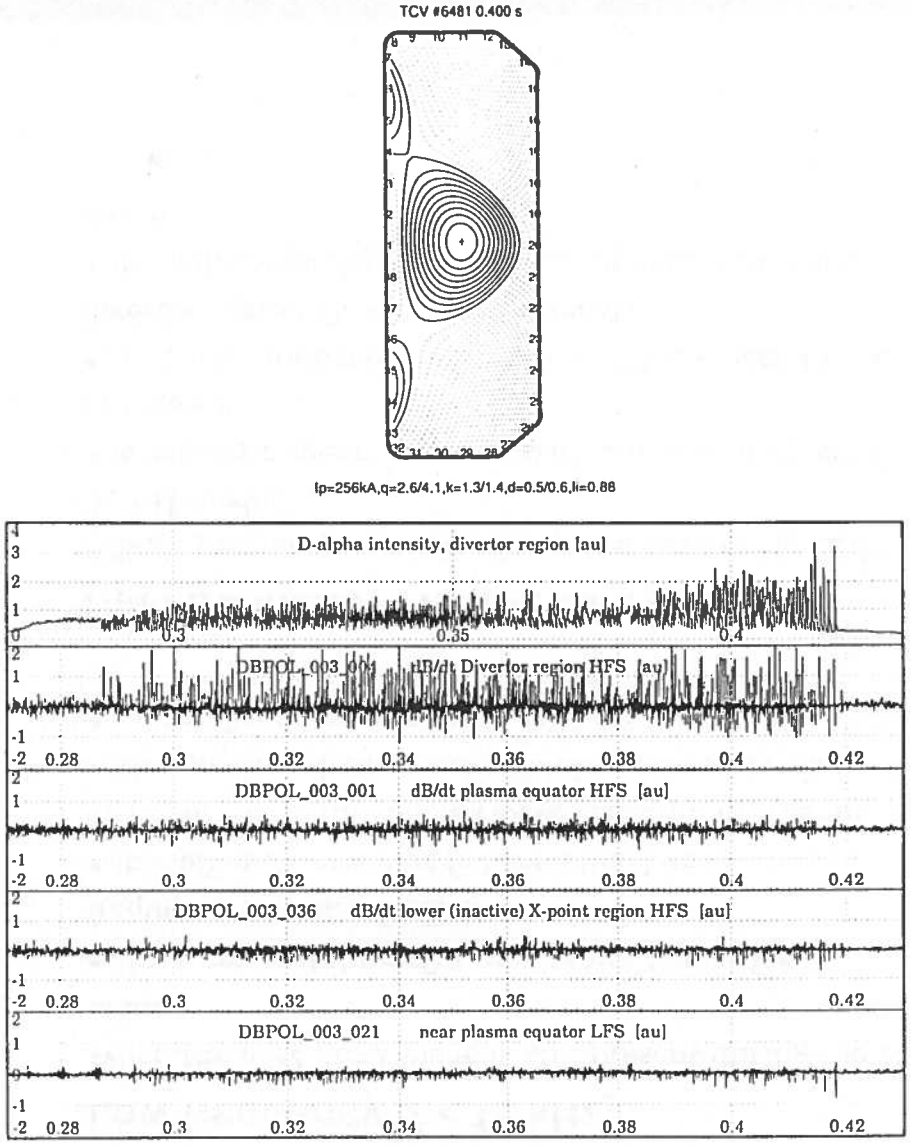

Typical dithering phase on TCV. The plasma configuration is shown on the upper part of the page. Note that the magnetic activity is more intense in the divertor region. The density (not shown here) behaves as during the L-mode.

Magnetic activity at the L-H transition

The L-H transition is generally seen on the magnetic probes as:

- a **20 dB drop in low frequency (4 kHz< f < 30 kHz) turbulence** occuring on a time scale of **100** μs. (see also section about turbulence).
- a marked decrease in Mirnov activity (m≥2 , n=1).

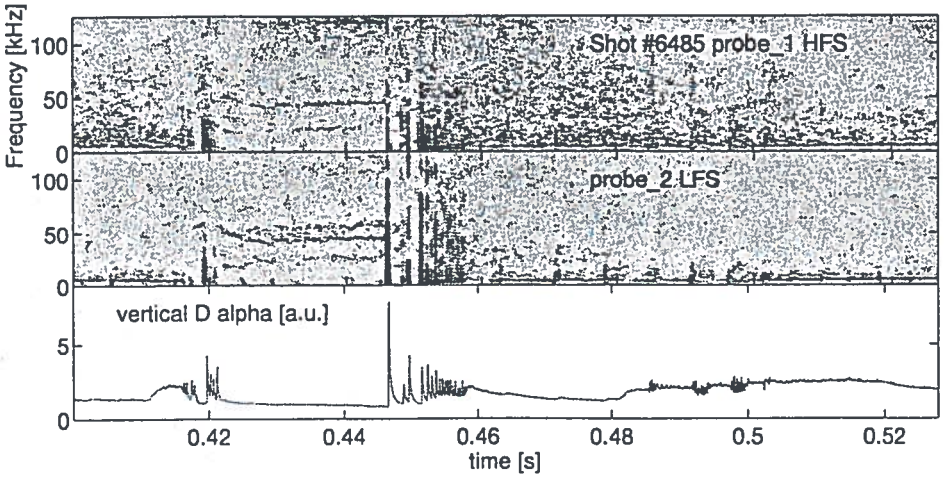

The two spectrograms show the numerous changes occuring at the transition time in MHD activity. The fact that the LFS probe is further away from the plasma than the HFS one should be taken into consideration. (The signals are normalized. In the spectrograms: Red=high intensity, Blue=low intensity).

Coherent magnetic activity during H-mode

Low frequency (f < 15 kHz)

When the m≥2 , n=1 mode is still present during the H-mode:

- it approximately maintains its pre-transition frequency (usually 5 kHz).
- it is often observed as fishbone-like bursts synchronised with the sawtooth crash and coherent with a m=1, n=1 oscillation visible on X-ray profiles.
- its amplitude is greater on the LFS than on the HFS.

High frequency (15 kHz < f < 40 kHz)

A high frequency mode is often observed during ELM free H-mode.

- it usually appears together with a double frequency harmonic.
- it occurs simultaneously with a 10% increase in the divertor region D_α emission intensity.
- its high frequency prevented us to determine the m and n.

ELM types

Large ELMs

Large ELMs appear on the magnetic probes as strong bursts of MHD activity (~100 μs duration). They are characterised by a broad frequency spectrum (at least up to 125 kHz) together with some **spatial coherence**. The **dominant mode (m=1, n=0, usually a fast upward plasma displacement)** often occurs together with a **less intense m=2,3 n=1 mode.**

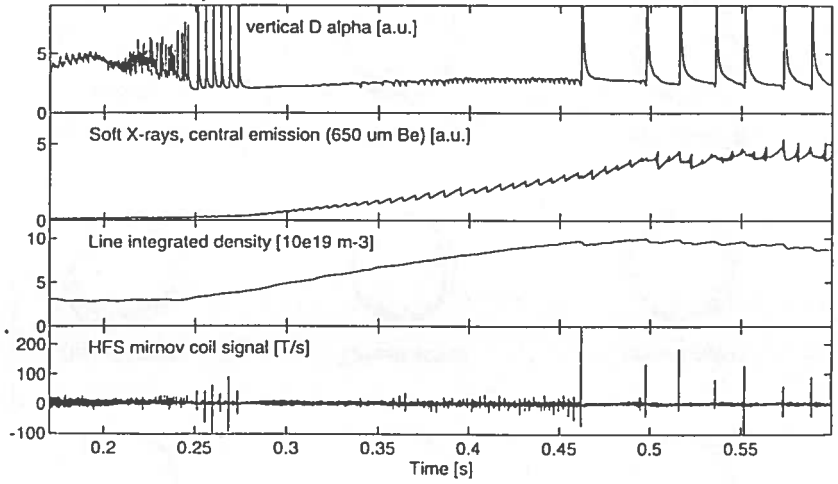

Typical experimental signals associated with the occurrence of grassy ELMs (t=0.35s-0.5s) and large ELMs (t=0.25-0.28s and from t=0.46s).

Grassy ELMs

Grassy ELMs are visible on the MHD diagnostic as repetitive bursts of activity located near the X-points.

- repetition frequency 300 Hz < f < 5 kHz
- tend to become stochastic at high density (typically $n_e > 10^{20}$ m^{-3})
- do not degrade energy confinement: they were present during the discharge showing the highest confinement time to date (see below).
- don't prevent the density rise typical of ELM-free H-mode.
- never appear immediately after the L-H transition, and have never been observed at a line averaged density lower than 4.9 10^{19} m^{-3}.

ELM m spatial structure

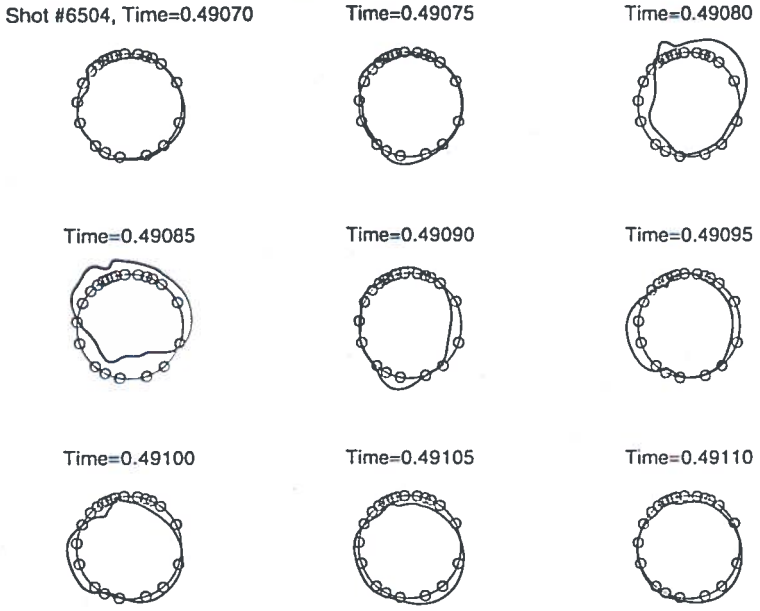

This plot shows the magnetic signals on all available magnetic probes during a giant ELM. They are normalized and displayed. The dominant m=1 component is clearly visible. The Dα maximum intensity is at t=0.4909 s.

Large ELMs type

The large ELMs on TCV may be identical to type III ELMs seen elsewhere. This conjecture will have to be confirmed when additional heating will be available.

Energy confinement with grassy ELMs

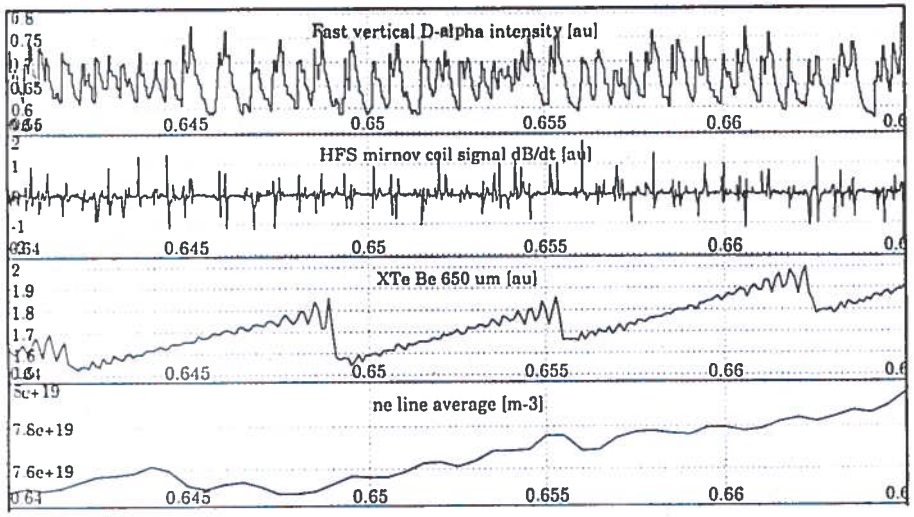

These typical grassy ELMs don't prevent the density rise. The confinement time is one of the highest ones observed to date in TCV. (τ_E=0.09s, shot #6143).

Grassy ELMs type

The grassy ELMs described in this poster have been named after the D_α intensity traces, which are 'grassy'. We do not pretend that they have anything in common with the grassy (type II) ELMs from DIII-D.

Large ELM precursors

Two precursor types have been observed:

- A turbulent precursor observed before most ELMs. It begins 0.5-1 ms before the rise of the D_α intensity.
- A coherent precursor observed before the first ELM after the dithering phase. It is similar to the dithering phase D_α peak precursors.

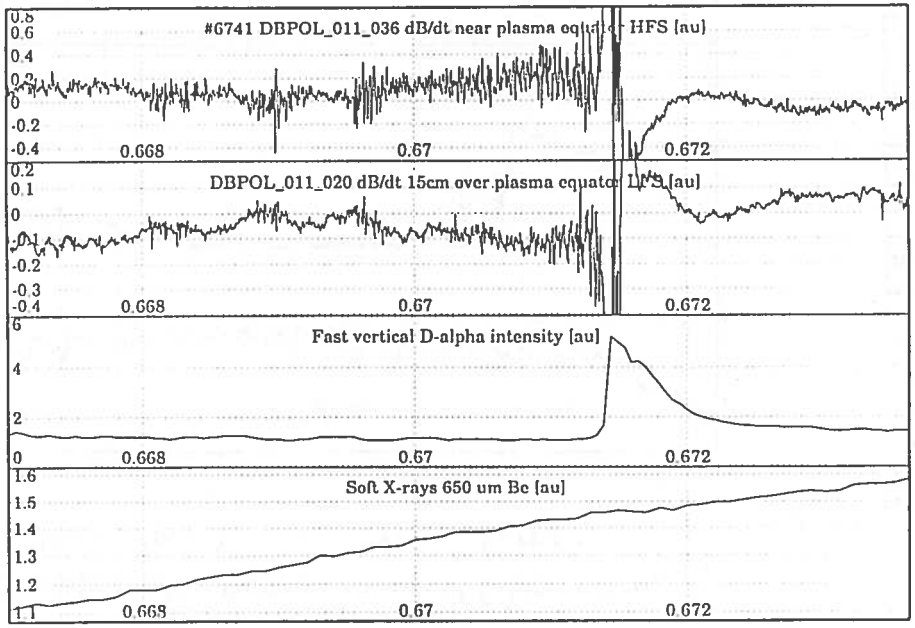

This is a typical Large ELM precursor (during a DND-L H-mode discharge). The HFS probe also shows the typical H-mode high-frequency activity, whereas the LFS probe only shows the ELM precursor (from t=0.67s).

Grassy ELM appearance

Grassy ELMs can appear:

- after a density increase during an ELM-free phase.
- after a plasma magnetic configuration modification

(for instance an active X-point switch, see B.P.Duval poster, this conference).

Localisation of grassy ELMs

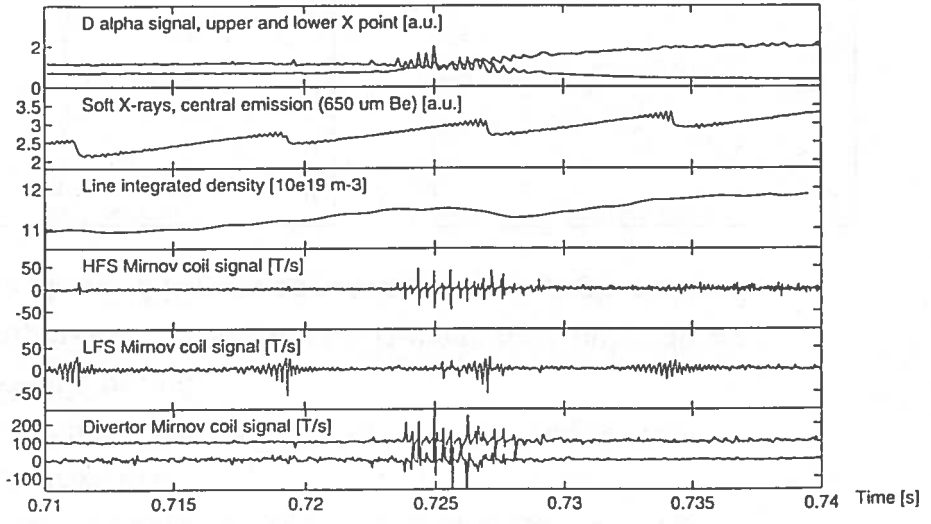

This plot shows that the grassy ELMs amplitude on the Dα and MHD diagnostic is largest near the X points. This group of grassy ELMs has been observed at the time of the active X-point switch. Note that the grassy ELMs are also more intense on the D_α light in the divertor region.

Edge confinement barrier

- Density profile flattens at the H-L transition, indicating creation of a particle barrier.

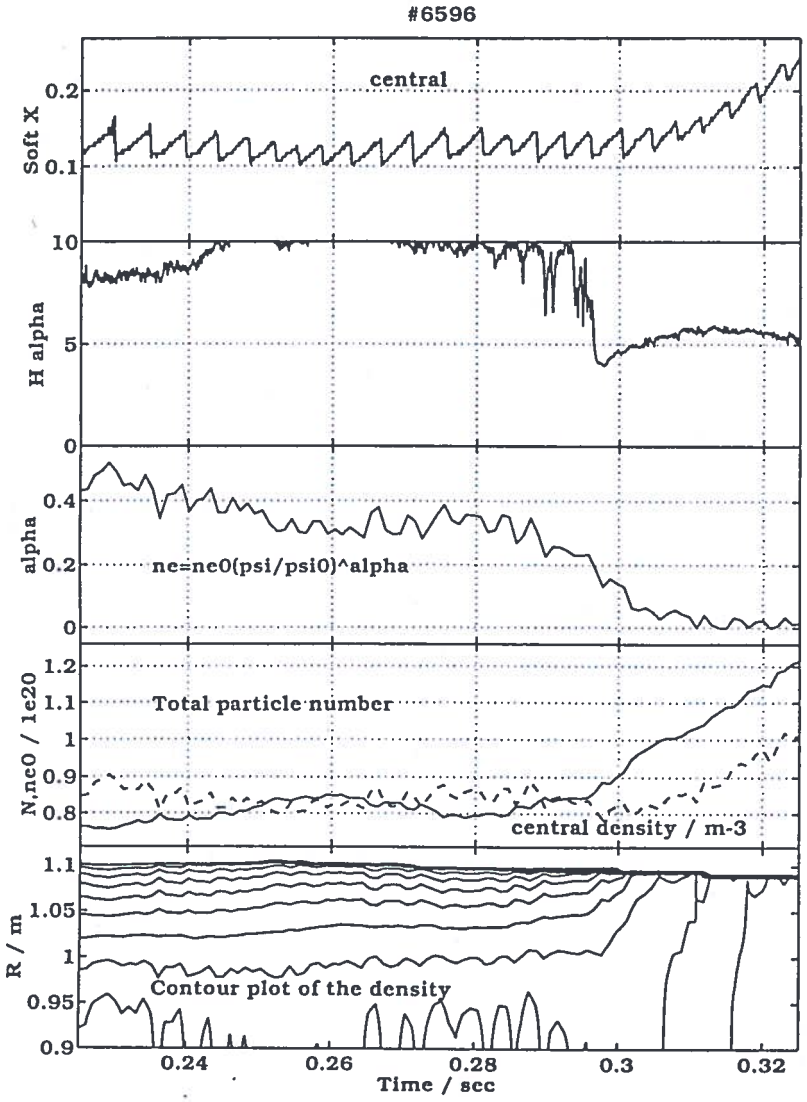

- During Elm-free H-mode transition heat pulses released by sawtooth collapses lead to step-wise increase in edge X-ray emission and (presumably) edge pressure.
- Heat pulse decay time becomes much longer than sawtooth period.
- Comparison of L-mode and H-mode heat-pulse decay time shows diffusive edge transport strongly reduced.

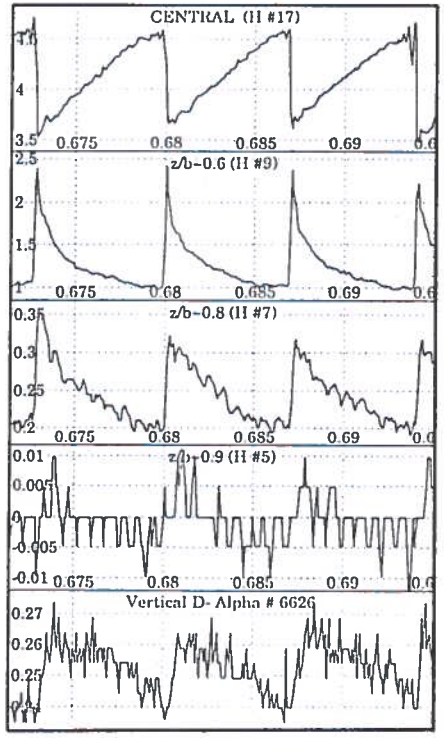

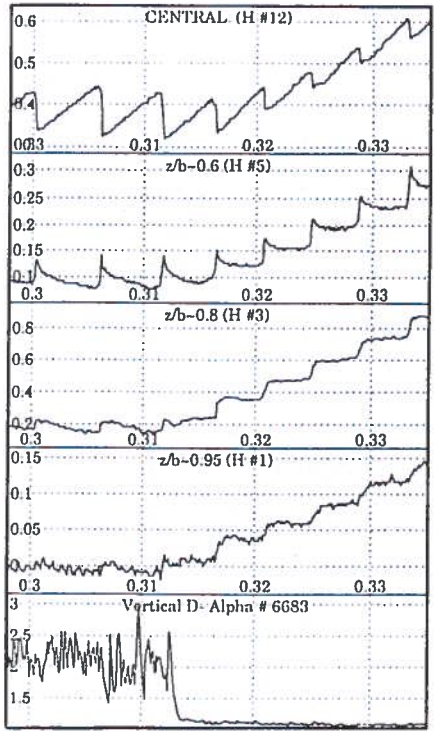

X-ray signals from horizontal system in Belt-limiter plasma (L-mode) and during L-H transition in SNU diverted plasma.

- In Elmy H-modes X-ray emission (and presumably pressure) near edge is mainly determined by a balance of macroscopic MHD events: Sawtooth collapses and Elms.

- Rise times (from heat pulses) and fall times (from Elms) observed are limited by diagnostic (0.1 ms).

- Confinement barrier restored within 1 ms after Elm.

Elmy H-mode --> ⇃

Single-Null Upper (SNU) configuration, 330 kA.

Top traces:	Central X-ray channel (vertical camera)
Middle:	Edge X-ray traces (r/a ~ 0.85)
Bottom:	D-α from vertical viewing line

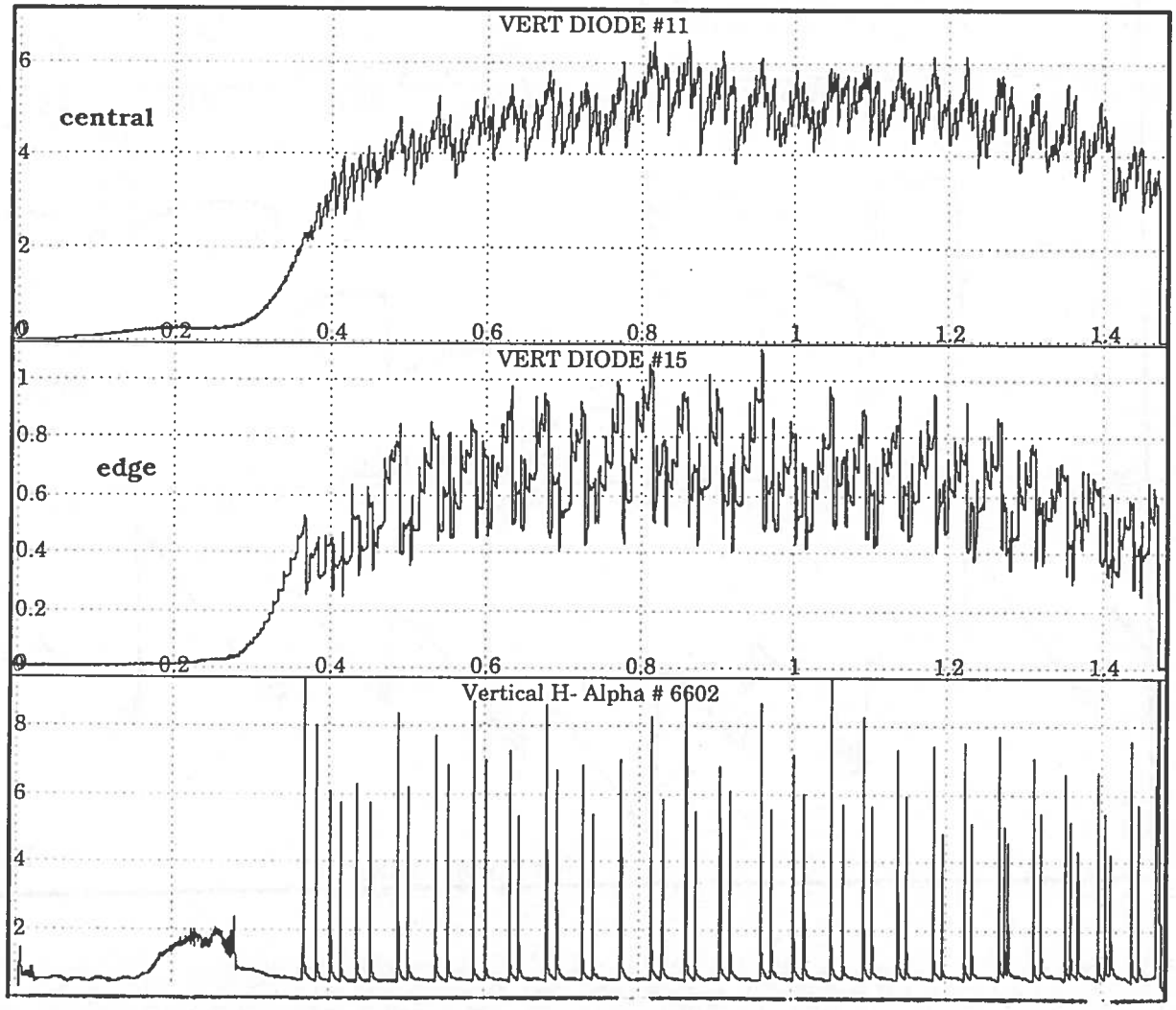

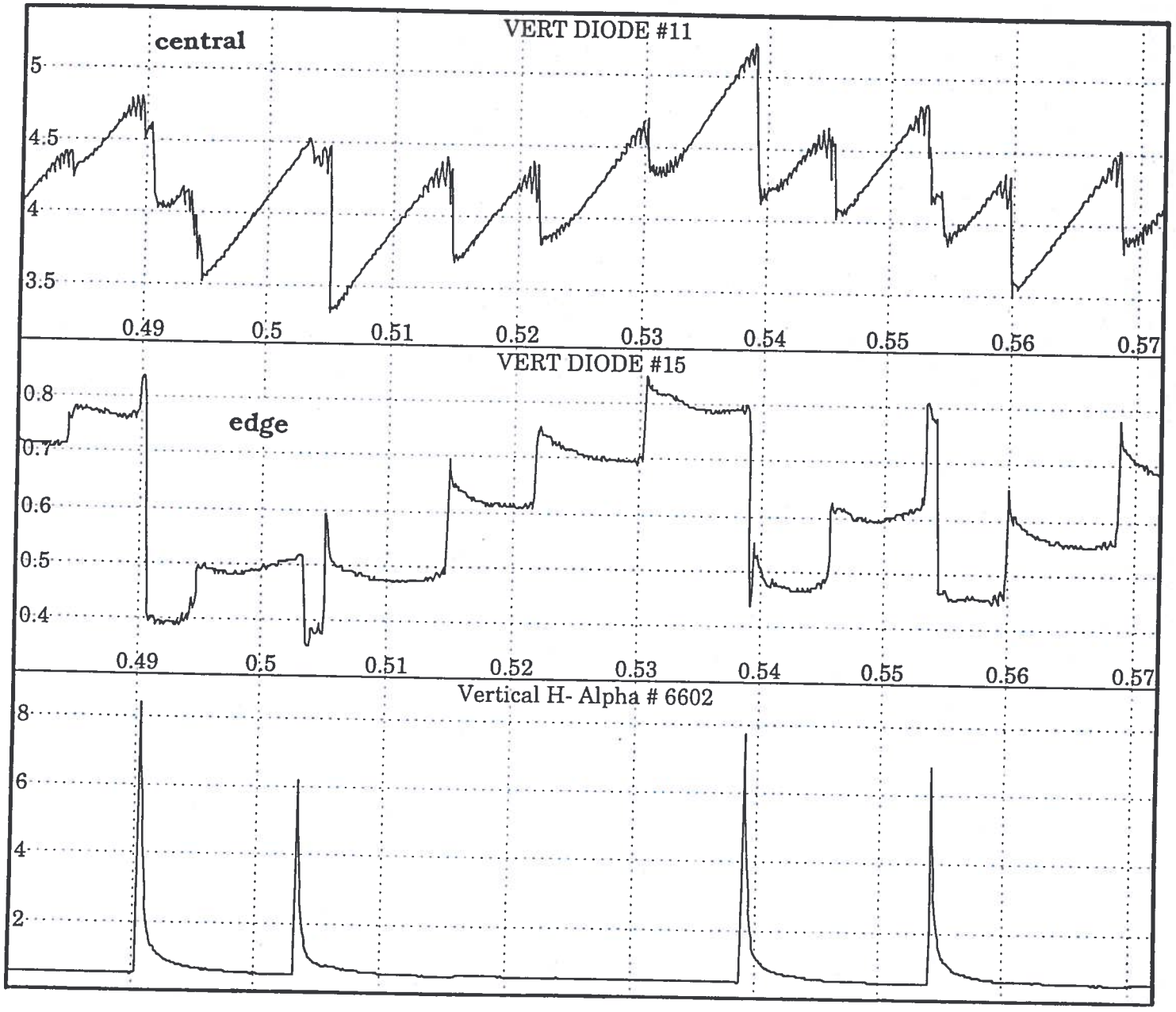
central
VERT DIODE #11
5
4.5
4
3.5
0.49
0.5
0.51
0.52
0.53
0.54
0.55
0.56
0.57
VERT DIODE #15
edge
0.8
0.7
0.6
0.5
0.4
0.49
0.5
0.51
0.52
0.53
0.54
0.55
0.56
0.57
Vertical H- Alpha # 6602
8
6
4
2

Effect of large Elms

- Large Elms briefly disrupt edge confinement barrier.
- 3-7 % of particle inventory lost in one Elm.
- 10-50 % reduction of edge X-ray emission by one Elm.
- Macroscopic plasma movements due to changes in equilibrium.

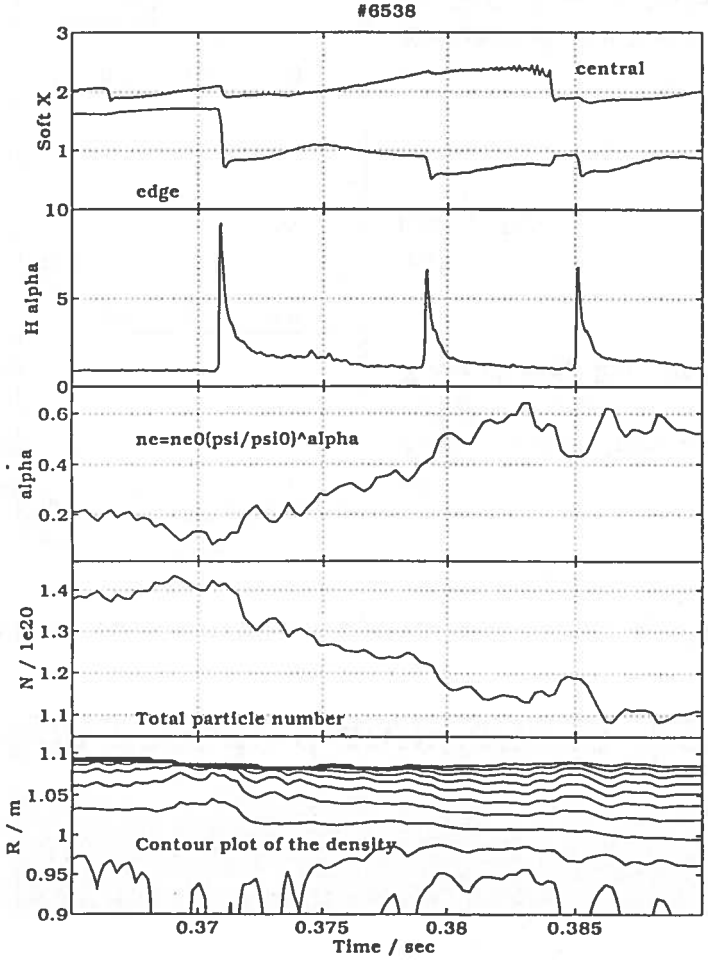

Elmy H-mode phases

- Large Elms stabilize or reduce n_e, depending on frequency and reduce profile broadness.
- Stabilize or reduce Z_{eff}, depending on frequency.
- Prevent density limit disruptions.
- Have lower τ_e than Elm-free H-modes.
- Controllable by slight changes of configuration.

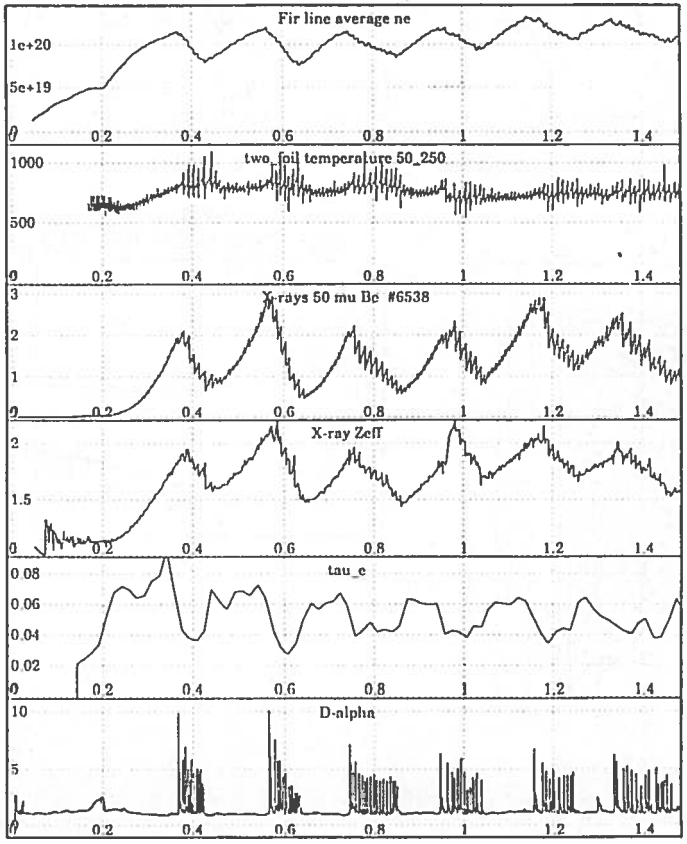

High density disruptions in H-mode

A) Disruption with central radiation collapse.

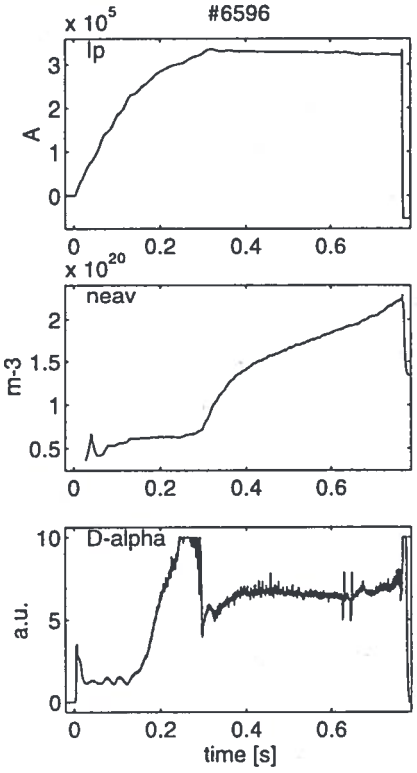

–>
X-ray emission from 1/2 profile.
–> –>
X-ray viewing lines and LCFS.

<–
I_p,<n_e>,D_α

–>
Evolution of raw X-ray profiles.
–> vertical, –> –> horizontal camera.

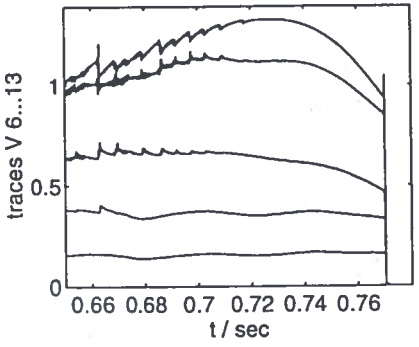

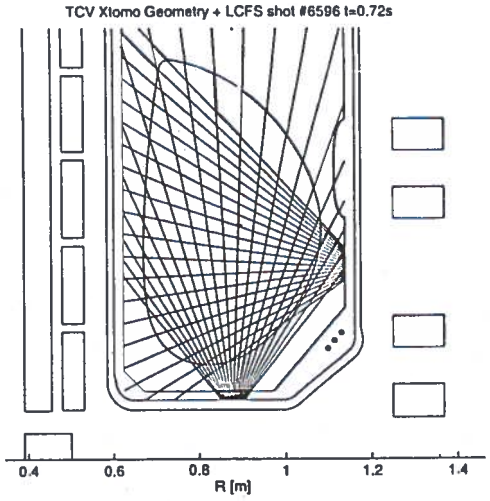

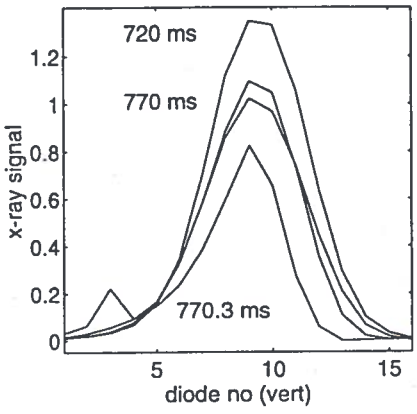

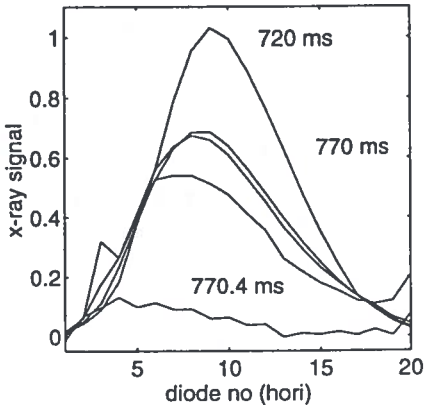

- Loss of sawteeth and m=1 oscillations at $2.1 \cdot 10^{20} m^{-3}$.
- No locked or quasi-stationary n=1, m=1 (magn & X).
- Reduction of central X-ray emission, edge unaffected.
- Accelerated drop of l_i ($l_i \cong 0.7$) after loss of sawteeth.
- <n_e> rises to $2.25 \cdot 10^{20} m^{-3}$ (1.2 times Greenwald).

- Peaking of n_e profile before loss of sawteeth.
- Final X-ray collapse within ≤ 0.3 ms.
- Plasma moves towards bottom and inner wall.
- Current disruption within 2ms.
- Odd-n, low-m perturbations (~ 0.03 T) on probes.

B) Disruption with H-L transition (# 6687).

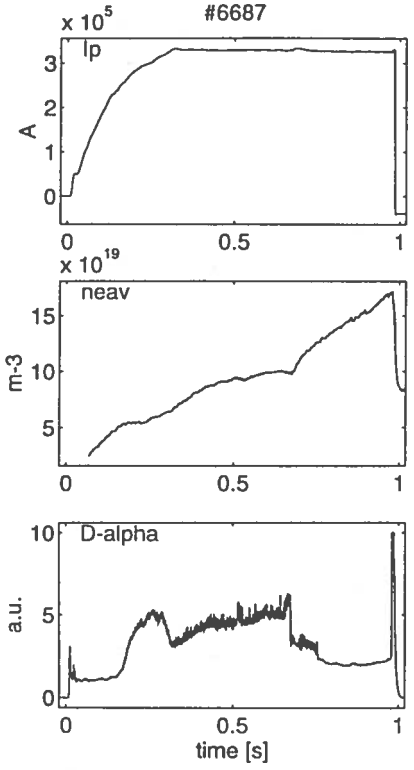

–>
X-ray half profile 7ms before disruption.
–>–>
Plasma position from X-rays.

<–
I_p,<n_e>,D_α

—>
X-ray profiles during last 5 ms
–> vertical –>–> horizontal
Continuous lines spaced 0.1ms from last sample in H-mode, broken lines 1ms.
Dashed lines spaced 0.1 ms in disruption.

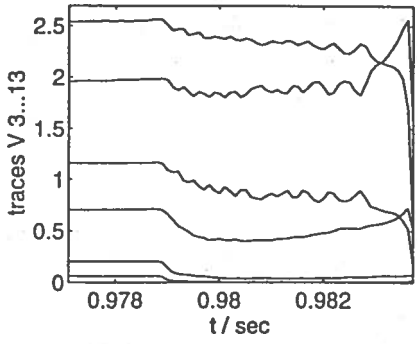

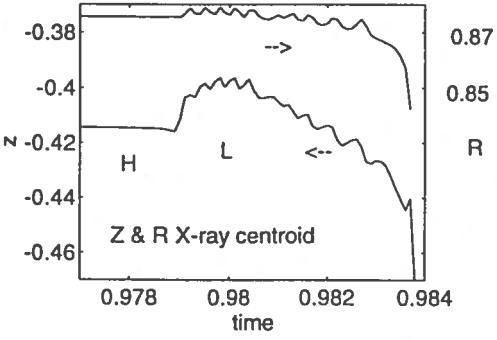

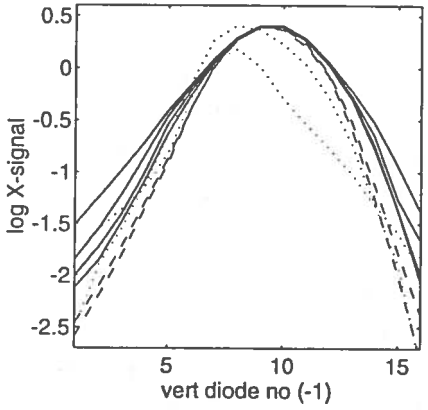

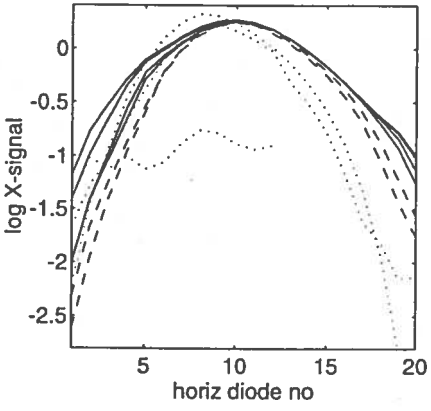

- H-L transition at <n_e> = $1.7 \cdot 10^{20} m^{-3}$ (90 % Greenwald)
- Drop of pripheral X-emission within ≤ 0.2 ms.
- Plasma jumps up 2 cm at transition, then drifts down slowly, with small rotating m=1 mode.
- Fast rise in l_i during L-mode (from 0.61 to 0.67).

- Disruption after 5 ms of L-mode.
- X-ray emission collapses within ≤ 0.3 ms.
- X-ray centroid moves down and inboard.
- I_p collapses within 2 ms.
- Odd-n, low-m (4 ?) perturbations (~ 0.03 T) on probes.

APS, Minneapolis, 7-11 November 1994

FIRST EDGE PHYSICS RESULTS FROM TCV

R. A. Pitts, M. Corboz, R. Behn, A. Burri, R. F. Chavan, M. Dutch, B.P. Duval, A, Hirt, F. Hofmann, P. F. Isoz, J. B. Lister, B.Marletaz, Ph. Marmillod, Y. Martin and H. Weisen

Centre de Recherches en Physique des Plasmas, Association EURATOM - Confédération Suisse, Ecole Polytechnique Fédérale de Lausanne, 21, Av. des Bains, CH-1007 Lausanne, Switzerland

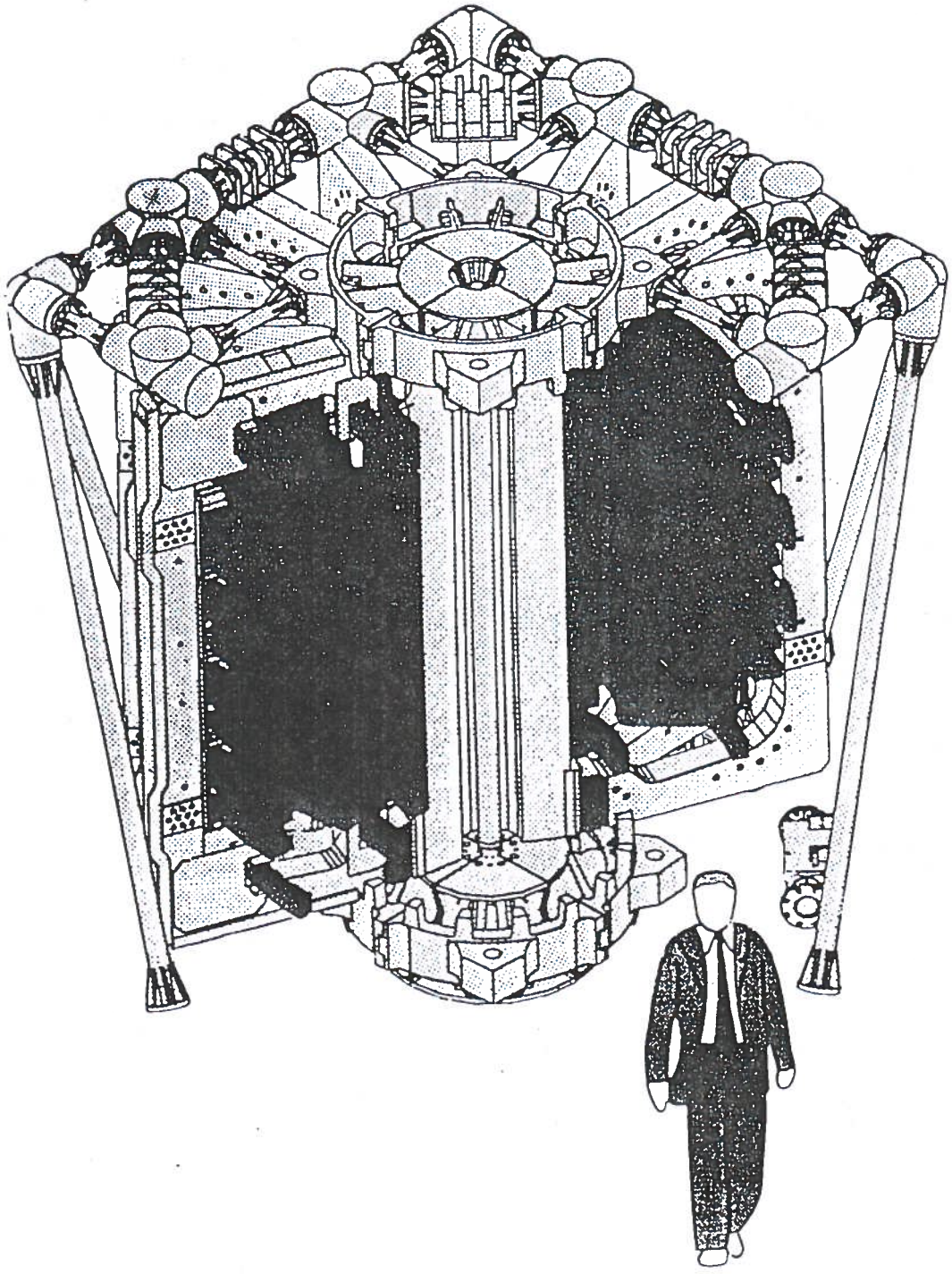

The TCV Tokamak

• Major Radius	0.88 m
• Vessel Inner Width	0.56 m
• Vessel Inner Height	1.54 m
• Toroidal Field	≤ 1.5 T
• Plasma Current	≤ 1 MA
• Plasma Elongation	≤ 3.0

Edge Physics on TCV

The enormous flexibility of TCV with respect to the variety of plasma configurations possible adds an extra dimension to the problem of characterizing the edge plasma. A preliminary programme comprises two main diagnostics:

- A poloidal array of **44 graphite single Langmuir probes** covering the lower part of the central column and the divertor floor.
- A **scanning Infra-Red camera** and accompanying relay optics, presently configured to view the outer full toroidal belt limiter, but which will soon be transferred to study equilibria diverted onto the vessel floor.

First results, described below, have been obtained with both diagnostics.

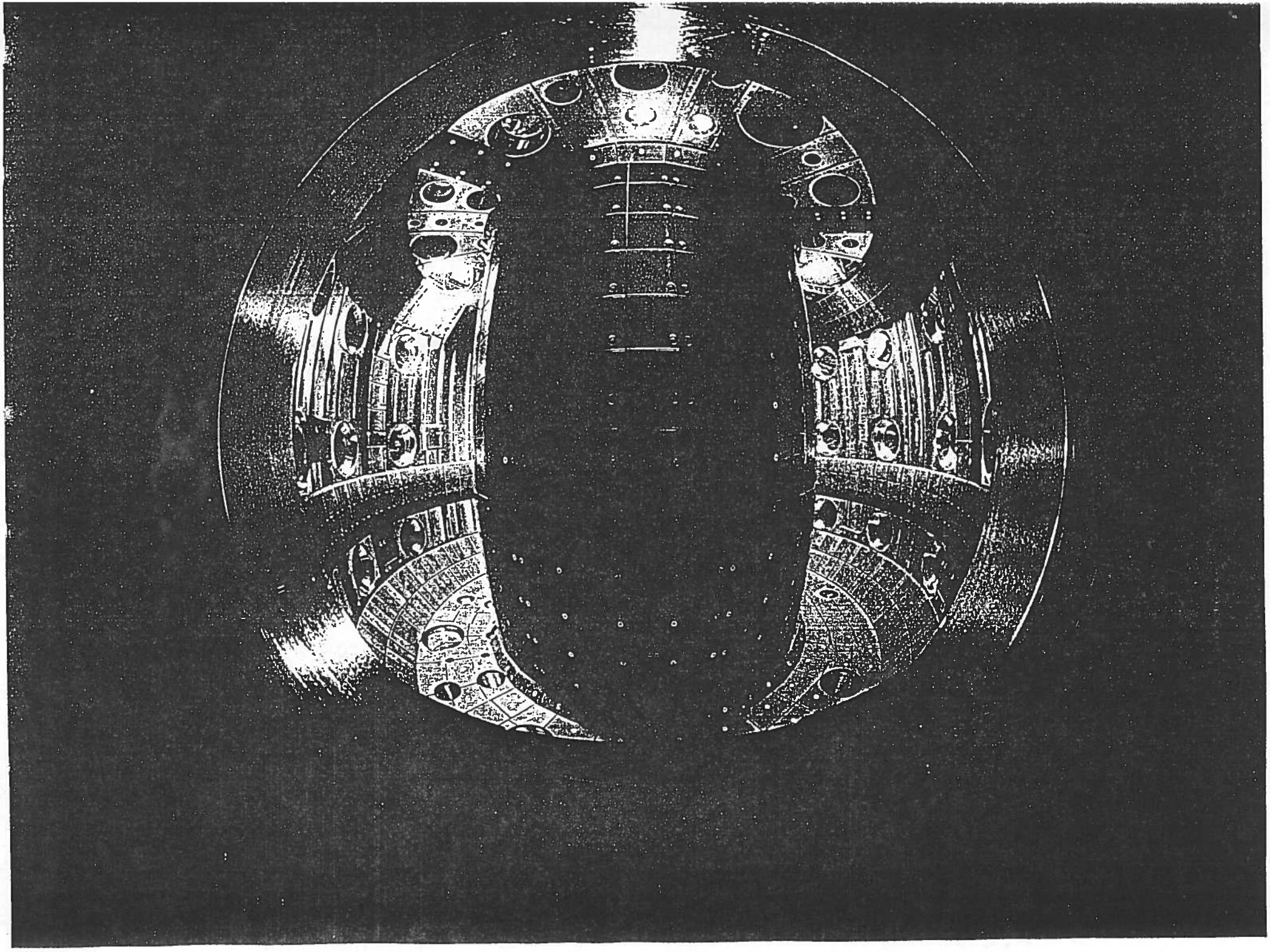

First Wall Protection

- Central column, divertor floor and internal fast stabilisation coils protected by a total of around 1000 tiles (Ringsdorff polycrystalline, isotropic graphite, type EK 986).
- Belt limiter centred 23 cm below the outside midplane and comprising 64 tiles (Schunk FP379, isotropic, polycrystalline).
- Graphite tile protection during the first full experimental campaign amounted to 46% of vessel internal surface area.
- Tile coverage currently being increased to ≈62% with the addition of 446 new upper and lower divertor tiles designed to optimize diagnostic access and power handling.

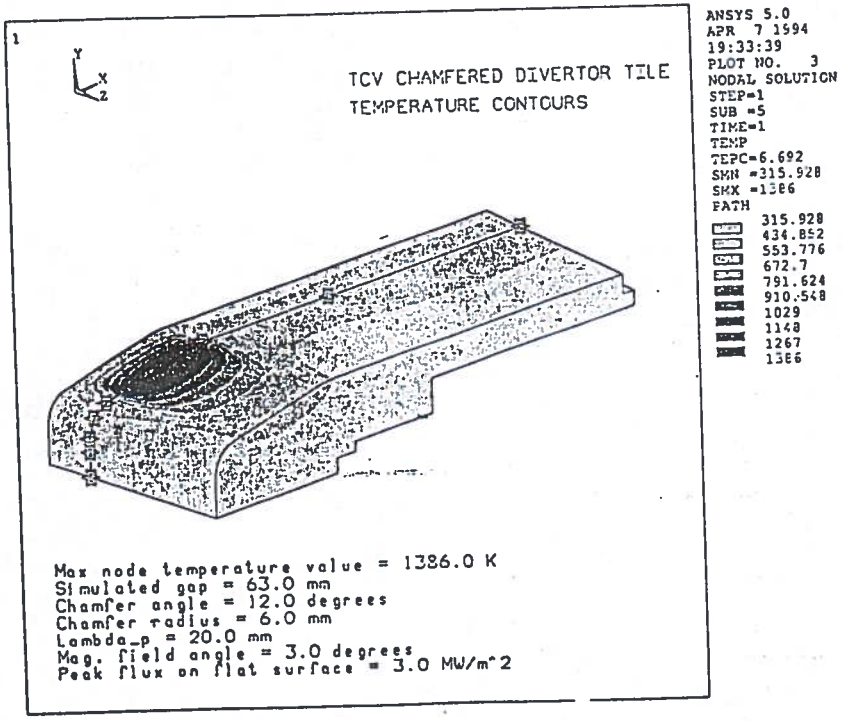

Example of finite element simulation of the new divertor tiles

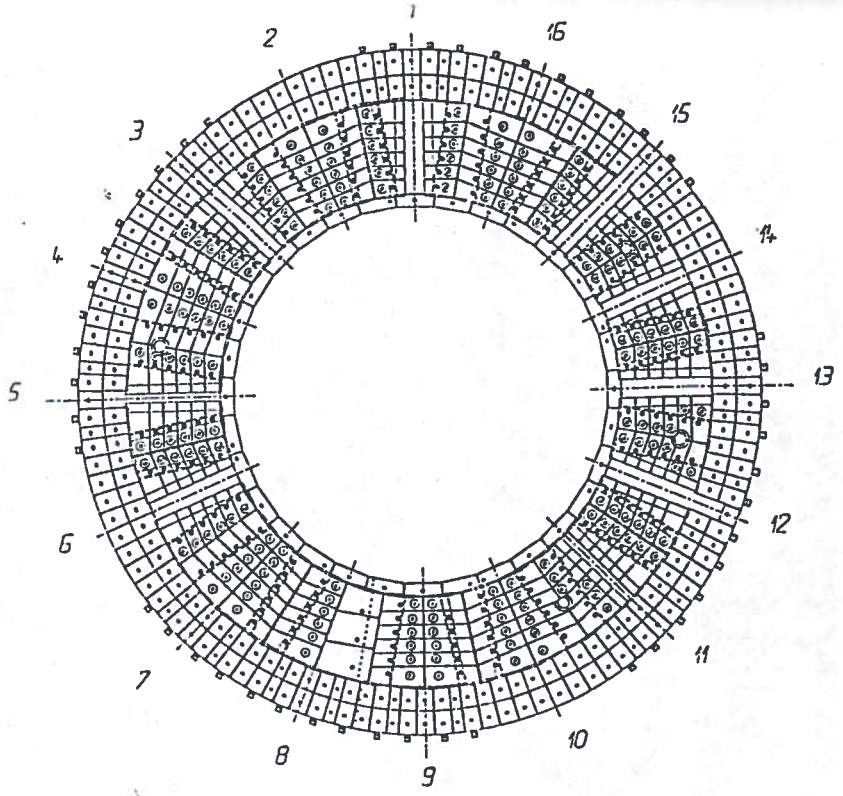

New floor tiling presently being installed

- TCV is equipped with an RF glow discharge system consisting of two diametrically opposed antennas mounted on the outside midplane (only one electrode is RF driven).
- The vacuum vessel was boronized for the first time on 4 May 1994 by glow discharge in a standard 10% deuterated diborane/90% He mixture with the chamber at 200°C. Boronization is now routine and has been performed a total of three times in 5 months. Pure He glow discharge cleaning is perfomed according to machine requirements.
- Typical chamber base pressure is 4×10^{-9} Torr

DIVERTOR LANGMUIR PROBES

Probe Layout

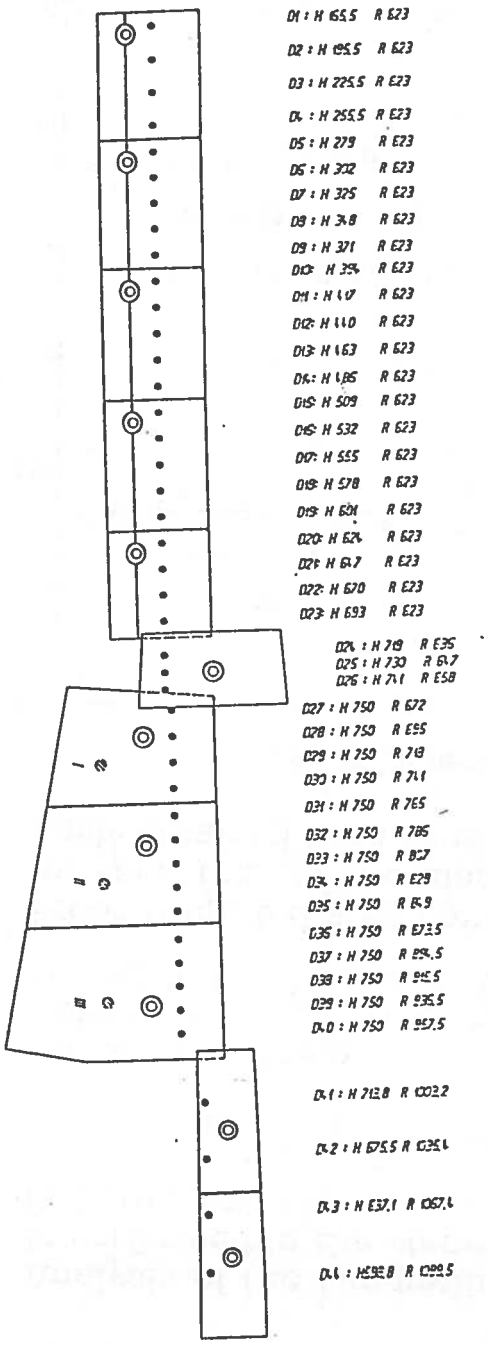

Probe Design

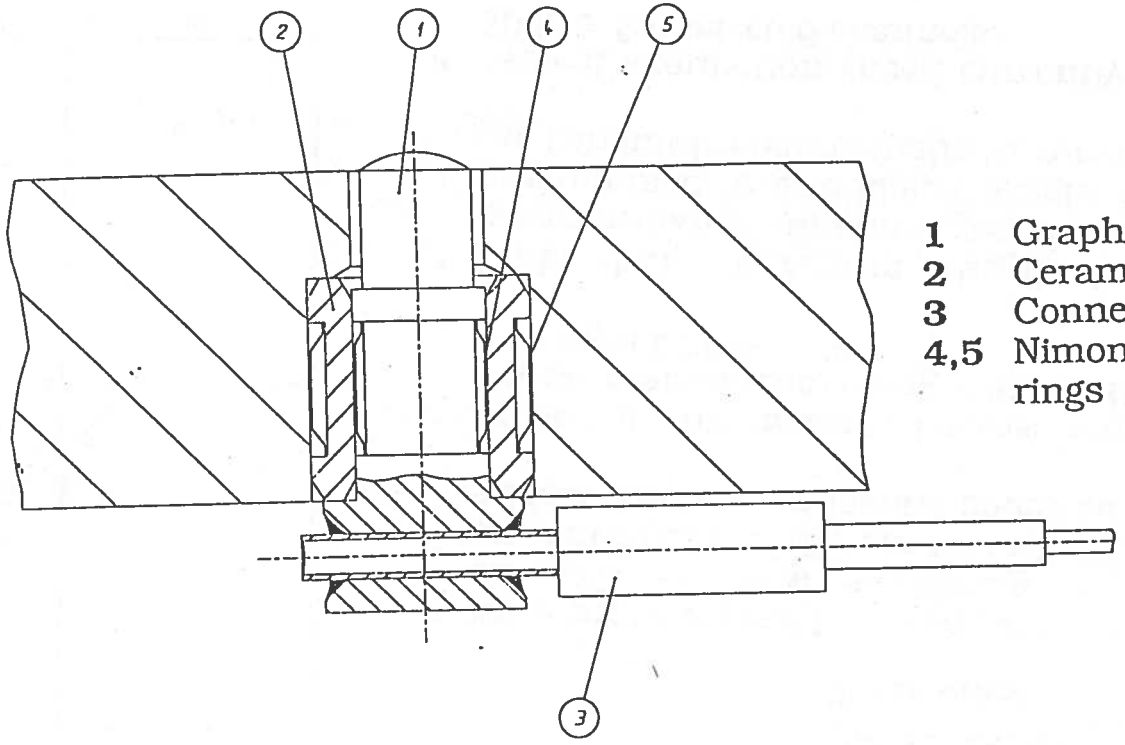

1 Graphite probe
2 Ceramic former
3 Connector
4,5 Nimonic tolerance rings

- Same graphite used for the probes as for the wall protection tiles.
- Probe head of the 'domed' type projecting **0.80 ± 0.15 mm** above the tile surface (probe diameter **5.0 mm**). Tile/probe clearance 0.5 mm, probes held in place in the tile by specially fabricated tolerance rings.
- Mineral insulated coaxial cable used to pass signals to the probe electronics. Cables terminated at each end by special purpose ceramic/metal connectors.
- Probe-connector liason assured by electrolytically coating the graphite probe base with ~20 μm of Nickel and vacuum brazing a small tube into pre-drilled hole in the base. Connector end is then brazed into this acceptance tube.
- 44 probes installed in the lower divertor. Average spatial separation **2.2 cm.**

Analysis

- Analysis of the Langmuir probe characteristics is performed in the standard way - 3 parameter fit to the function:

$$I_{pr} = I_{sat}(1 - \exp[e(V_{pr} - V_f)/kT_e])$$

- Initial non-linear least squares fit to entire characteristic gives starting parameters for a second fit to all points with $V_{pr} \leq V_f$
- Probe projected area computed by interpolation for each time of the magnetic field line impact angle obtained from equilibrium reconstruction.

Typical characteristic

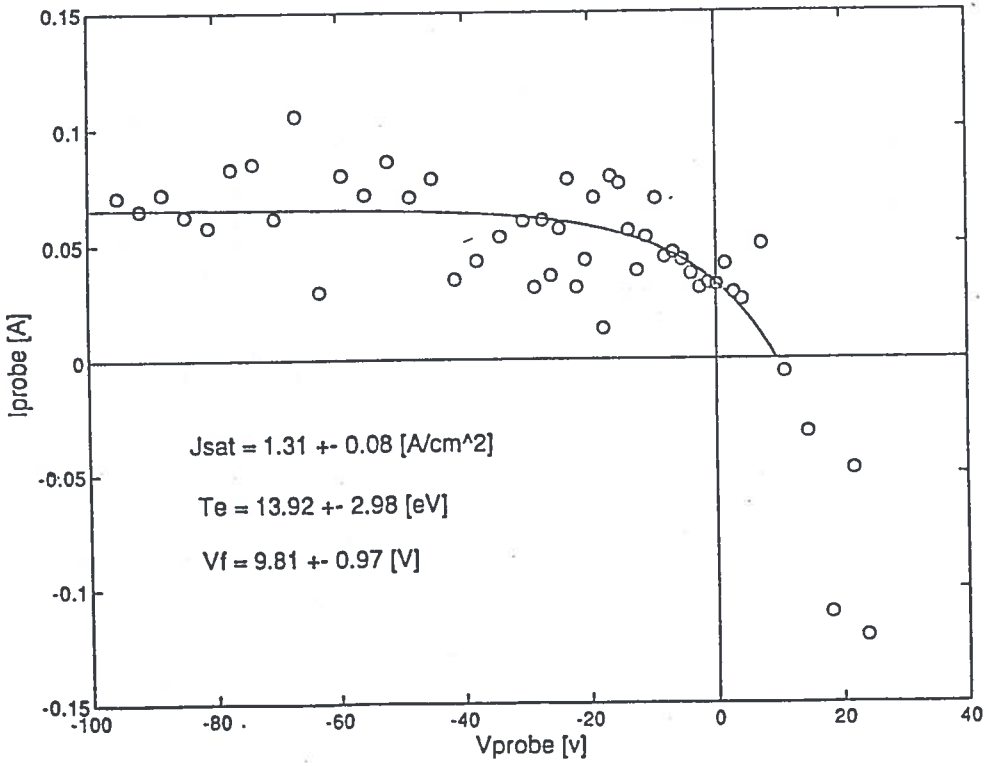

Probe projected area vs. field line impact angle

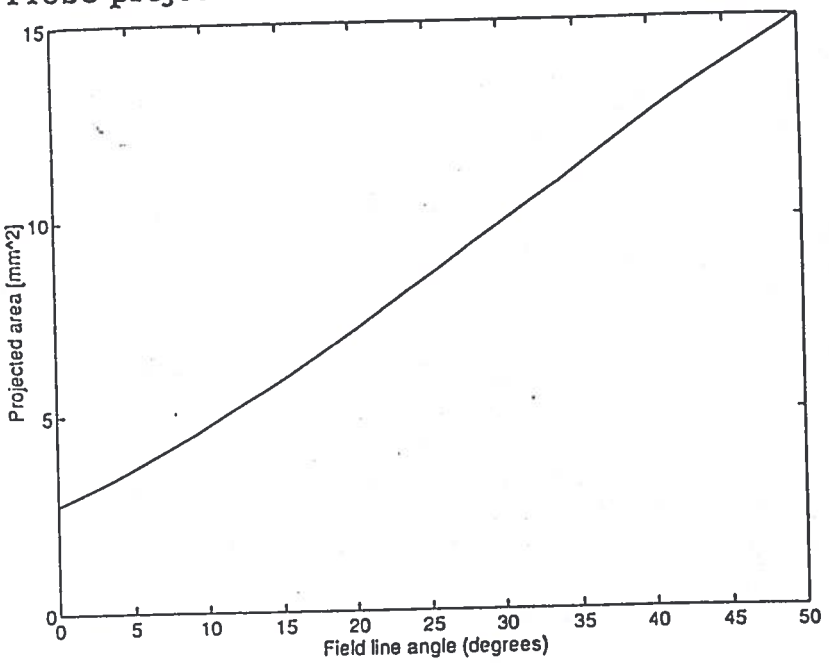

Electronics

- Each probe served by a dedicated amplifier (based on APEX-PB58A) supplying ± 2A up to a maximum of ± 110V, slew rate ≥ 10V/μs. Remote selection of bias or floating potential modes.
- Probe currents measured across remotely selected shunt resistances using differential amplifiers with high CMRR.
- Probe bias waveform supplied by remotely programmable function generator. Waveform programmed to give higher weight to points near the Langmuir characteristic turn-over.
- Typical acquisition speed currently at 10 kHz or 50 kHz for selected channels.

Example of profile measurements at lower strike point of a double null diverted discharge

- During the first full TCV camapign, ∇B has been exclusively directed upwards. Emphasis on H-mode studies has limited the machine time available for investigation of single null diverted equilibria with a lower X-point. Measurements with the divertor probe array have thus been possible so far only in discharges with double null plasma configurations.
- Probe signal intensity is always in good agreement with nominal strike point positions from equilibrium reconstruction.
- Campaign in 1995 will include discharges with inverted toroidal field permitting much more extensive use of probes

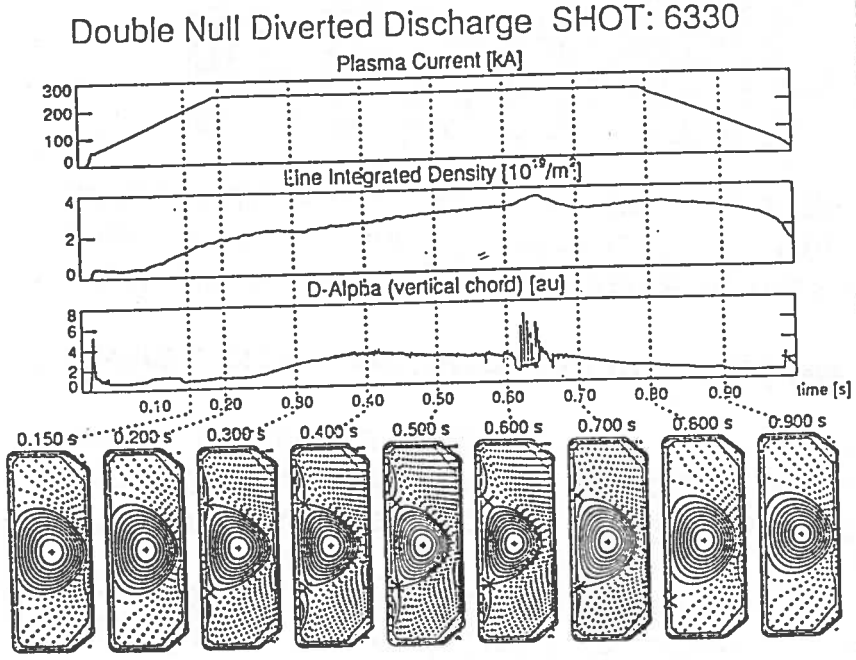

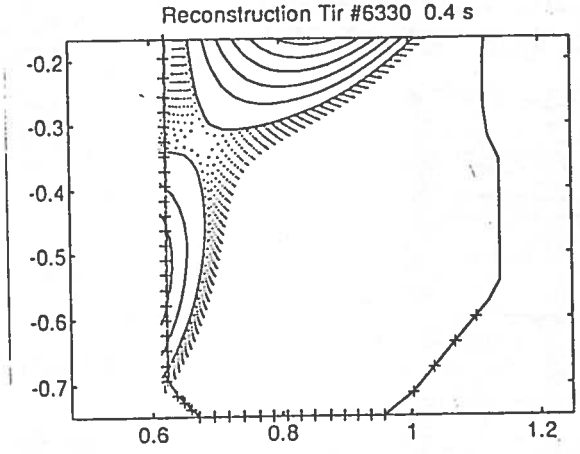

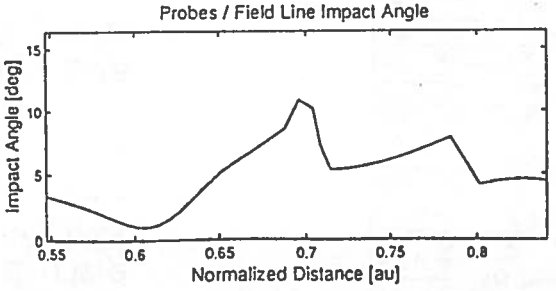

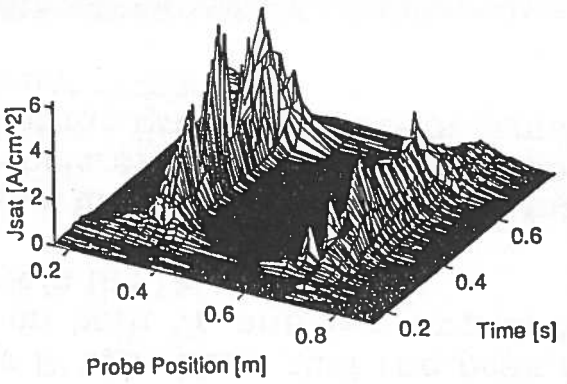

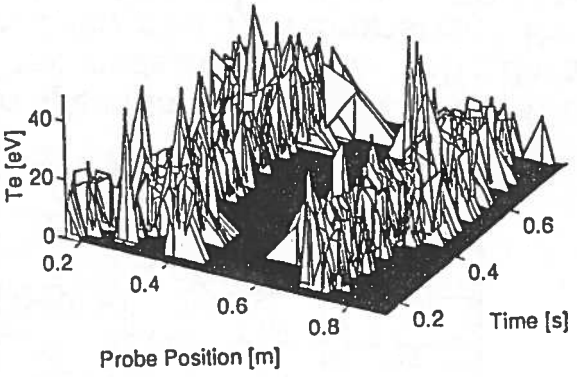

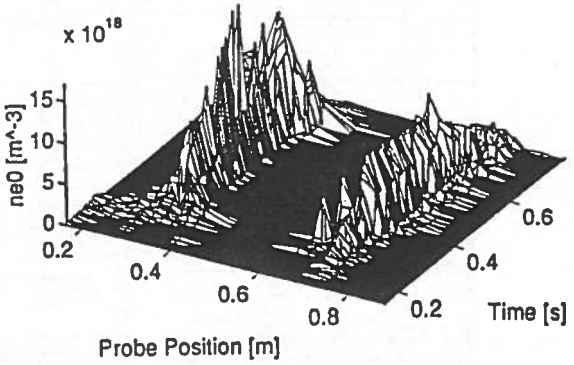

Measurements during X-point toggling

- Interesting results have been obtained during X-point toggling experiments - magnetic axis of DNX equilibrium is modulated vertically to move the X-points alternatively away from the LCFS.

- Plasma oscillates between ELM/ELM-free periods with ELMy periods corresponding to lower X-point 'active' (see poster 2S25).

- Divertor probes operated both in V_f and I_{sat} modes.

- On both signal types, **negative spikes** observed consistently on those probes near the **upper strike point** of the lower X-point before each large ELM

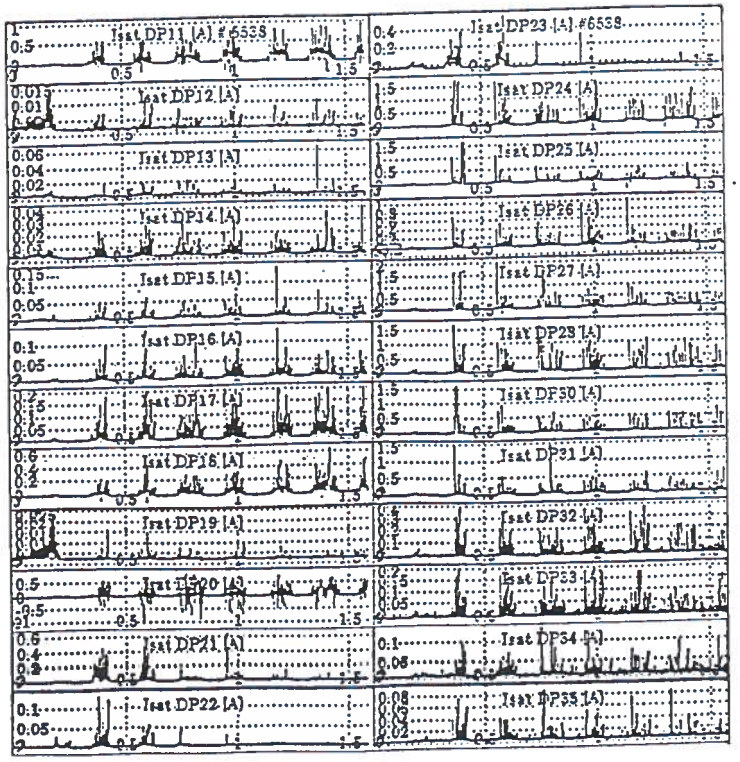

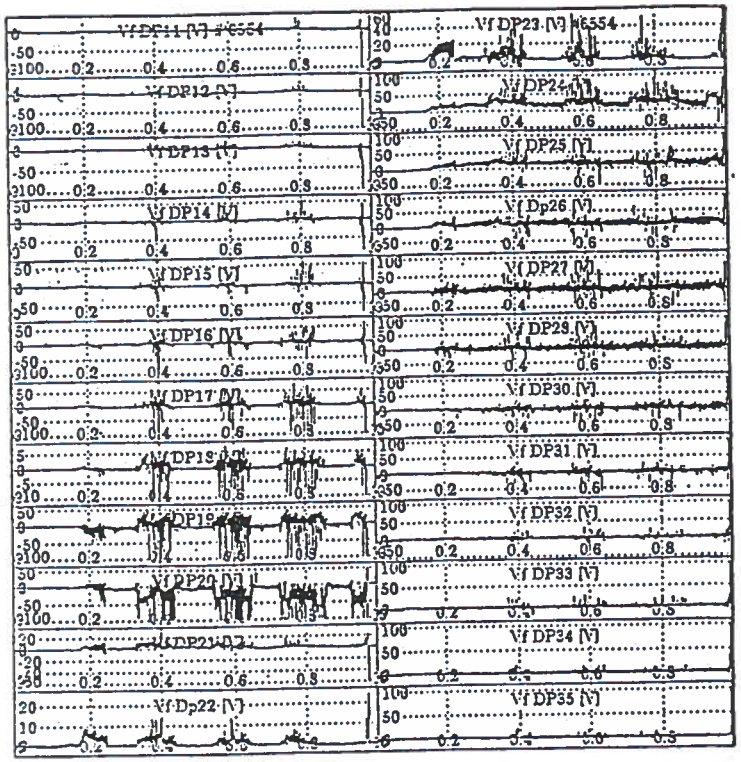

- The 10 kHz acqusition speed is insufficient to see the detailed structure of the negative spikes. The data below, obtained at 50 kHz, clearly demonstrate the effect. Comparison is possible only with the 50 kHz vertical Dα signal measured along a central chord.

- Averaging over many ELM's shows that the peak of the negative spikes on both V_f and I_{sat} appear to coincide with the peak in the Dα signal.

- Limited database seems to indicate that the V_f signal begins to decrease before that of the saturation current. But note that the two mesurements cannot be performed in the same discharge.

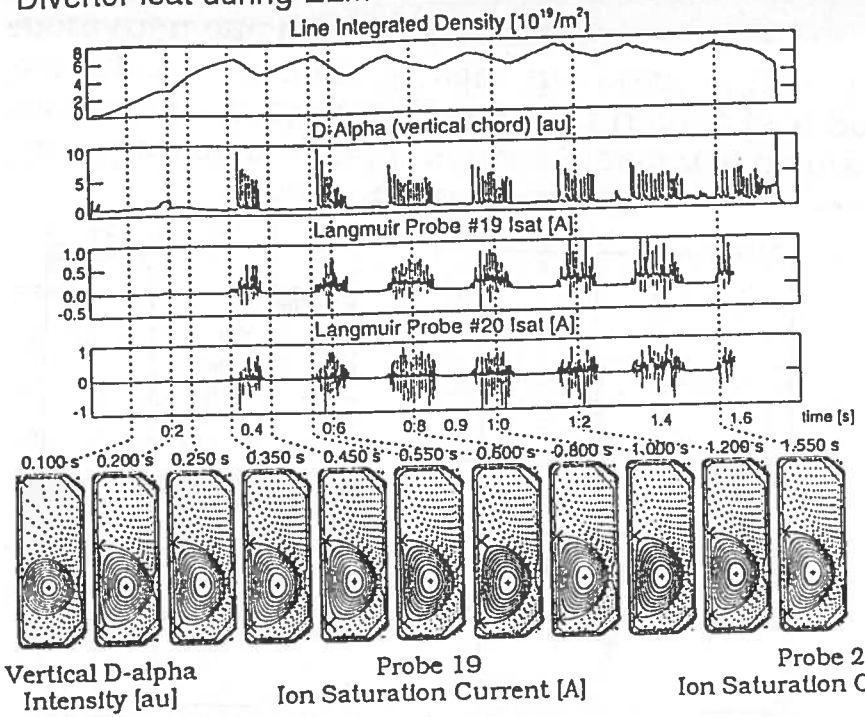

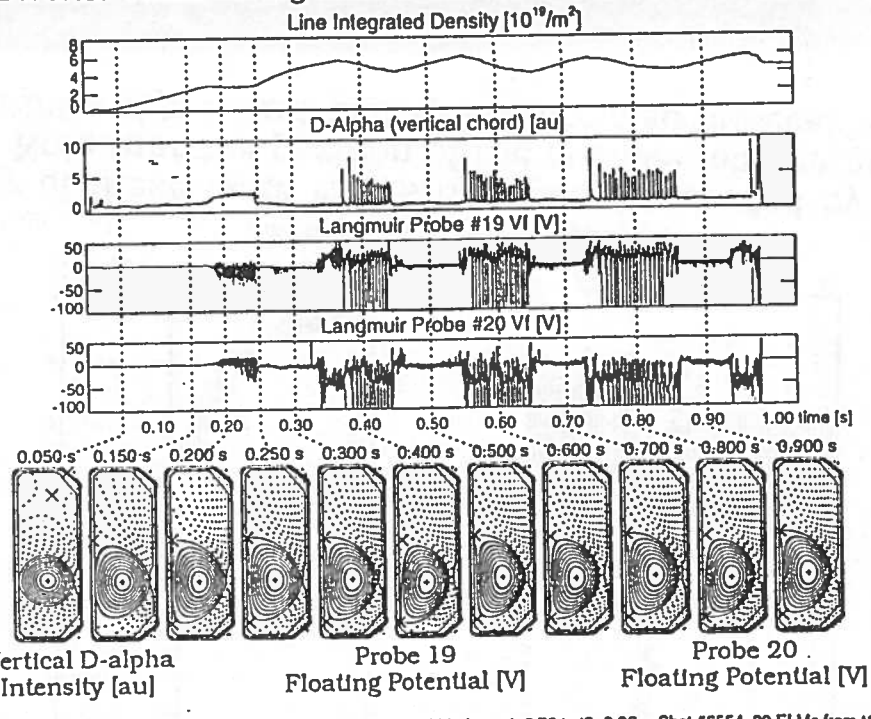

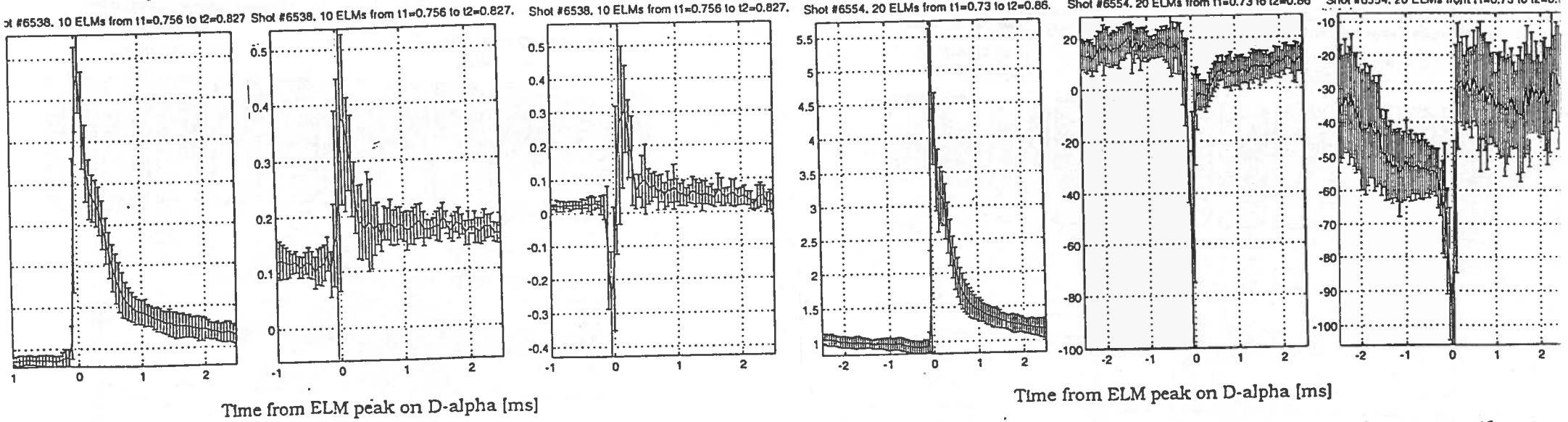

- Note that in Isat mode the probes are held at a constant bias of -100V (w.r.t. the torus potential). Since the floating potential falls to nearly this value, the negative current is likely to be a consequence of the fall in Vf. The effect is most marked on the probe closest to the strike point.

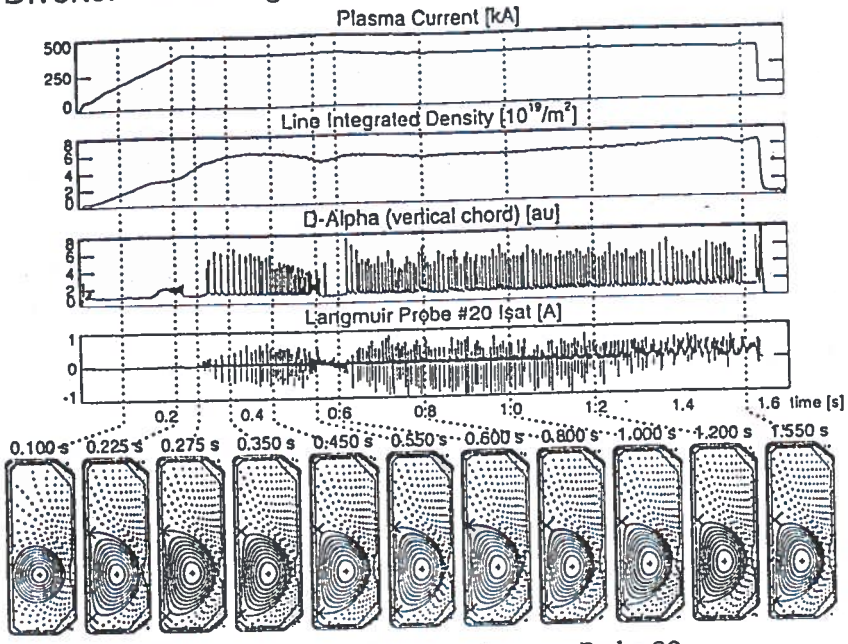

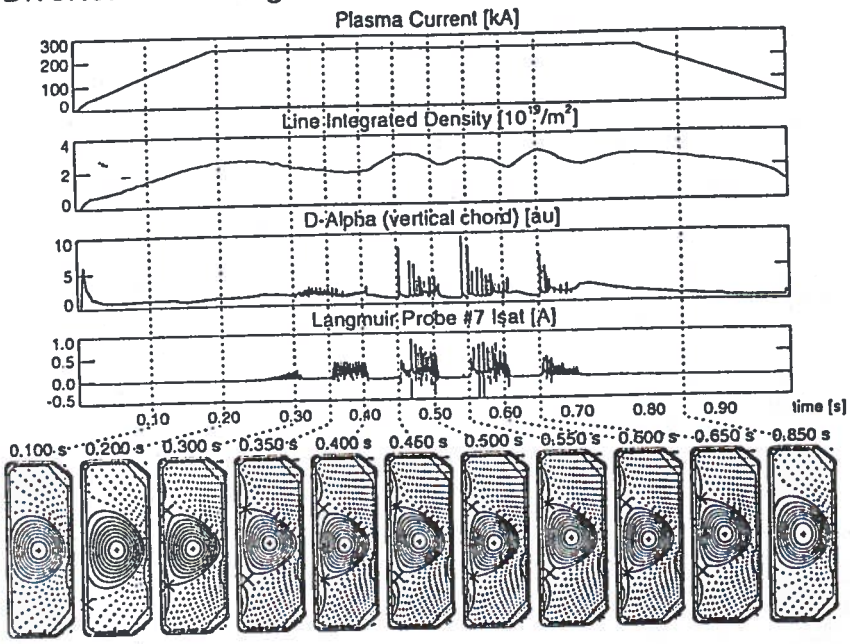

Vertical D-alpha Intensity [au]

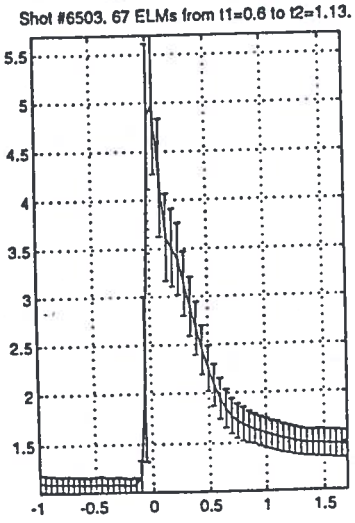

Probe 20 Ion Saturation Current [A]

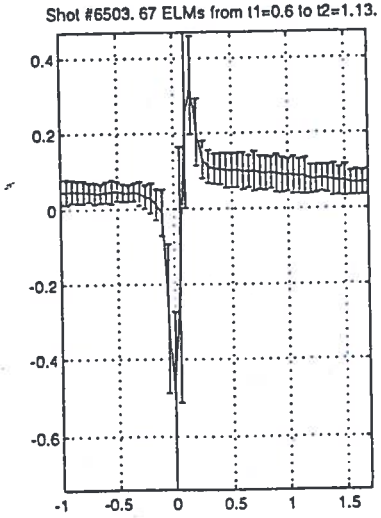

Time from ELM peak on D-alpha [ms]

Vertical D-alpha Intensity [au]

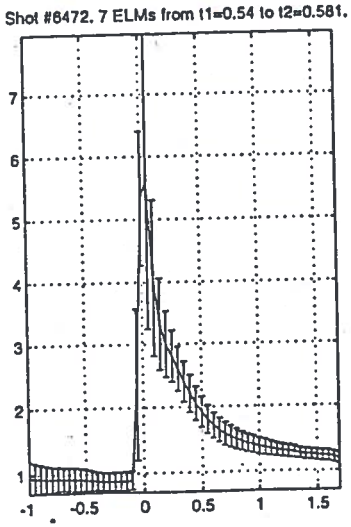

Probe 20 Ion Saturation Current [A]

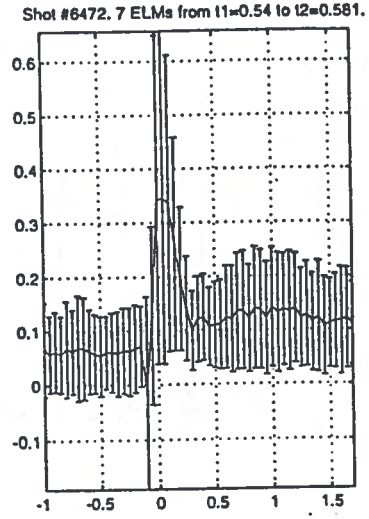

Time from ELM peak on D-alpha [ms]

- No coherent magnetic activity observed before the majority of these large ELM's but most preceeded by an increase in level of magnetic turbulence (see poster 2S24). Note that the position of the positive maximum in I_{sat} appears to coincide with the point of inflexion in the D-alpha signal and that spikes are also noticeable in more than one type of equilibrium.

INFRA-RED CAMERA

Camera

- Second element of the basic edge physics programme on TCV is an Infra-Red camera for measurements of first wall surface power deposition.
- First camera measurements (presented here) have been made on the toroidal belt limiter tiles, but the system is intended primarily for divertor viewing and is presently being reconfigured.
- Inframetrics series 600 scanning camera, single HgCdTe detector cooled thermoelectrically to 77K, . used in spectral bandpass 3-14μm. Detector FOV 2 mRad horiz. and vert. with 175 (IFOV's) digitized to 256 pixels per line and 120 (IFOV's) per field giving 240 lines per frame (CCIR-PAL standard). Time resolution 20 ms/frame

Data Acquisition

- Video data acquisiton achieved with UNIX based Synoptics-DASH electronics and host PC. An Identical system is also employed for TCV visible CCD cameras.
- Acqusition is real time and data access is immediate.
- 30 MB RAM storage capacity permits max. 69 frames digitized to 384(horiz.) x 288(vert.) pixels per colour (RGB system).
- Video processor piloted remotely from VAX host with data transfer via TCIP-FTP protocol at 0.5 MB/s.
- User interface programmed in-house (B. P. Duval) using comercially available software library.

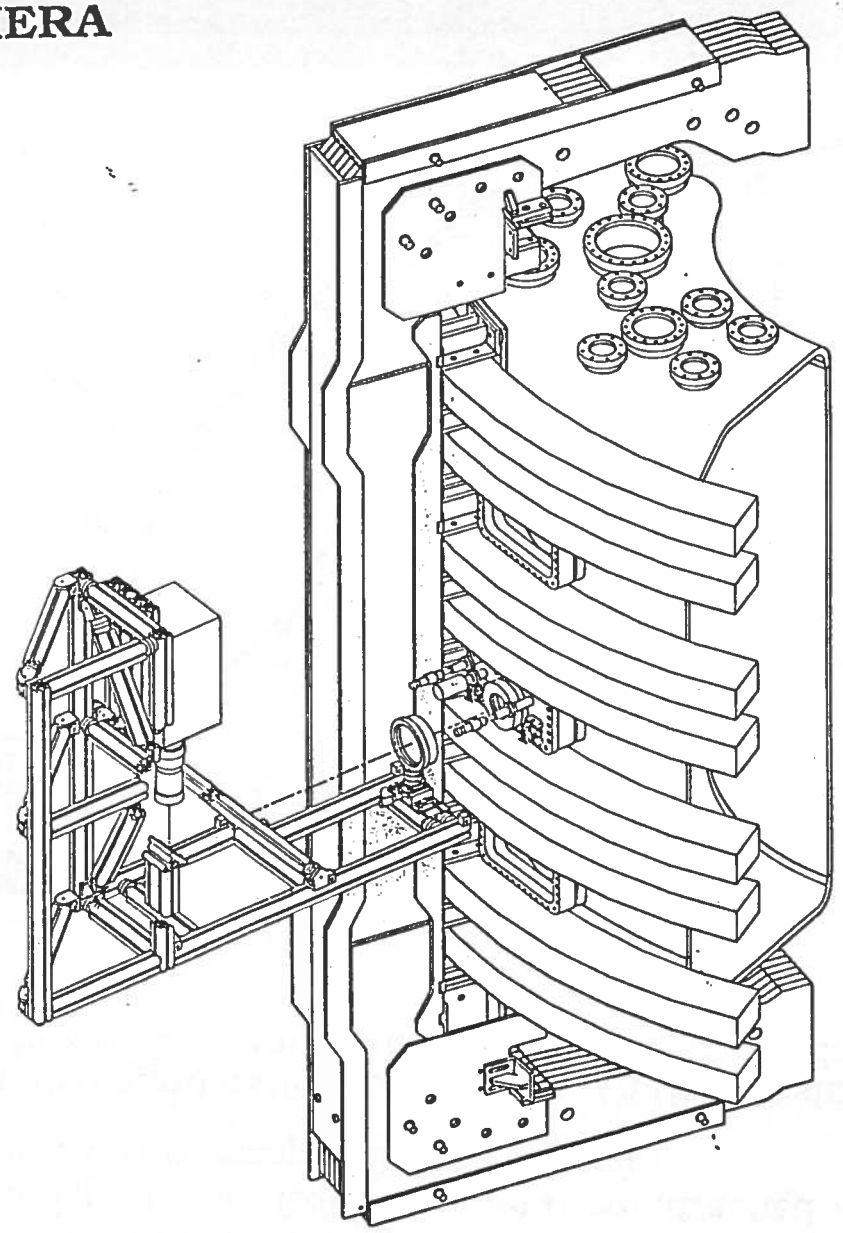

View of the system installed for limiter viewing. The camera is magnetically shielded by 2 cm of soft iron.

Nearest

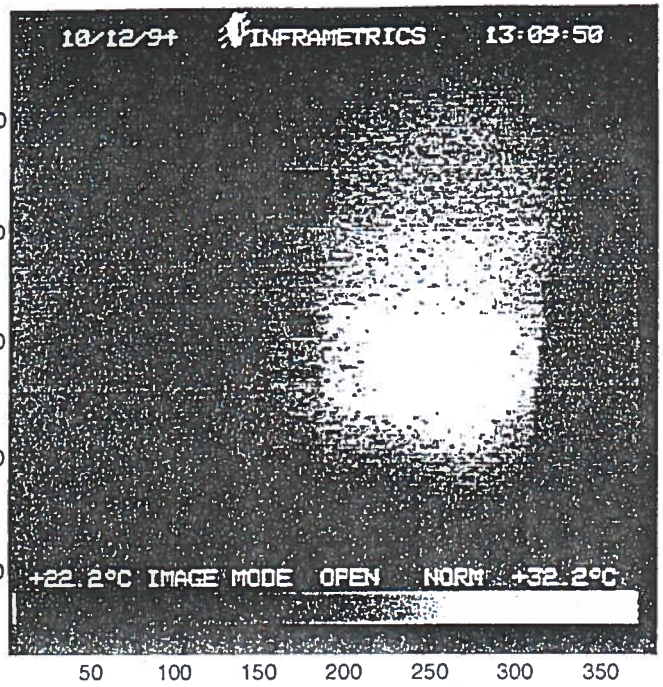

Bottom of the machine

Top of the machine

Furthest

- First results are reported below for a 3 discharge density scan. The image above shows the appearance in IR of the belt tiles in the camera field of view after the series of shots.

- The hottest (brightest) tile in this image is located between two toroidal field coils and has heated up noticeably higher than those beside (evidence for toroidal field ripple). The surface temperature of this tile has been used exclusively in the analysis below.

Relay Optics

- Limiter tiles imaged by a system of relay optics consisting of:
  - Two adjustable folding mirrors built into viewing port.
  - Vacuum window in ZnSe (82 mm diam., 10 mm thick).
  - Objective lens in Ge, $f_{eff}(5\ \mu m) = 21.5$ cm.
  - Field lens in Ge, $f_{eff}(5\ \mu m) = 18.8$ cm.
  - Close-up lens in Ge, $f_{eff}(5\ \mu m) = 84.6$ cm attached to Inframetrics 3x telescope (all Ge elements).

- Total system demagnification of 0.0052. Optics design performed in-house (R. Behn with Sinclair Optics, 'Optics Analyst' software).

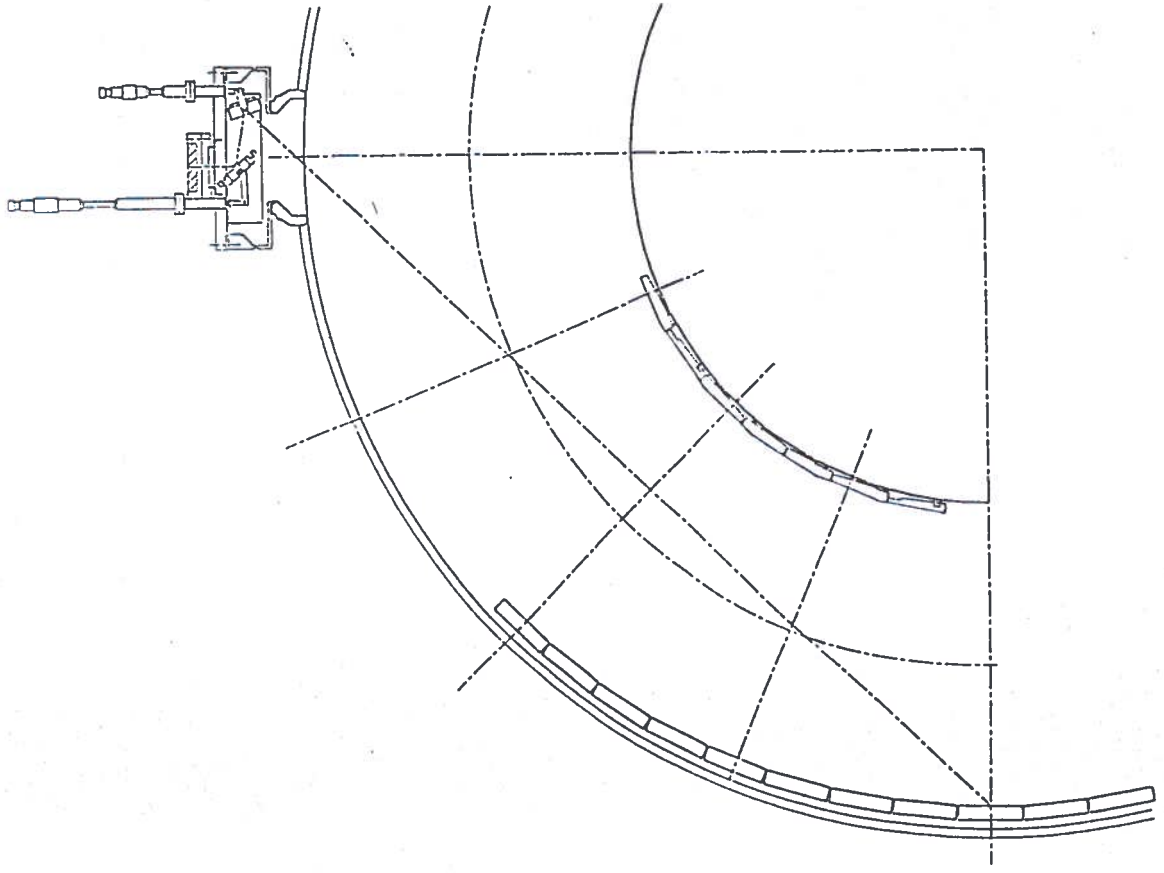

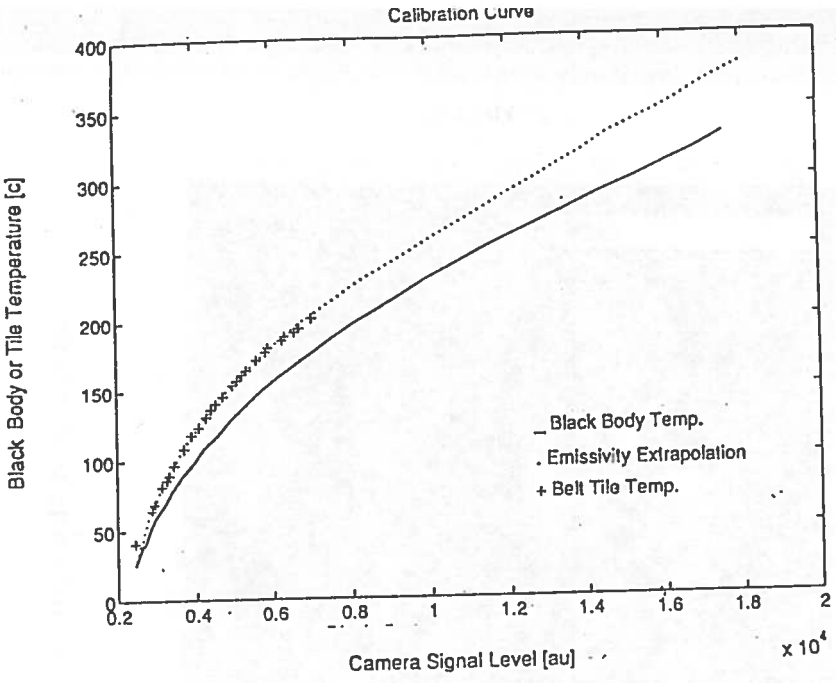

Data Analysis

- Time evolution of surface temperatures analysed numerically on a 2-D mesh to compute the heat flux.
- Real limiter tile geometry built in.
- Temperature dependence of thermal coefficients included but the coefficients assumed to remain constant during each time step, Δt.
- Heat diffusion computed using the Forward Backward Substitution Method (FBSM) with the measured surface temperature as boundary condition.
- Code fully tested against commercial finite element software

Camera Calibration

- Performed on the bench with the full system of relay optics and a home-made black body source

and

- During vessel cooling following baking using thermocouples built into the belt limiter tiles.

- The reconstruction is simplified by recasting the problem in terms of an effective temperature scale or 'heat potential':

$$U(T) = \int_0^T k(T')dT'$$

whence

$$\mathbf{q(surf)} = -k\nabla T = -\nabla U$$

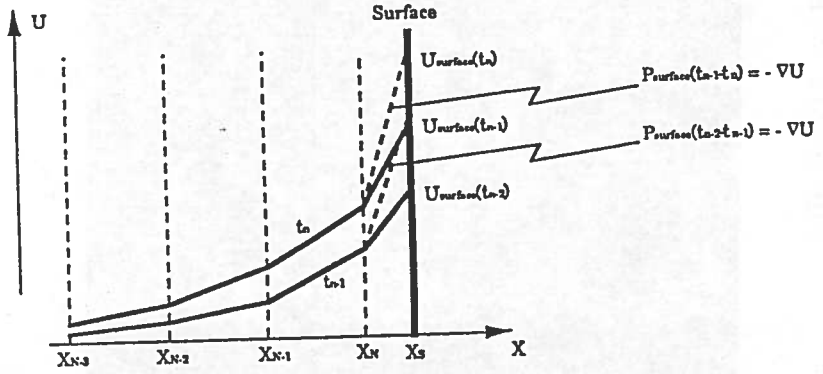

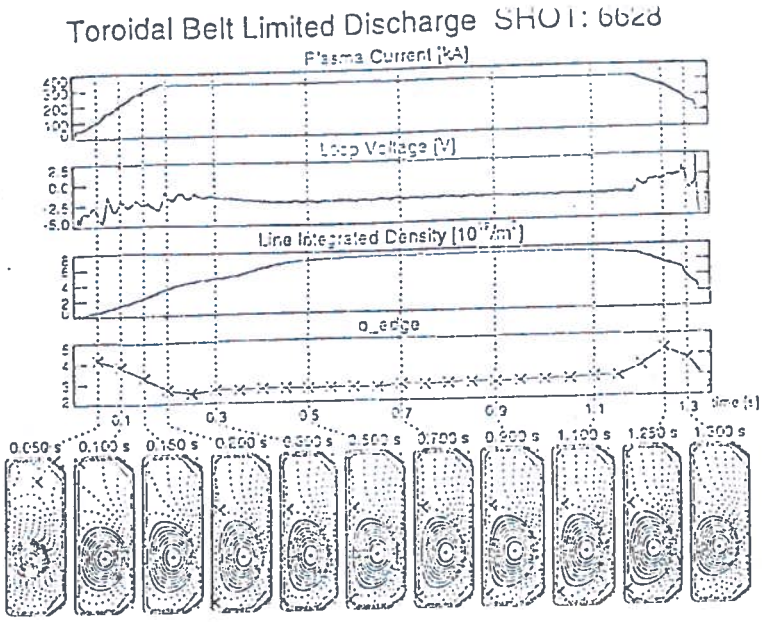

IR image at higher resolution to emphasize the heat deposition zones.

Nearest

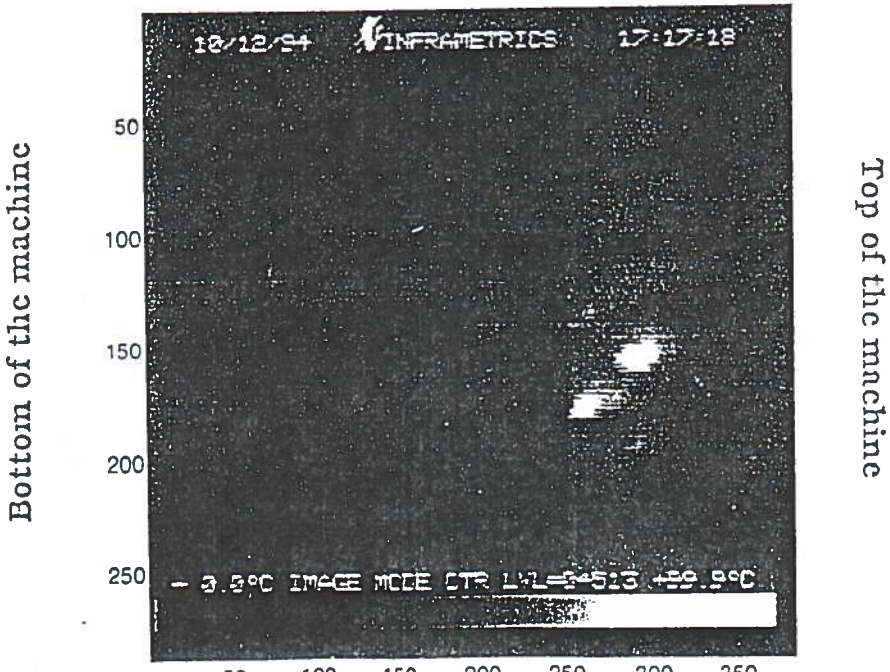

Nearest

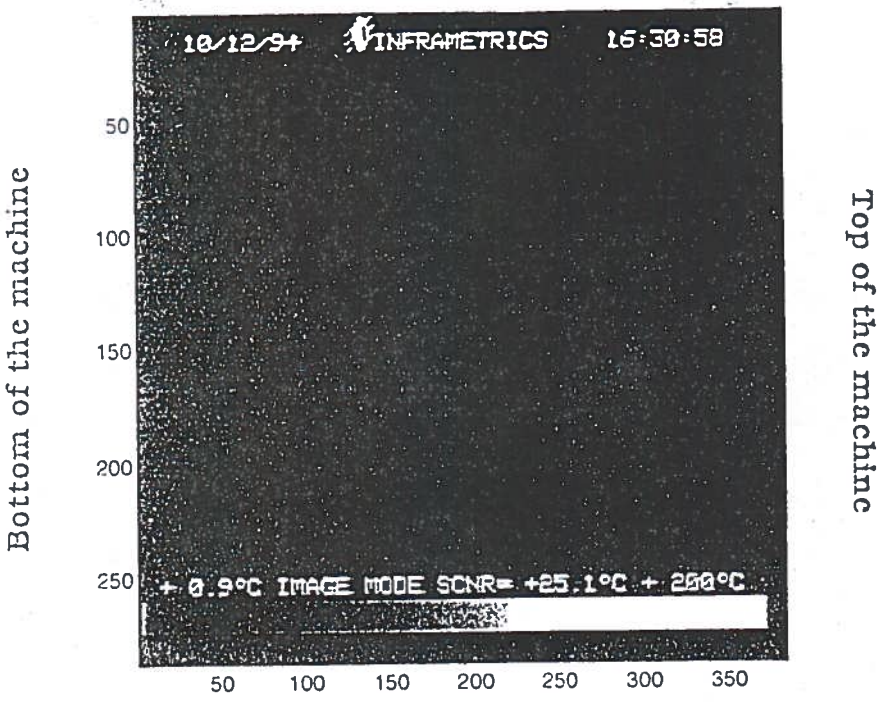

Langmuir probe ion current signals from limiter tile probes.

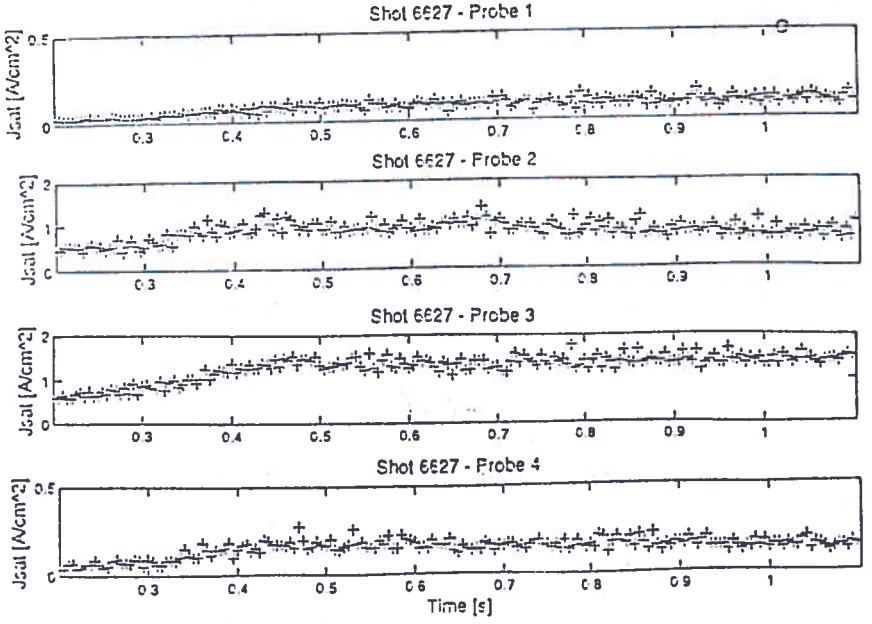

- Data analysis performed for poloidal strips passing through each of the wetted zones evident on the tile surface. Surface temperature averaged at each poloidal position inside these strips. Approximate power scrape-off lengths obtained by extrapolating the computed heat flux at the tile surface back into the SOL for the ion and electron drift sides of each strip.

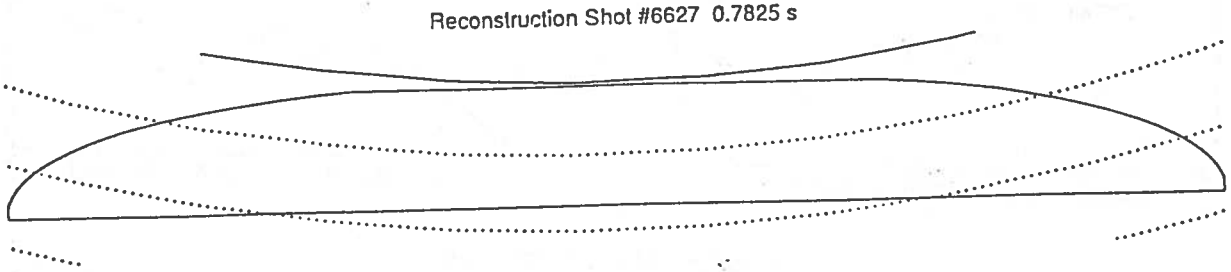

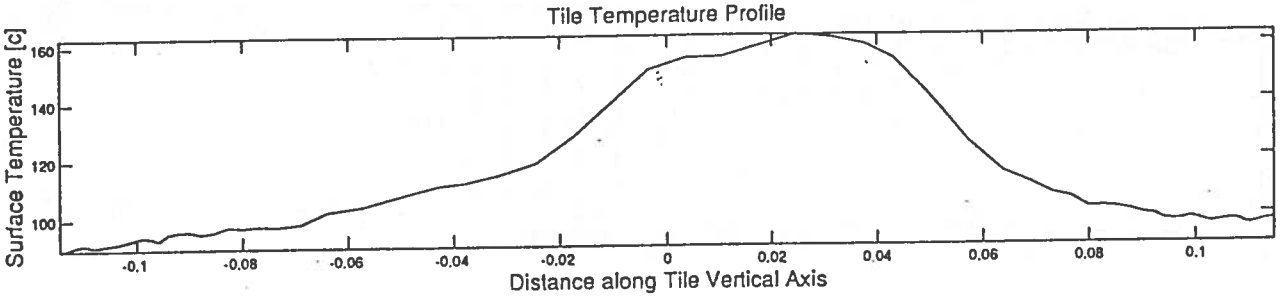

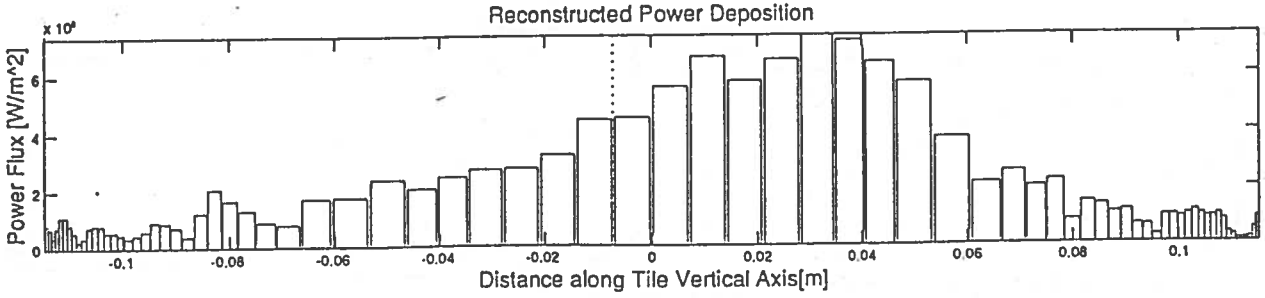

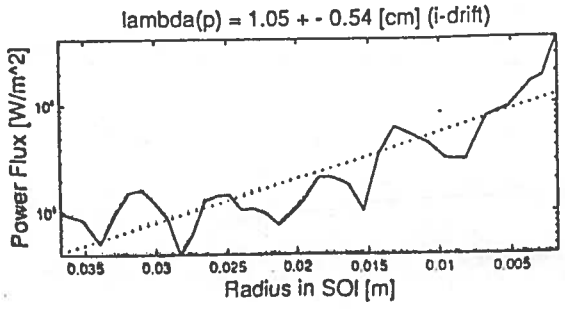

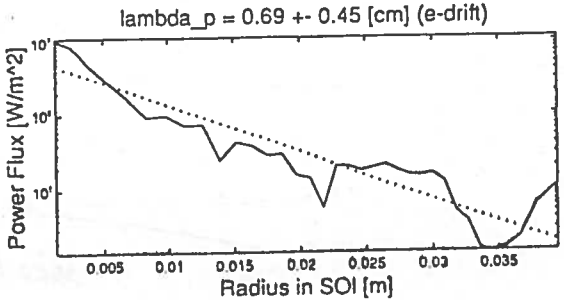

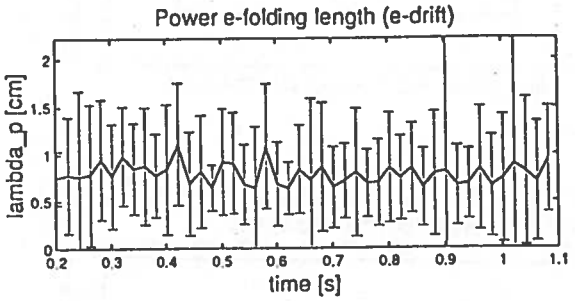

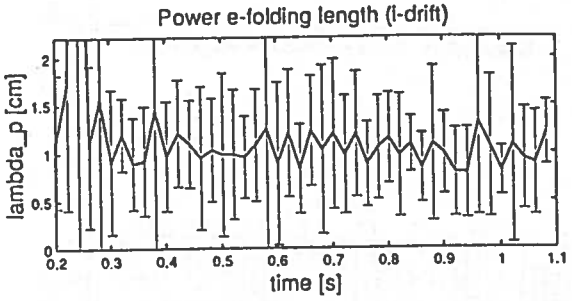

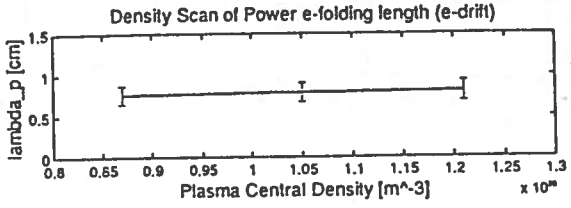

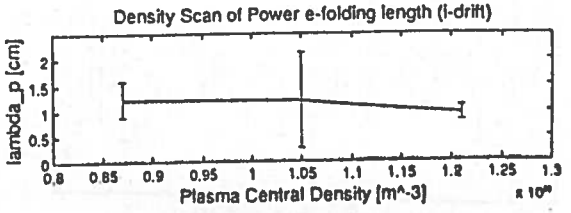

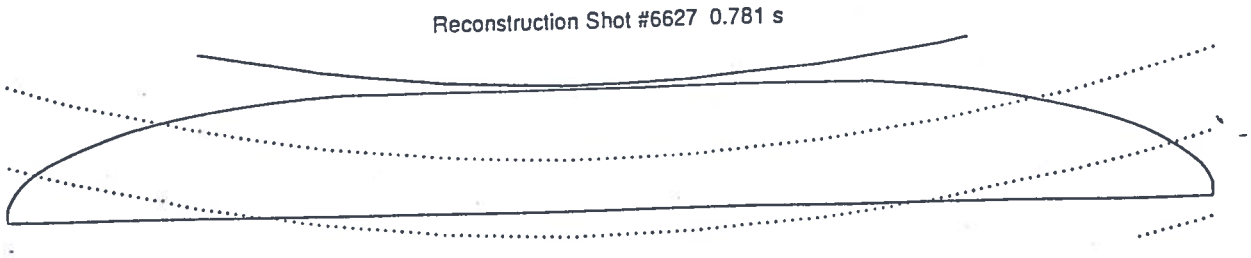
Reconstruction Shot #6627 0.781 s

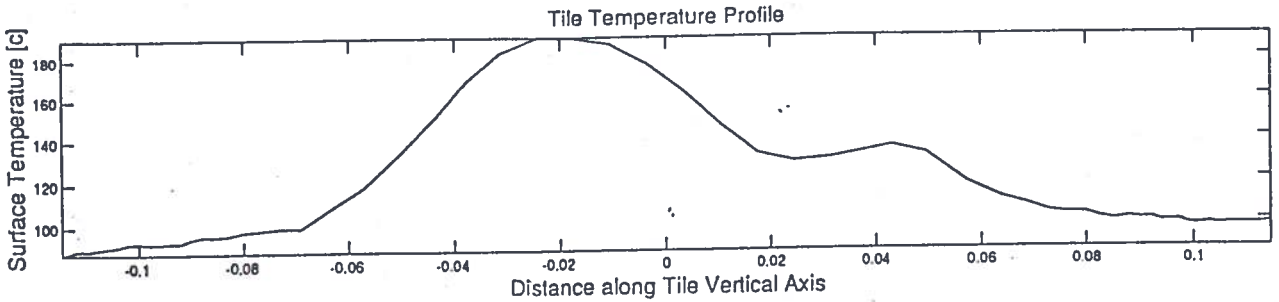
Tile Temperature Profile
Surface Temperature [c]
Distance along Tile Vertical Axis

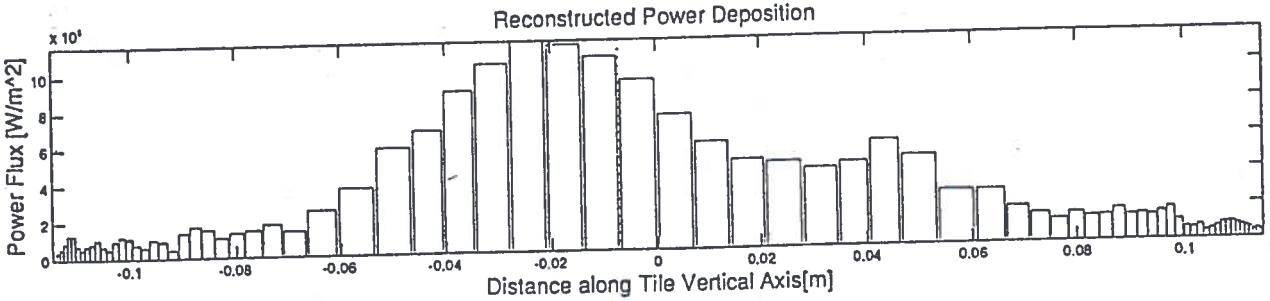
Reconstructed Power Deposition
Power Flux [W/m^2]
Distance along Tile Vertical Axis[m]

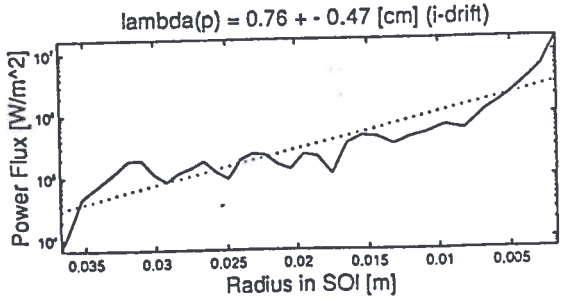
lambda(p) = 0.76 + - 0.47 [cm] (i-drift)
Power Flux [W/m^2]
Radius in SOI [m]

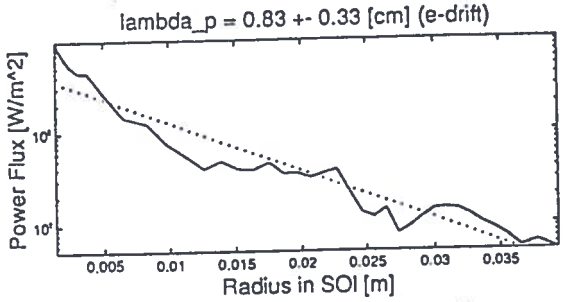
lambda_p = 0.83 +- 0.33 [cm] (e-drift)
Power Flux [W/m^2]
Radius in SOI [m]

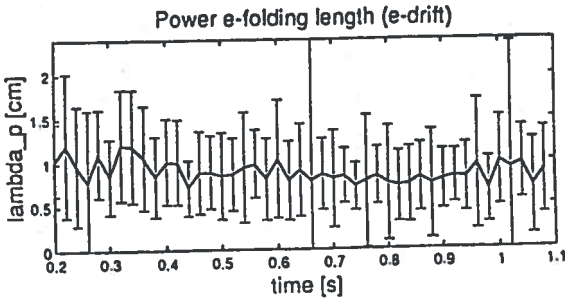
Power e-folding length (e-drift)
lambda_p [cm]
time [s]

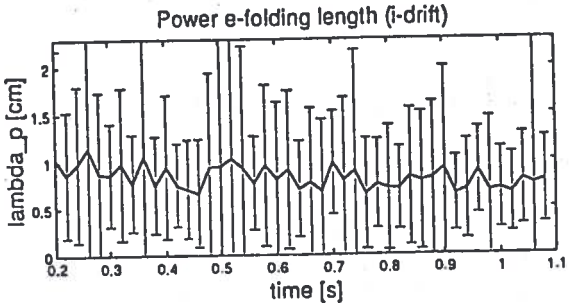
Power e-folding length (i-drift)
lambda_p [cm]
time [s]

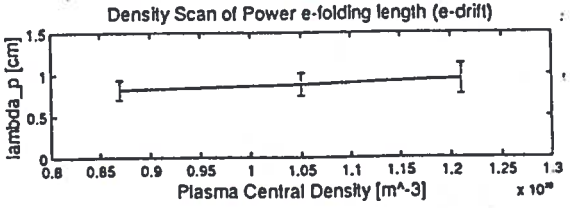
Density Scan of Power e-folding length (e-drift)
lambda_p [cm]
Plasma Central Density [m^-3]

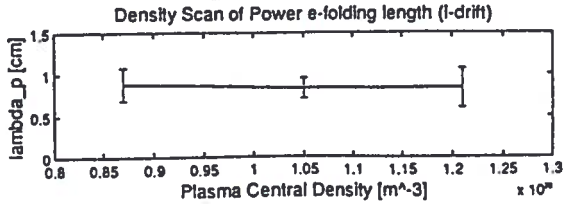
Density Scan of Power e-folding length (i-drift)
lambda_p [cm]
Plasma Central Density [m^-3]

EXPERIMENTAL AND MODELLING STUDY OF THE PLASMA DYNAMIC RESPONSE IN TCV

Y. Martin, J.B. Lister and J.-M. Moret

Centre de Recherches en Physique des Plasmas,
Association EURATOM - Confédération Suisse,
Ecole Polytechnique Fédérale de Lausanne,
21, Av. des Bains, CH-1007 Lausanne, Switzerland

Introduction

- TCV Aims:
  - Studies of confinement and transport in highly shaped plasmas.
  - Plasma shapes to study: $\kappa \leq 3$, $-1 \leq \delta \leq 1$.
  - Vertical displacement of elongated plasmas is unstable.
  - Optimized feedback control is necessary to achieve highest performances.

- TCV Plasma Control System (PCS):
  - 128 conditioned signals measuring the plasma characteristics mainly by magnetic probes and flux loops.
  - Matrix A maps these input signals onto 24 control parameters (CP).
  - 24 CP references are subtracted.
  - 24 CP errors are injected into the PID controller (Matrices G), to give18 current changes.
  - Matrix M decouples 18 current changes into 18 voltage corrections.
  - 18 voltage corrections are summed with feedforward voltage references.
  - 16 shaping coils + 2 OH coils are driven by 1 kHz rectifiers.

  - CP are defined in the MDS+ data structure.
  - CP 's values are:
    - directly drawn by the operator in the MDS+ Wavedit interface (MIT).
    - computed from drawn physics references through a neural network, MLP type.

- Experiment:
  - Perturbation injection into the CP errors (z*Ip).
  - System identification of the dynamic response.
  - Determination of the poles of the closed loop system.
  - Optimization of coil selection for feedback control.

- Modelling:
  - Matrix representation of the plasma-vessel- coils system.
  - Computes the poles in the open loop system.

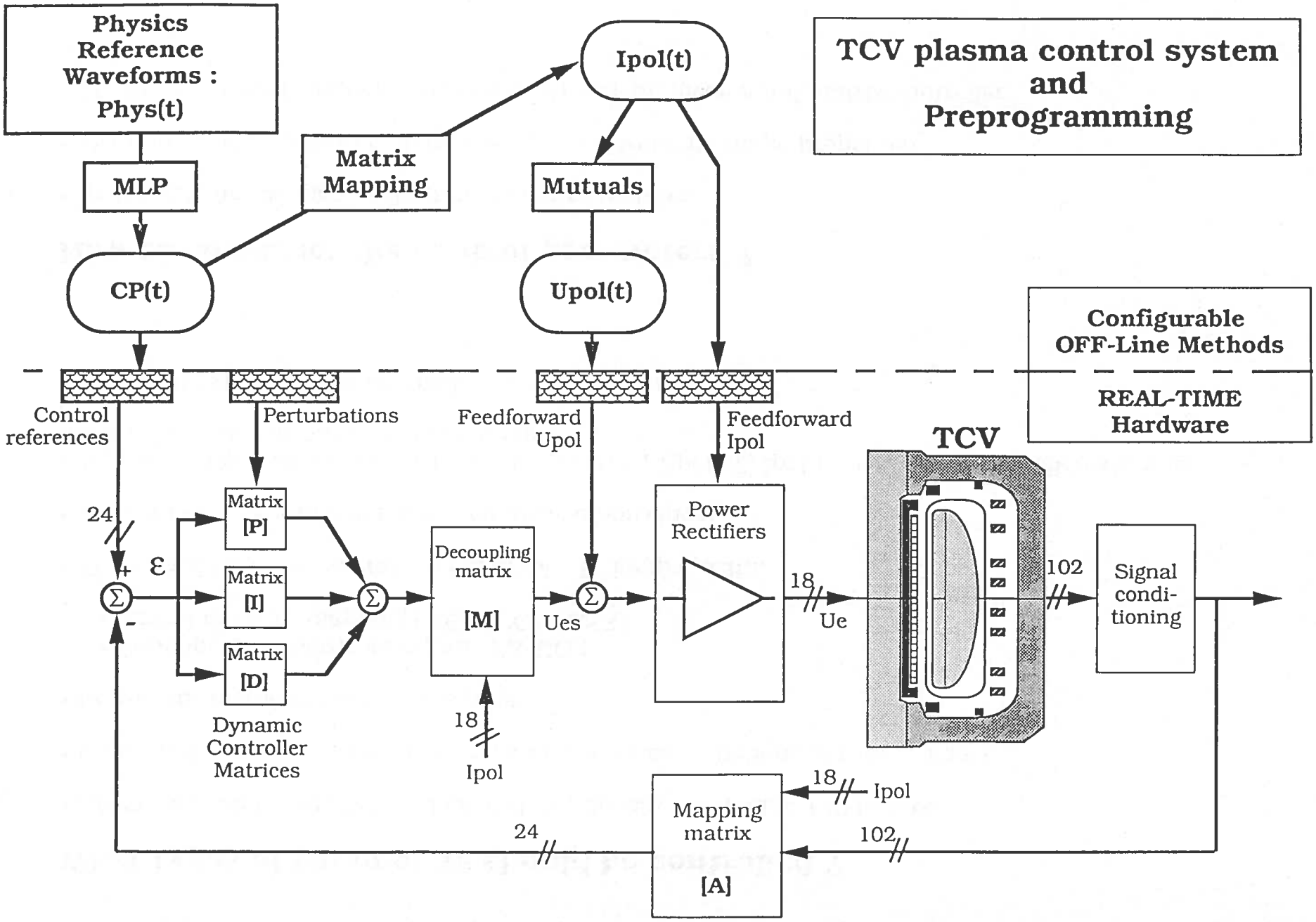
TCV plasma control system and Preprogramming
Physics Reference Waveforms : Phys(t)
MLP
CP(t)
Matrix Mapping
Ipol(t)
Mutuals
Upol(t)
Configurable OFF-Line Methods
REAL-TIME Hardware
Control references
Perturbations
Feedforward Upol
Feedforward Ipol
TCV
24
Matrix [P]
Matrix [I]
Matrix [D]
Dynamic Controller Matrices
ε
+
-
Decoupling matrix [M]
18
Ipol
Ues
Power Rectifiers
18
Ue
102
Signal condi-tioning
Mapping matrix [A]
18
Ipol
24
102

What types of parameters should be controlled ?

- Signals available are Bpol, Ψ, Ipol and line density - a total of 120 inputs.
- Controlled parameters could be linear or non-linear functions of these signals.
- Non-linear methods have been studied:
  - Function parametrisation (ASDEX-UG)
  - Neural network mapping (TCV, COMPASS)
- These methods can generate, for example, R, kappa, delta.
- Problem - the controllers must then also be non-linear.
- A linear set of control parameters CP = [A] * [Bpol, Ψ, Ipol] can use a controller which is linear, constant and valid for many shapes.
- This is the approach we adopted.

How to construct the control parameters ?

- Ip and z*Ip are defined as discrete contour integrals.
- Heuristic field and flux combinations define dominant shape properties.
- These CPs should simply be linearly independent, given a full matrix controller.

How to program the control parameter waveform references ?

- A problem using heuristic linear control parameters is to generate the reference waveforms.

- We must map non-linearly starting from "physics variables" such as R, kappa, delta.

- Initially, this was done by operator "feel".

- Subsequently we have used a neural network mapping, multi layer perceptron type.

- This mapping was learned from a data base of achieved discharges.

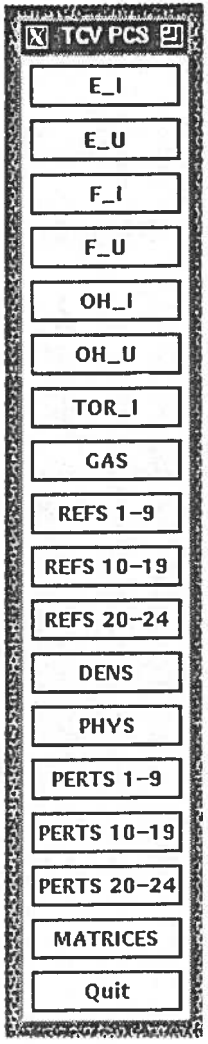

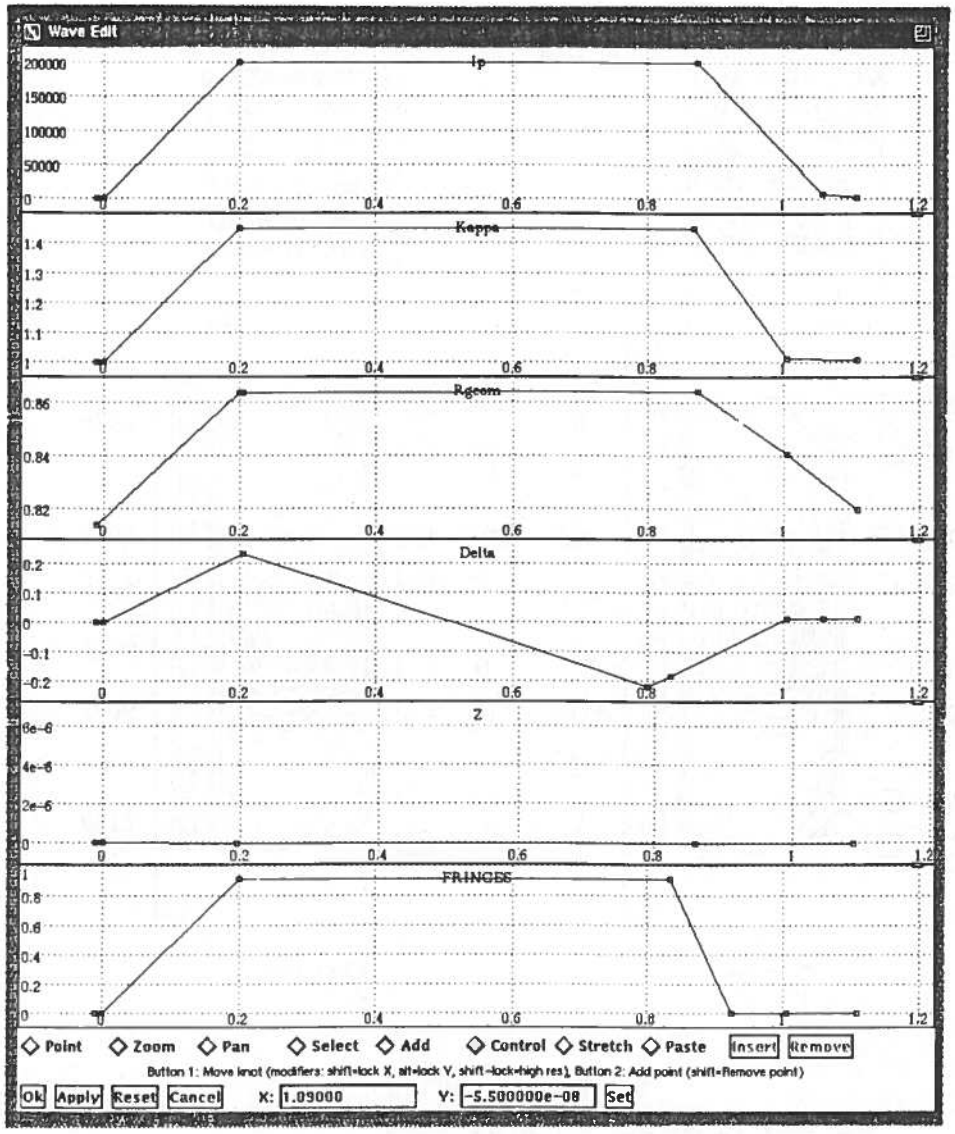

How to program the feedforward waveforms ?

• Shaping currents were also initially defined by operator "feel".

• Subsequently this has been automated using a linear mapping.

• This mapping was learned from an SVD of data from achieved discharges.

• The precision is adequate for feedback control.

• Coil voltage are provided from the vessel-less and plasma-less mutual matrix.

• All this is done off-line during the shot preparation.

How to perform the feedback ?

• The hardware allows all controllers of the form

$$\dot{\vec{\delta I}}_p = \left[\mathbf{P}\cdot \mathrm{diag}\left(\frac{1}{\vec{\tau}_P}\right) + \mathbf{D}\cdot \mathrm{diag}\left(s\cdot\frac{\vec{\tau}_D}{\vec{\tau}_P}\right) + \mathbf{I}\cdot \mathrm{diag}\left(\frac{1}{s\cdot\vec{\tau}_I\cdot\vec{\tau}_P}\right)\right]\cdot \vec{\varepsilon}_{CP}$$

What range does this approach cover ?

• A **single fixed A-matrix** was able to generate a wide range of shapes.

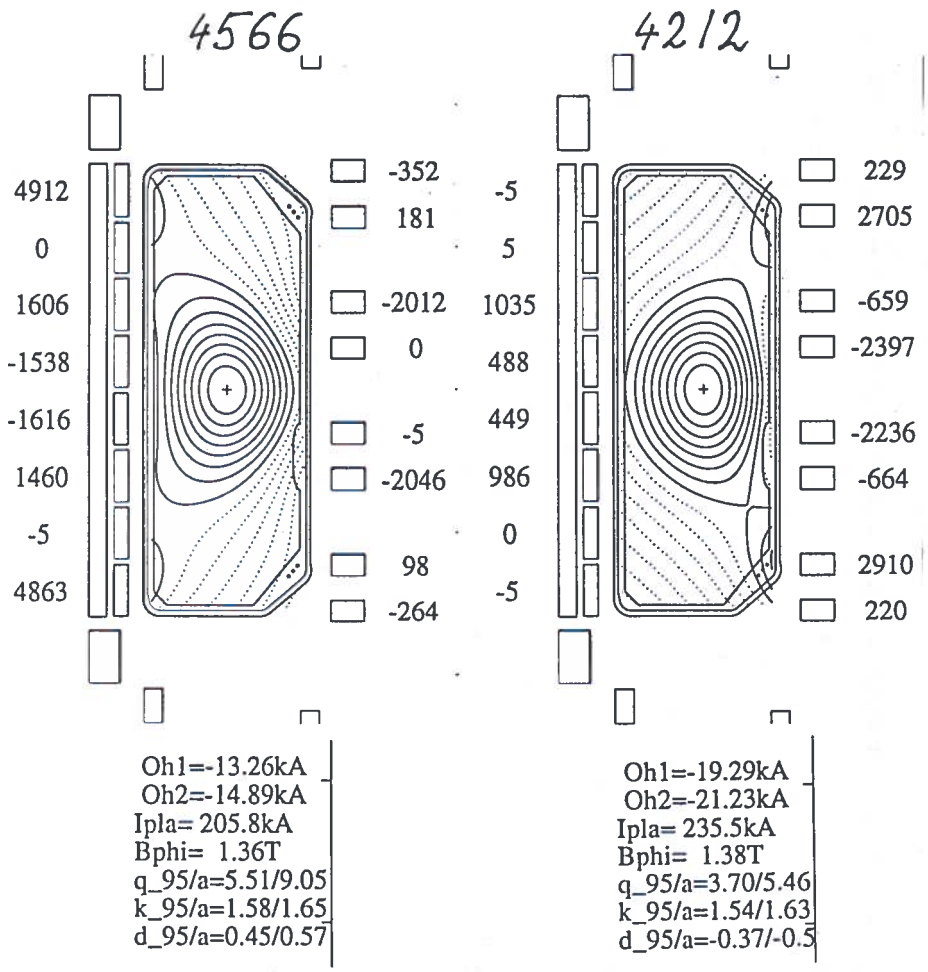

How to choose the controllers ?

• Ip is fed back on the mid-plane flux loop, assuming a typical plasma inductance.

• z*Ip is fed back on a specifiable combination of shaping coils.

• Shaping CPs are fed back via

$$\overrightarrow{\delta I_{pol}} = \left(\mathbf{A} \cdot \frac{\partial [\, B, \psi, I_{pol}]}{\partial\, I_{pol}} \right)^{-1} \cdot \overrightarrow{\varepsilon_{CP}}$$

calculated with no plasma and no vessel.

• The independence of the CPs must be such that the matrix is well conditioned.

• The elements of [**P**], [**I**] and [**D**] are the same except for z*Ip.

• Integral and proportional feedback is used for all CPs.

• Derivative feedback is only used for z*Ip and Ip.

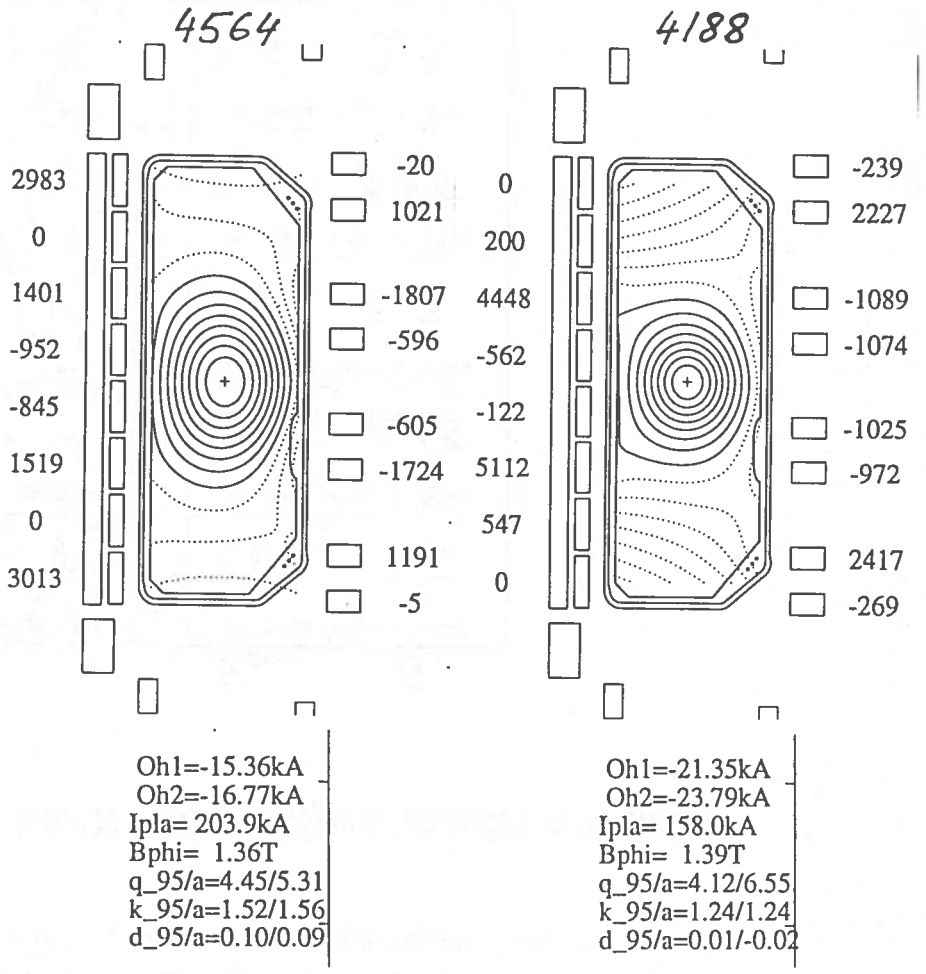

How to measure the vertical motion dynamics in TCV ?

A - Measure the closed loop system

- Inject z*Ip perturbation into the P-matrix.
- Closed loop stability with given controller settings.
- Follows the evolution during the shaping.
- Allows visual optimisation of the controller.
- Includes power supply transfer function.

Plasma elongation ramps in shots with feedback controllers modifications

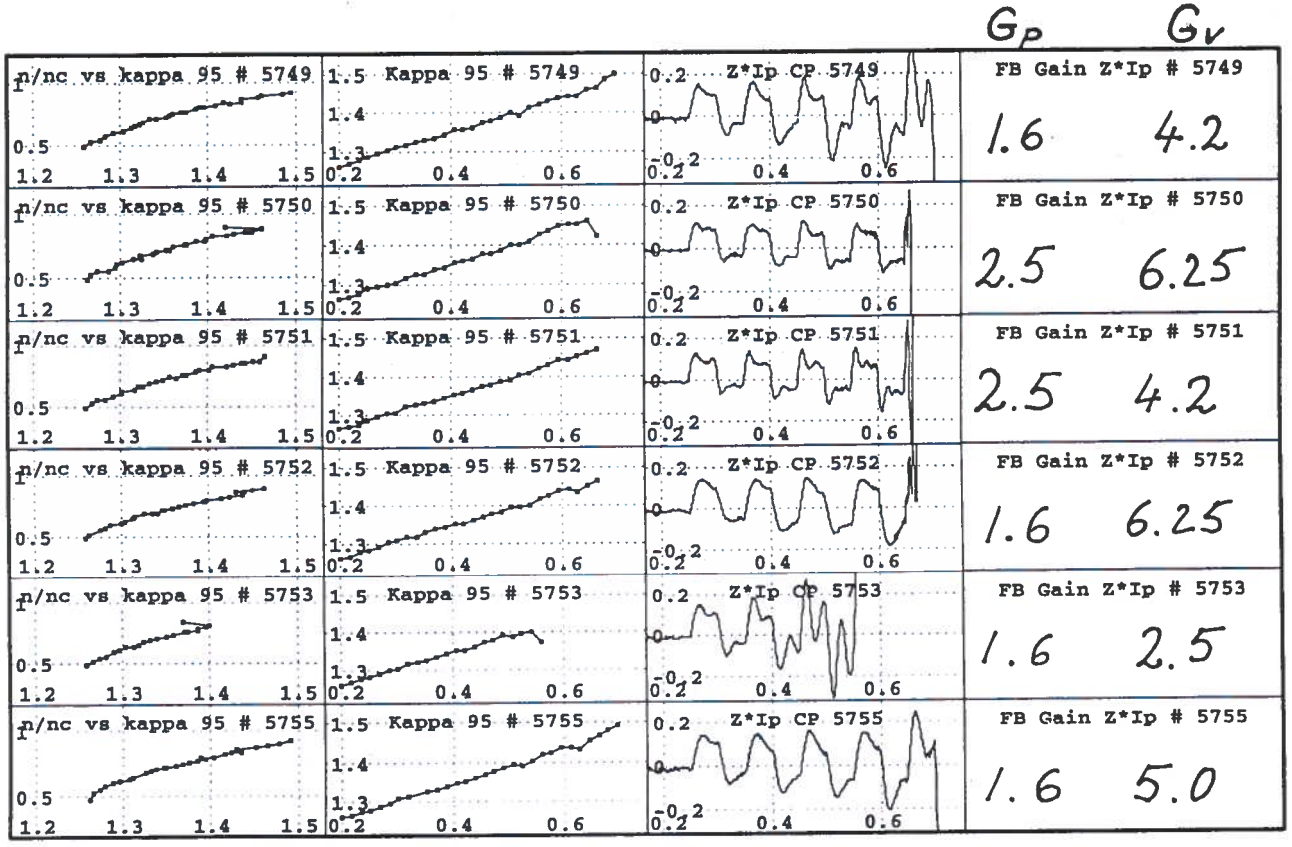

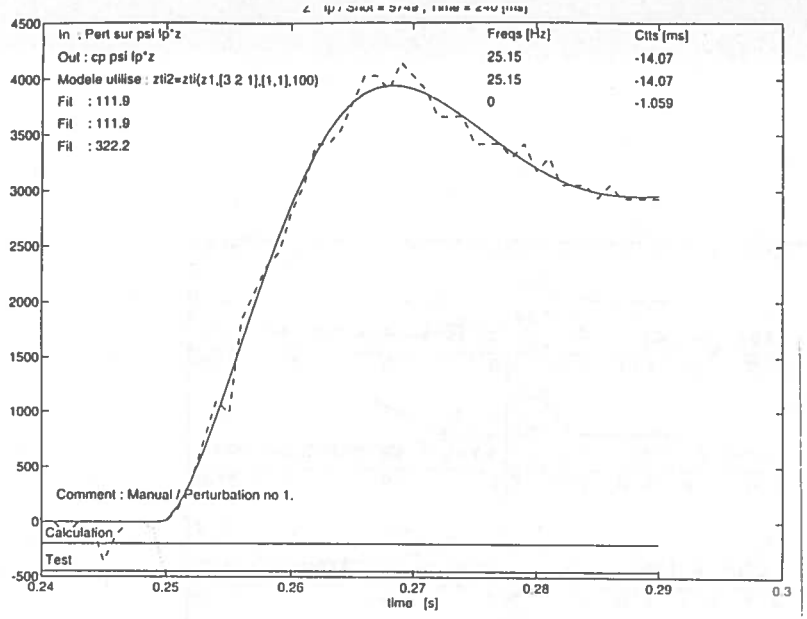

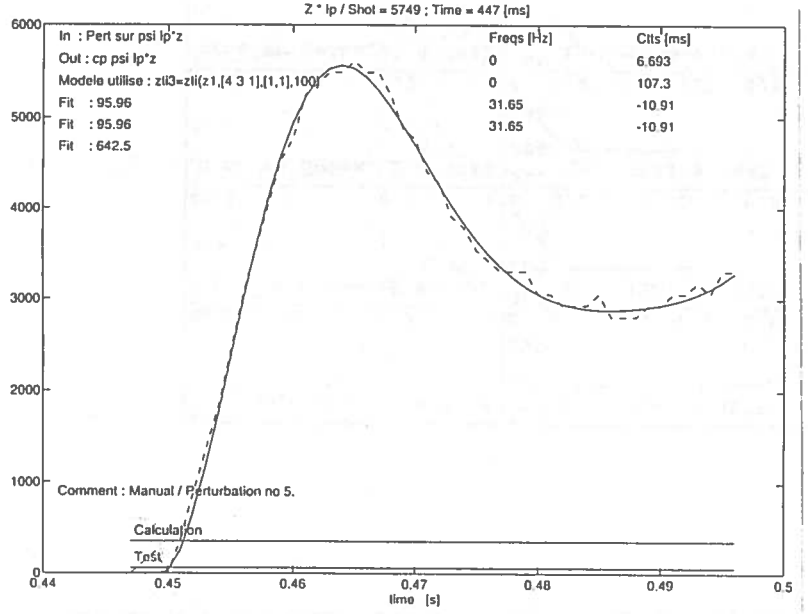

Poles displacements during k ramp
A: k = 1.28 B: k = 1.35

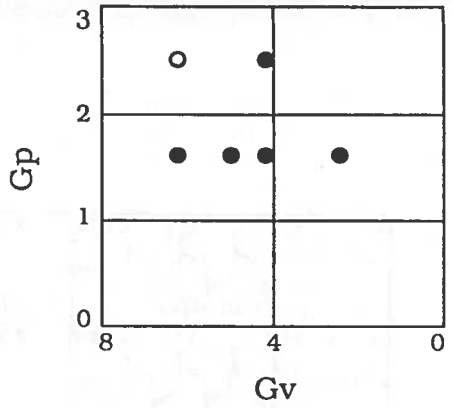

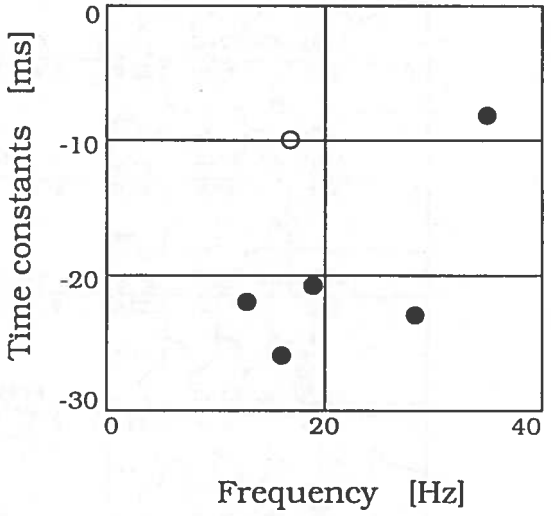

Poles displacements due to controller modifications

Plasma shots with triangularity ramps: 0.3 > δ > -0.1 and Ip scan: 150 < Ip < 300 kA.

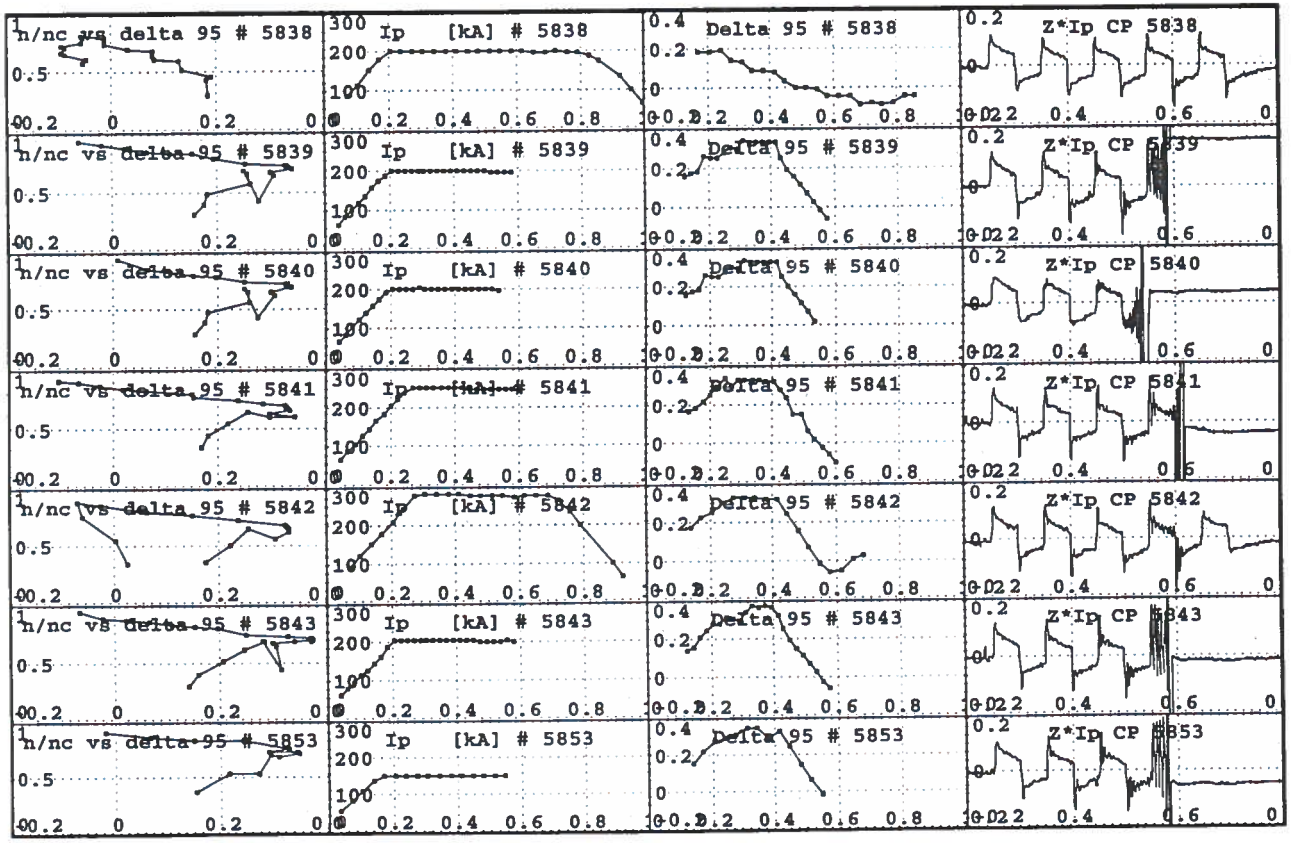

LIUQE Equilibrium Reconstruction SHOT: 5842 triang_6

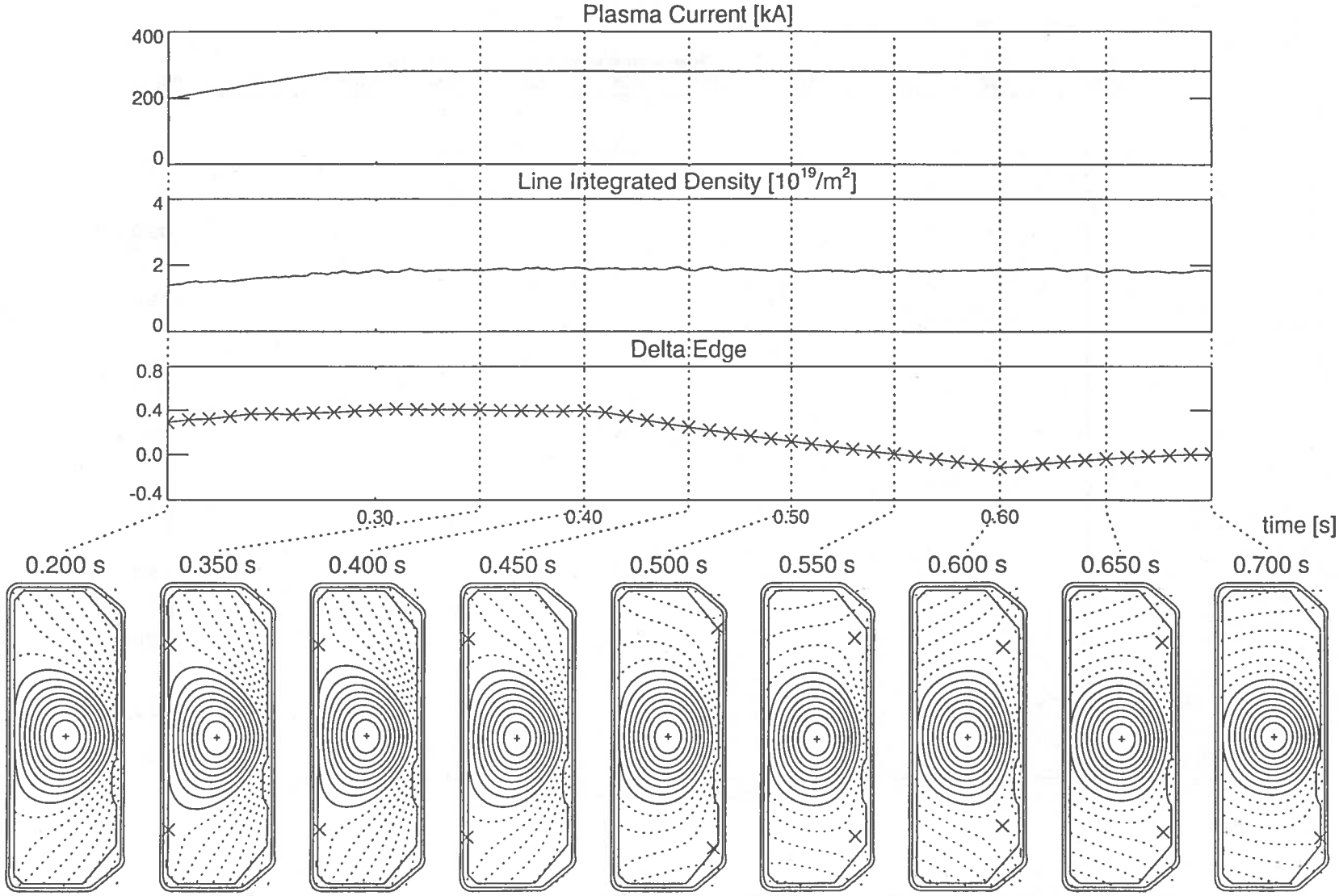

Relationship between plasma current and decay index for shots with the same elongation ($\kappa = 1.4$), triangularity ($\delta = 0.$) and corrector.

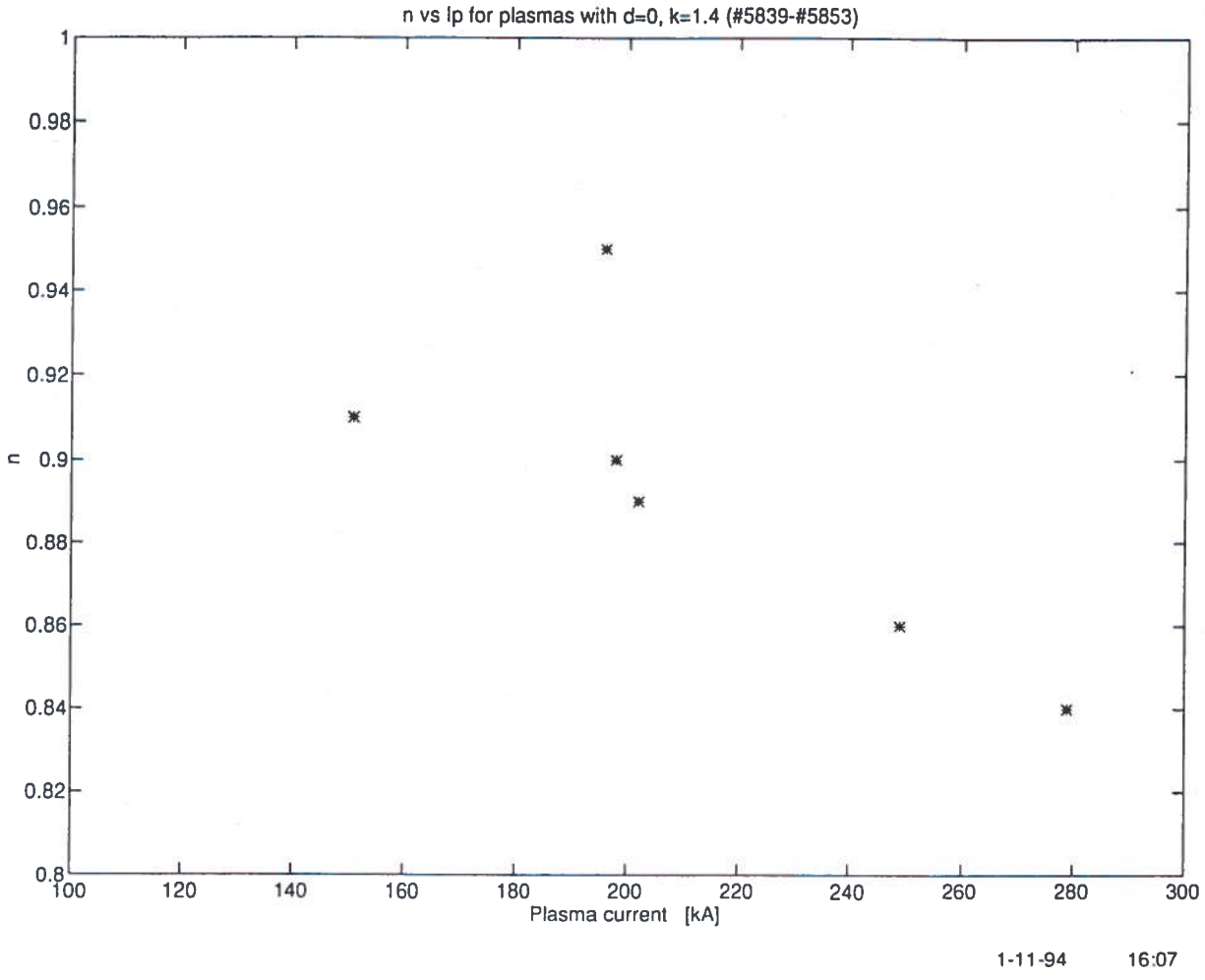

How to model TCV vertical motion simply ?

- We extend the simple model used on DIII-D.
- Force balance is still calculated for a filament on axis.
- Several eigenmodes are necessary due to
  - Irregular vessel shape.
  - Variation in z of the plasma axis.
- All shaping coil pairs are considered together.
- The coil - vessel - plasma model becomes:

$$\begin{bmatrix} s\cdot M_{aa} + R_a & s\cdot M_{ae} & s\cdot \frac{\partial M_{ap}(z)}{\partial z} \\ s\cdot M_{ae} & s\cdot M_{ee} + R_e & s\cdot \frac{\partial M_{ep}(z)}{\partial z} \\ -s\cdot \frac{\partial M_{ap}(z)}{\partial z} & -s\cdot \frac{\partial M_{ep}(z)}{\partial z} & -s\cdot \sum_e \frac{\left(\frac{\partial M_{ep}(z)}{\partial z}\right)^2}{L_e}\cdot \alpha(z, I_{pol}) \end{bmatrix} \cdot \begin{bmatrix} I_a \\ I_e \\ z\cdot I_p \end{bmatrix} = \begin{bmatrix} V_a \\ 0 \\ 0 \end{bmatrix}$$

- Each eigenmode makes a contribution to the stabilising field.

$$2\pi R\cdot \delta B_r = \frac{\left(\frac{\partial M_{ep}(z)}{\partial z}\right)^2}{L_e}\cdot \delta(z\cdot I_p)$$

Z • Ip response as a function of coil pairs

Coil / Pairs / RMS

E 1-8: 0.6

E 2-7: 1.3

E 3-6: 2.5

E 4-5: 2.0

F 1-8: 0.4

F 2-7: 0.5

F 3-6: 1.1

F 4-5: 0.8

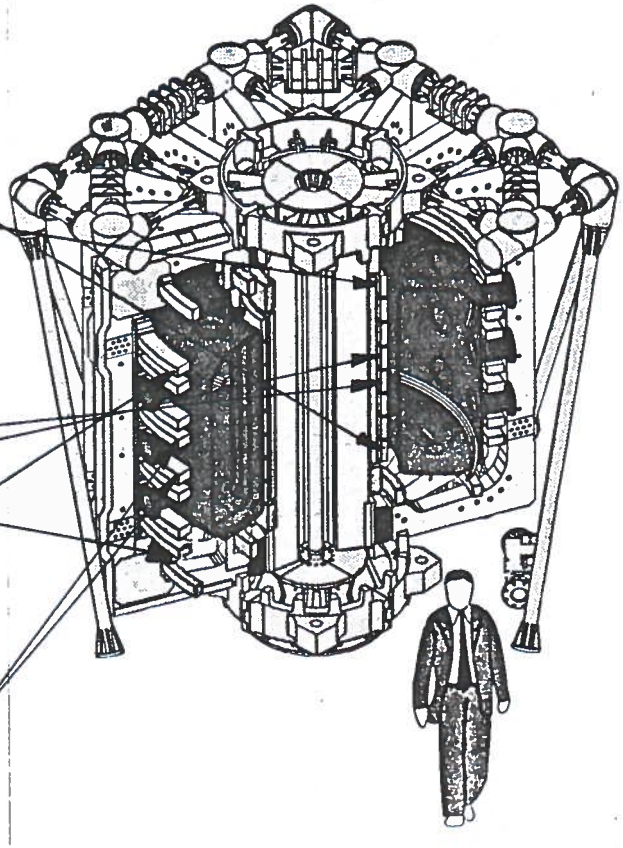

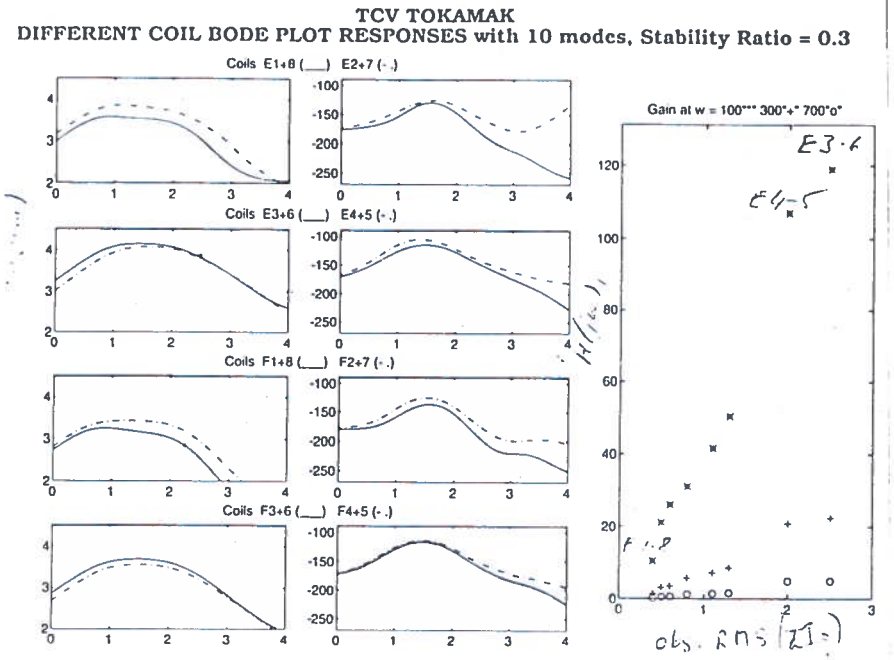

- The model predicts significant differences between the usefulness o f different coil pairs for controlling Z•Ip.
- Experimentally, the observed pulse-response shows large variations between coil pairs excited.
- Experimentally, the observed RMS response is in good agreement with the modelled response

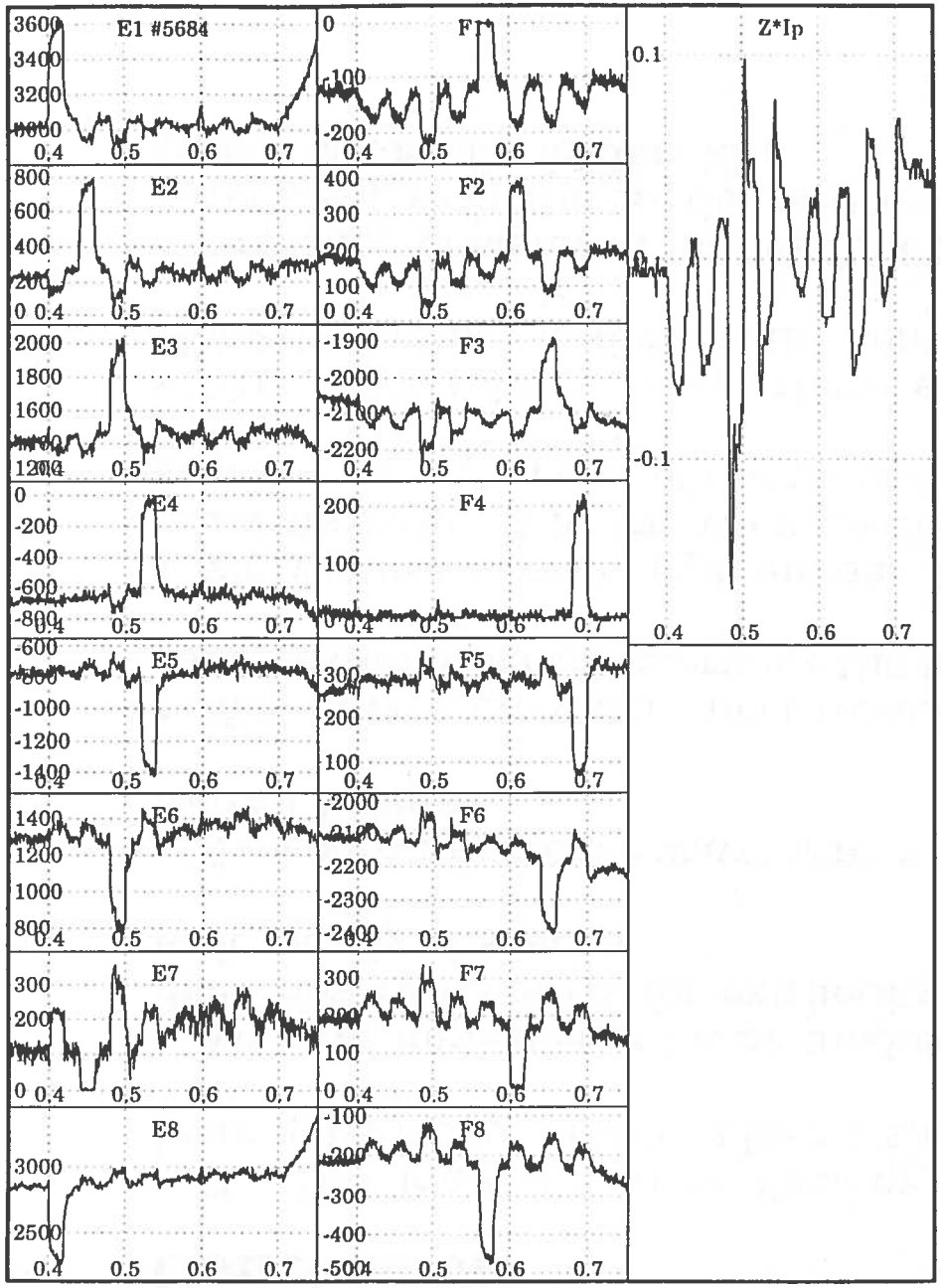

Illustrative model

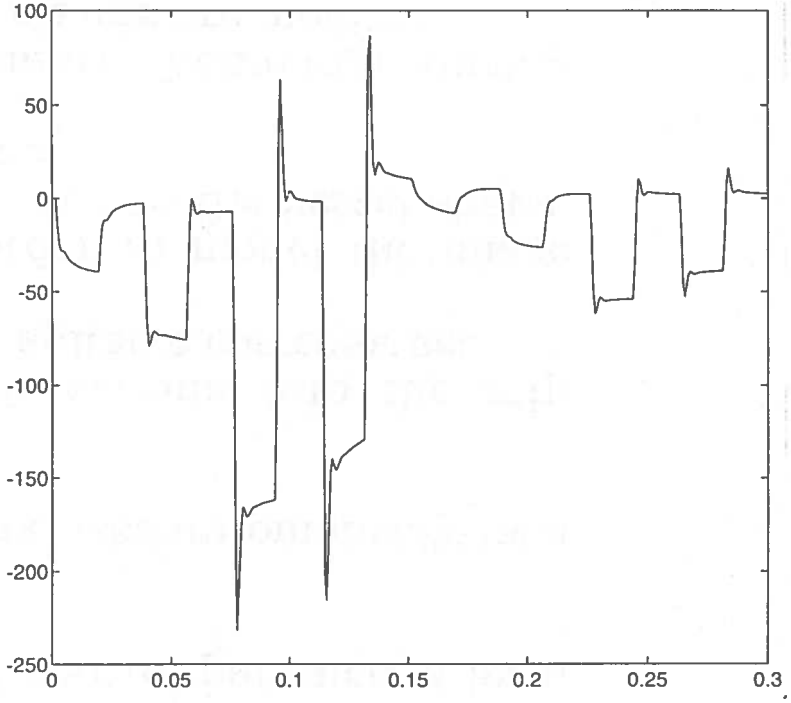

Conclusions

- The TCV Plasma Control System has the required flexibility for testing many methods for plasma shaping and control.

- We have implemented a methodology which allows the use of a fixed observer matrix for extracting the control parameters for a wide variety of shapes.

- The control reference waveforms are produced automatically by a Neural Network.

- We have performed perturbation injections into the z*Ip feedback, in order to determine the most suitable corrector set.

- We require several eigenmodes in order to model the image currents induced in the vacuum vessel, due to the vessel shape, and the varying height of the magnetic axis.

- The closed loop poles show systematic behaviour during elongation ramps and when the controller gains are modified.

- Injection of signals into different coils shows a response in good agreement with the model and confirms the importance of the choice of coils for feedback.